Methods[1]

K.M. Gillis, J.E. Snow, A. Klaus, G. Guerin, N. Abe, N. Akizawa, G. Ceuleneer, M.J. Cheadle, Á. Adrião, K. Faak, T.J. Falloon, S.A. Friedman, M.M. Godard, Y. Harigane, A.J. Horst, T. Hoshide, B. Ildefonse, M.M. Jean, B.E. John, J.H. Koepke, S. Machi, J. Maeda, N.E. Marks, A.M. McCaig, R. Meyer, A. Morris, T. Nozaka, M. Python, A. Saha, and R.P. Wintsch[2]

Chapter contents

Introduction

This chapter documents the procedures and methods employed in the various shipboard laboratories during Integrated Ocean Drilling Program (IODP) Expedition 345. This information applies only to shipboard work described in the Expedition Reports section of the Expedition 345 *Proceedings* volume. Also described is the information architecture for the population and extraction of curatorial information and shipboard scientific observations and data from the Laboratory Information Management System (LIMS) database and the Sample Master and DESClogik interfaces. Methods for shore-based analysis of Expedition 345 samples and data will be described in the individual scientific contributions to be published in articles in the open literature and in the Expedition Research Results section of the Expedition 345 *Proceedings* volume.

Numbering of sites, holes, cores, and samples and computation of depth

Drilling sites are numbered consecutively from the first site drilled by the *Glomar Challenger* in 1968. Starting with IODP Expedition 301, the prefix "U" designates sites occupied by the U.S. Implementing Organization (USIO) vessel, the R/V *JOIDES Resolution.* At a site, multiple holes are often drilled. For all IODP drill sites, a letter suffix distinguishes each hole drilled at the same site. The first hole drilled is assigned the site number modified by the suffix "A," the second hole takes the site number and the suffix "B," and so forth. Although all cored holes are routinely given these letter designations, during Expedition 345 jet-in tests were also given hole designations. This permitted documentation of jet-in test location and penetration information in the LIMS database.

While on site, the ship's location over a hole is maintained using a Neutronics 5002 dynamic positioning system that utilizes positioning information from both a positioning beacon deployed on the seafloor and the shipboard GPS. Given the seafloor morphology surrounding the Hess Deep drill sites, the seafloor positioning beacons were conveyed to and placed on the seafloor using the camera system.

The cored interval is measured in meters below rig floor (mbrf) and reported in meters below seafloor (mbsf). Depth below seafloor is determined by subtracting the seafloor depth measured

from the rig floor from the rig floor measurement of the depth of the bit below seafloor. Note that according to IODP Depth Scales Terminology v.2 (www.iodp.org/program-policies/), the mbsf scale is defined as meters core depth below seafloor, method A (CSF-A). The computations of mbsf and meters CSF-A depths are exactly the same.

The cored interval was generally a maximum of ~9.5 m long, which is the length of a standard core barrel. However, one potential cause of poor recovery during hard rock coring is core jamming in the bit or in the throat of the core barrel. Once the opening in the bit is jammed, core is prevented from entering the core barrel. Thus, core barrels were sometimes retrieved after shorter penetration intervals (usually ~4.7 m) to improve core recovery. In addition, core barrels were often deployed without a plastic liner.

Two types of cores were recovered with the rotary core barrel (RCB) coring system during Expedition 345. The first type includes RCB cores that penetrate into new formation at the bottom of the hole; these cores have the "R" designation in the core identifier. The second type includes cores in which the material enters the core barrel during substantial hole cleaning operations in previously cored or drilled intervals. These are termed "ghost cores" and are identified with a "G" core identifier instead. See "Operations" in each hole chapter for a listing of core intervals.

Each recovered core was divided into 1.5 m sections numbered serially from the top. The sections were numbered sequentially as recovered, starting with 1 at the top of the core; the last section may be shorter than 1.5 m (Fig. F1). For the purpose of nominal depth calculation, the top depth of the core is equated with the top depth of the cored interval (in mbsf) by convention to achieve consistency in handling analytical data derived from cores. All pieces recovered were placed immediately adjacent to each other in the core tray. Core pieces were designated by distance, measured in centimeters from the top of the section to the top and bottom of each sample or interval. A full identifier for a core piece consists of the following information: expedition, site, hole, core number, core type, section number, section half identifier (if applicable), top and bottom offsets in centimeters measured from the top of section (half), and additional subsample names if applicable. For example, the sample identifier "345-U1415A-5R-1W, 0–1 cm" represents a piece from the interval between 0 and 1 cm at the top of working section half 1W in Core 5R (R designates that this core was taken with the RCB) of Hole U1415A from Expedition 345. Core pieces are numbered sequentially from the top of each section, and if core pieces can be reassembled

into a single coherent piece, the piece numbers are annotated with the suffix "A," "B," and so forth.

Core reference frame for sample orientation

Each core piece that has a length exceeding that of the core liner diameter is associated with its own core reference frame (CRF) (Fig. F2). The primary reference is the axial orientation (i.e., the top and bottom of the piece) based on the piece's orientation when extracted from the core barrel; the bottom was marked by red grease pencil on the bottom of the core piece. The core axis defines the z-direction, where positive is downcore. The secondary reference is an arbitrarily marked axis-parallel line on the whole-round surface of the piece. This is the cut line, which marks the plane through the cut line and the core axis where the piece will be split. The cut line was selected by a structural geology specialist to maximize the dip angle of planar features on the split surface, which facilitated accurate structural measurements. The x-axis of the CRF is defined orthogonally to the cut plane, positive (000°) into the working half and negative (180°) into the archive half. The y-axis is orthogonal to the x–z plane and, using the right-hand rule, is positive (090°) to the left and negative (270°) to the right when looking upcore onto the archive half. When viewing the working half upcore (e.g., for sampling), 090° is to the right and 270° to the left. Cube samples and thin sections taken from the working half were marked as shown in Figure F2.

Core handling and core flow

The 15 steps of the core handling and core flow process, from coring to shipboard sampling, are summarized in Figure F3. Routine steel core barrels were used unless otherwise noted in the operations sections. Cores may be recovered with or without a plastic liner, which is believed to reduce core jamming caused by angular fragments. When cores without liners came to the rig floor, the Curator, supported by technicians, waited with presplit core liners at the end of the catwalk. Once the core barrel was lowered horizontally, each rock piece was removed from the core barrel and placed in consecutive order in 1.5 m split plastic liners labeled A through D (A through F for 9 m cores), with A being the lowermost split liner section. Blue and colorless liner caps denote the top and bottom of each split liner, respectively. This convention was used throughout the curation process. Before each piece was removed from the core barrel, the bottom of all pieces long enough to ensure vertical orientation was marked with an "X" using a wax pencil. In some

cases, pieces too small to be oriented with certainty may have been marked as they were extracted from the core barrel but later identified to be a roller. Any core catcher sample recovered was added to the bottom of split section A. To minimize contamination of the core with platinum group elements and gold, all personnel handling and describing the cores or other sample material removed jewelry from their hands and wrists before handling. In addition, no magnetic materials were used in the vicinity of the core to minimize the impact on the magnetic properties of the core.

Once all core material was removed from the core barrel and placed in split plastic liners, the liners were transferred to the core splitting room, and the rock material in each section was measured and entered into Sample Master as "Recovered length" (Fig. F4). This parameter was used to compute core recovery. While the core was being recovered from the core barrel on the catwalk, identification labels were put on prescribed split liners. After transport of the cores to the splitting room, core pieces were transferred into the prescribed and labeled liners. After all pieces were placed in the labeled split liners, the Curator and one other technician washed the whole-round pieces, one piece at a time, and allowed them to dry.

The rocks in each section were placed into sample bins with plastic core dividers between individual pieces. These spacers may represent substantial intervals of no recovery. Adjacent core pieces that could be fitted together along fractures were curated as single pieces. Core pieces that appeared susceptible to crumbling were encased in shrink-wrap. Once binning activities and curatorial measurements were completed, a designated scientist (structural geology specialist) was then called to the splitting room to check the binning and reconstruction of fractured pieces. A splitting line was marked on each piece with a red wax pencil so that the piece could be split into representative working and archive halves, ideally maximizing the expression of dipping structures on the cut face of the core while maintaining representative features in both archive and working halves (Fig. F2). To ensure a consistent protocol for whole-core imaging (see "Core section image analysis"), the splitting line was drawn so that the working half was on the right side of the line with the core upright. The working half of each piece was marked with a W to the right of the splitting line. Where structural fabrics were present, cores were marked for splitting with the fabric dipping to the east (090°) in the CRF. This protocol was sometimes overridden by the presence of special features (e.g., xenoliths, mineralized patches, and dike margins)

that were divided between the archive and working halves to ensure preservation and/or allow shipboard or postcruise sampling.

Once the split line was drawn, the plastic spacers were permanently secured with acetone between individual pieces into matching working and archive half split core liners. Spacers were mounted into the liners with the angle brace facing uphole. This ensured that the top of each piece had the same depth as the top of the curated interval for each bin. The length of each bin was entered into Sample Master as "Bin length." The cumulative length of all bins, including spacers, was entered as the "Curated length" of the section. Oriented pieces were recorded at this stage. Later, at the start of core description, the igneous petrologists measured the longest vertical dimension of each piece and entered by the curator into Sample Master as "Piece length" (Fig. F4). Once all curatorial information had been entered and uploaded, the empty section half with bins was placed over the full half and taped together in a few places to dry and equilibrate to core laboratory conditions (usually <1 h from arrival from the catwalk).

Once thermally equilibrated, the magnetic susceptibility and natural gamma radiation (NGR) signal of each section was measured using the shipboard Whole-Round Multisensor Logger (WRMSL) and the Natural Gamma Radiation Logger (NGRL), respectively (see "Whole-Round Multisensor Logger measurements" and "Natural Gamma Radiation Logger measurements"). The outer cylindrical surfaces of whole-round pieces were then scanned with the adapted Section Half Imaging Logger (SHIL) using the split line marking for registration (see "Core section image analysis").

Each piece of core was then split into archive and working halves, with the positions of plastic spacers between pieces maintained in both halves. Piece halves were labeled sequentially from the top of each section, beginning with number 1; reconstructed groups of piece halves were assigned the same number but were lettered consecutively. Pieces were labeled only on the outer cylindrical surfaces of the core. If the piece was oriented with respect to vertical, an arrow was added to the label, pointing to the top of the section. Digital images of the dry, cut faces of archive halves were captured with the SHIL. Sections were then transferred to the Section Half Multisensor Logger (SHMSL), with which color reflectance and contact probe magnetic susceptibility were measured (see "Section Half Multisensor Logger measurements").

Following core curation, whole-round and section-half measurement and imaging, and splitting (Fig.

F3), the archive section halves of each core were described by expedition scientists, and observations were recorded using the DESClogik interface and uploaded to the LIMS database (for details, see individual disciplinary sections in this chapter). Archive section halves were also passed through the cryogenic magnetometer for magnetic remanence measurements (see **"Paleomagnetism"**) and selected half-round core pieces were measured for thermal conductivity measurements (see **"Physical properties"**).

Digital color close-up images were taken of particular features for illustrations, as requested by individual scientists. Working section halves of cores were sampled for both shipboard characterizations of cores and, later during the expedition, for shore-based studies. Samples were routinely taken for shipboard physical properties (8 cm³ cubes), paleomagnetism (8 cm³ cube), thin section (billet or slab), and geochemical (billet, slab, or quarter round) analyses, as described in the sections below. Each extracted sample was logged into the LIMS database using the Sample Master program, including the sample type and either the shipboard analysis (test) conducted on the sample or the name of the investigator receiving the sample for postcruise analysis. Records of all samples taken from the cores were stored in the LIMS database and are accessible online. Extracted samples were sealed in plastic vials, cubes, or bags and were labeled.

Following initial shipboard scientific observations, measurements, and sampling, both core halves were shrink-wrapped in plastic to prevent rock pieces from moving out of sequence during transit. Working and archive halves were then put into labeled plastic tubes, sealed, and transferred to cold-storage space aboard the drilling vessel. At the end of Expedition 345, the cores remained on the ship. After the ship transited to Victoria, Canada, they were shipped to the IODP Gulf Coast Repository in College Station, Texas (USA).

Information architecture

Laboratory Information Management System

The LIMS database is an infrastructure to store all operational, sample, and analytical data produced during a drilling expedition. The LIMS database comprises an Oracle database and a custom-built asset management system, along with numerous web services to exchange data with information capture and reporting applications. More than 30 data capture applications, most of them custom tools built to support specific shipboard workflows, collect information and store it in the LIMS database. Several data retrieval applications are available to access the data from the system for different purposes (Fig. F5).

Data capture tools

All core pieces collected and samples taken during Expedition 345 were registered in the LIMS database using the Sample Master application. The program has workflow-specific interfaces to meet the needs of different users. Core piece registration began with the driller entering information about the hole and then the cores retrieved from the hole. IODP staff entered additional core information, sections, pieces, and any other subsamples taken from these, such as cubes or thin section billets.

Five imaging systems available on the *JOIDES Resolution* were used to produce six types of images:

1. Whole-round section surface (360°) images using the converted SHIL (see **"Core section image analysis"**),
2. Section-half surface images using the SHIL,
3. Core composite images combining multiple section-half images into the traditional "core table" view,
4. Close-up images taken to meet special imaging needs not covered with routine line scan images,
5. Whole-area thin section images using a custom-built system, and
6. Photomicrographs using cameras mounted on optical microscopes.

All images were uploaded to the LIMS database immediately after capture and were accessible through browser-based reports. Images were provided in at least one generally usable format (JPG, TIFF, or PDF) and in multiple formats if appropriate.

Physical property, paleomagnetism, and geochemistry analytical systems in the shipboard laboratories were used for the capture of instrumental data, as described in the following sections. In cases where no further user interaction was required, the data upload to the LIMS database was triggered automatically. In cases where quality control or data processing was needed before upload, the user explicitly triggered the upload to the LIMS database when the data were ready.

Descriptive and interpretive information (DESCINFO) was captured using the DESClogik custom software application, and all information was stored in the LIMS database. The main DESClogik interface is a spreadsheet with extensive data entry and data validation support. The columns and tabs were entirely configurable by USIO staff based on users' definitions of what information should be collected

(see "Core description overview"). USIO staff then enabled entry columns based on sets of parameters that made up the DESCINFO data structure.

Data retrieval

Data tables were mostly populated using LIMS Reports (Fig. F5), with which the user selected the type of desired information from ~30 available reports, selected a hole (and core pieces and sections), and used additional report-specific filters as desired to view a report online or download information in a standard comma-separated value (CSV) file. For information reporting not yet implemented in the LIMS Reports, another program (Web Tabular Report [WTR]) was used to access data. Information retrieved from the WTR generally represents all valid data stored in the LIMS database for a given analysis.

Another alternative was to use LIMS2Excel, a highly configurable Java-based data extractor with which users save a specific configuration for any combination of data parameters and export it into a Microsoft Excel workbook.

Many data sets could also be viewed on LIMSpeak, a browser-based application that plots cores, sections, and samples along with a user-selected data set, including images and other data sets, against depth. The application is particularly useful for monitoring data acquisition, real-time quality control, and browsing images.

Core description overview

Work flow

Three teams were formed to describe igneous petrology, metamorphic petrology, and structural geology in all core sections and thin sections prepared onboard. This disciplinary team approach ensured that all members of a specialty group were able to see all recovered material and work in a coordinated fashion to produce consistent data sets. Each team was assigned shifts that were intended to provide time and space to examine the cores and also to ensure overlap with the other teams for information exchange.

At the beginning of the expedition, each group defined observables as Excel spreadsheet columns, with descriptive terminology and definitions defined as appropriate for each measurement. These specifications were subsequently implemented as columns, tabs, and workbooks in the DESClogik application. Observable parameters were of three types: controlled values, free text, and numbers. For the controlled value columns, value lists were configured as drop-down lists to facilitate consistent data capture. These values are defined in each description team's

section. Free text fields had no constraints and were used for comments. Number columns were used to log, for example, abundance percentage, size, intensity, and rank (for plotting) of physical constituents, texture, and structures.

Descriptive data capture workbooks

The three core description teams defined data capture columns. Columns were arranged in tabs and workbooks as agreed upon within each description team as well as among the three teams. Arrangements were optimized to support the description workflow and to avoid overlaps and gaps in data collection.

Section summary graphic (visual core descriptions)

With all observables specified, the science party selected a few of the parameters to be represented graphically on the core section summary graphic, historically referred to as the visual core descriptions (VCDs). All information for VCDs was retrieved from the LIMS database with the LIMS2Excel tool. VCD information was plotted as symbols, patterns, and line plots with depth, along with some instrumental data, using the commercial plotting program, Strater. Tabulated data summaries for the sections were generated using DESClogik and printed next to the plots. All information displayed on the VCDs were plotted or otherwise collected from the LIMS database in a semiautomated process supported by USIO staff.

Thin section description overview

Work flow

Thin sections were prepared on board after the daily shipboard sample party. Metadata, including the rationale for taking each section, were recorded and entered into the LIMS database. Finished thin sections were available ~1 day after sampling and were given an immediate preliminary description by the igneous petrology team. Detailed descriptions were conducted by each of the three teams in turn, and observational data were recorded in DESClogik and all digital imaging (whole-round sections, split sections, and close-up images, and photomicrographs) uploaded into the LIMS database. Concise summaries of findings are presented in the section-by-section VCDs and thin section summaries.

Core section image analysis

During Expedition 345, external surfaces of both archive-half and whole-round core sections were

scanned using an experimental system involving multiple passes through the SHIL. Core imaging during this expedition had four main objectives:

1. To provide a comprehensive suite of digital core images, including both unrolled 360° and section-half surface images, to aid petrological interpretation;

2. To identify and measure features on unrolled 360° images for comparison with core structural analysis;

3. To correlate core images with Formation MicroScanner (FMS) images of the borehole wall to determine true core depth as opposed to curated depth calculations in intervals with <100% recovery; and

4. To match structures observed on core images with FMS images to permit reorientation of core pieces and associated structural data to magnetic north obtained from the General Purpose Inclinometer Tool (GPIT) on the FMS tool.

Core orientation was particularly important for Expedition 345 because Hess Deep is at low paleolatitude, which means the expected paleomagnetic inclination would be nearly horizontal and the magnetic polarity would be indeterminate from azimuthally unoriented cores. Similarly, without a known polarity, the paleomagnetic declination cannot be used to orient the core for structural analyses or for the determination of anisotropy of physical properties.

Section Half Imaging Logger core scanning system

A system was developed at IODP-Texas A&M University to use the existing, higher resolution SHIL generally used for section-half surfaces to image the outer surface of the core. The main element of this system is an aluminum frame that can simultaneously hold the cylindrical pieces of a single core section and rotate them in 90° increments (Fig. F6). The frame consists of four aluminum strips ~155 cm × 4 cm in dimension, all of which latch at each end into a pair of rotatable spindles. Each strip is milled with a concave surface that rests against the core pieces. Four images of the core surface are later processed to simulate a continuous image of the unrolled 360° surface.

Methodology

On each core piece, a vertical line was drawn with a wax pencil to define the core split. Convention is such that, with the core upright, the archive half is to the left of this line and the working half is to the right. The split line therefore corresponds to the 90°

direction (+*y*) in the core-reference coordinates used for structural geology and paleomagnetism (Fig. F2). When the core images are processed to a simulated unrolled image, nonhorizontal planar structures (e.g., veins, faults, or fractures) should produce sinusoidal-shaped curves. These can be matched to similarly shaped features imaged along the borehole wall by the four pads of the FMS logging tool. Other distinct petrological features or structures that are imaged on the outer surface of the core and the borehole wall can be similarly matched to determine the depth of the core in the borehole and reorient the core azimuth (e.g., MacLeod et al., 1994; Morris et al., 2009).

In detail, the process for generating the simulated unrolled image includes the following steps:

1. The vertically oriented pieces for a single section are placed at their curated-relative depths within the aluminum frame, with two of the aluminum strips in place to hold the core and two removed for access.

2. After the frame is moved to the SHIL, three of the aluminum strips secure the core surface and one is removed to allow imaging.

3. After imaging one surface, the aluminum strip is replaced, the section is turned 90°, and the next strip is removed to allow imaging.

This process is repeated to generate four images. The individual images are automatically uploaded to the LIMS database. The imaging specialist then downloads the images, aligns them visually, labels them by section, and makes them available to the science party.

For matching core-surface features to borehole features, one generally must assume the features are planar to extrapolate across the material destroyed by the drill bit. An obvious point to consider is that the vertical extent of a planar feature will scale with the ratio of the borehole diameter to the core diameter, generally between 4 and 5. A less obvious point is that the usual presentation of images looking inward toward the core surface but outward toward the borehole wall results in mirroring geometric relations, clockwise downcore (increasing angle in IODP coordinates) left-to-right in the logging image but right-to-left in the core surface image.

Igneous petrology

Rock description procedures during Expedition 345 closely followed those used during IODP Expeditions 335, 304/305, and 309/312 (Expedition 335 Scientists, 2012; Expedition 304/305 Scientists, 2006; Expedition 309/312 Scientists, 2006). These, in turn,

were based on Ocean Drilling Program (ODP) Leg 209 and earlier "gabbro" legs (ODP Legs 118, 147, 153, and 176) to maintain a relatively high degree of consistency of description between legs (Shipboard Scientific Party, 1989, 1993a, 1995, 1999a). As during Legs 176, 206, and 209 and Expeditions 304/305 and 309/312, core descriptions were performed by the entire igneous petrology team working together (Shipboard Scientific Party, 2003, 2004). Each member was responsible for one or more aspects of the description (igneous contacts, textures, mineral modes, and habits) and data entry on the entire core to ensure consistency of recorded observations throughout. Commonly, the entire team worked together, particularly when defining units and contacts.

Recovered core was described both macroscopically and microscopically, and its characteristics were entered into the LIMS database through the DESClogik portal. Key information was entered into the Section-unit summary tab in the DESClogik Macroscopic template. This information was then used for the production of VCDs, which summarize the description of each section of core (see "Core descriptions"). The key to symbols used on the VCDs is given in Figure F7.

Piece descriptions and igneous units

Core characterization was based on the description of individual pieces from a recovered section of a core. If neighboring pieces were homogeneous with respect to magmatic features, they were combined to one lithologic interval and accordingly described macroscopically in the corresponding DESClogik tab. Lithologically and texturally similar pieces from consecutive core sections were curated as belonging to the same lithologic interval. The upper and lower ends of each piece were directly taken from the curated piece log available within DESClogik. If within a given piece a contact (e.g., chilled margin, change in primary mineralogy, color, grain size, and structural or textural variation) was recognized, a new lithologic interval was defined and described. In this way, all of the important information about the igneous stratigraphy was preserved on a truly descriptive basis. Where contacts and/or boundaries deviated from horizontal within the core reference frame, their depth was logged at the midpoint on the cut face. A summary of the lithologic intervals, including the description of the igneous contacts, was logged into the corresponding DESClogik tab. The numbering of lithologic intervals started with "1" for each hole and consecutively continued throughout the whole core. Within a given interval, no subdivisions were made. Based on the description of the different lithologic intervals and their contacts, igneous units of coherent rock type were defined on a broader, more interpretative scale after discussions within the whole scientific party. Description, characterization and explanations, and reasons why lithologic intervals were combined into units for each hole separately at the beginning of each igneous hole report. For those cores for which units were defined, tables are presented at beginning of the descriptions of the hole, listing the lithologic intervals in each hole and their classification into units. For each lithologic interval, core-section-interval, interval depth (in mbsf) of top and bottom, piece numbers, a complete lithologic name (name of the principal lithology and modifiers, if used), and a description of the contacts is given. Average grain sizes and modal contents of the principal minerals for individual intervals can be obtained from the VCDs (see "Core descriptions").

Macroscopic core description

Lithology

Plutonic rock

Plutonic rock was classified on the basis of mineral abundance, grain size, and texture (as inferred prior to alteration) based on the International Union of Geological Sciences (IUGS) system (Streckeisen, 1974; Le Maitre, 1989; Le Maitre et al., 2002). This classification defines the following rock types (Figs. F8, F9):

- Troctolite: olivine + plagioclase > 95%, olivine > 10%, and plagioclase > 10%.
- Olivine gabbro: olivine + plagioclase + clinopyroxene, none of which is <5%.
- Gabbro or diorite: plagioclase + clinopyroxene > 95%, plagioclase > 10%, clinopyroxene > 10%, and quartz < 5%.
- Gabbronorite: plagioclase + clinopyroxene + orthopyroxene, none of which is <5%.
- Quartz diorite: quartz 5%–20% of quartz + alkali feldspar + plagioclase (QAP), with alkali feldspar <10% of QAP.
- Tonalite: quartz 20%–60% of QAP, with alkali feldspar <10% of QAP.
- Trondhjemite: tonalite with total mafic mineral content <10%.

In the IUGS classification, diorite is distinguished from gabbro by the anorthite content of plagioclase, with diorite having plagioclase containing <50 mol% An and gabbro having plagioclase containing >50 mol% An. Because the anorthite content of was not determined from macroscopic description, we used the following convention: if a gabbroic rock contained quartz (<5%) or primary amphibole (indi-

cating a relatively high degree of fractionation), the rock was classified as diorite. If no quartz or primary amphibole was observed, the rock was classified as gabbro. For plutonic rock rich in chromian spinel, we followed the classification of Leg 209 (Shipboard Scientific Party, 2004): a sample that contains >10% chromian spinel was called chromitite.

We use the rock name "oikocryst gabbro" for troctolite or, less commonly, gabbro containing >40% clinopyroxene oikocrysts. This term describes gabbroic rock characterized by a high concentration of centimeter-scale clinopyroxene oikocrysts, which makes this rock unique and easily recognizable macroscopically. Because of the uniqueness of this rock, we introduced this name to distinguish from normal gabbro, based wholly on the mineral mode, in order to identify oikocryst gabbro in the VCDs and lithology distribution diagrams. For the definition of oikocryst, see below.

Minor modifications to the IUGS system were made to divide the rock types more accurately on the basis of significant differences rather than arbitrary cutoffs based on the abundance of a single mineral. We attempted to follow as closely as possible the descriptions from Leg 209 and Expeditions 304/305, 309/312, and 335 to facilitate intersite comparison.

For gabbroic rock, the following modifiers based on modal mineralogy were used:

Disseminated oxide = 1%–2% Fe-Ti oxide.
Oxide = >2% Fe-Ti oxide.
Olivine bearing = 1%–5% olivine.
Orthopyroxene bearing = 1%–5% orthopyroxene.
Clinopyroxene bearing = 1%–5% clinopyroxene.
Troctolitic = 5%–15% clinopyroxene; >20% olivine.
Olivine rich = >70% olivine.
Anorthositic = >80% plagioclase.
Clinopyroxene oikocryst bearing = 5%–40% clinopyroxene oikocrysts.

Additional descriptive modifiers were defined as

- Leucocratic: light colored; high proportions of plagioclase.
- Doleritic: applied to fine- or medium-grained gabbroic rock with dominant ophitic or subophitic textures (Fig. F10).

Volcanic and hypabyssal rock

For volcanic and hypabyssal rock, we used the following definitions:

- Basalt: all igneous rock of basaltic composition in the size range glassy to fine grained.
- Dolerite: holocrystalline, fine- to medium-grained rock of basaltic composition with well-developed subophitic or ophitic textures.

- Olivine dolerite: dolerite with >5% olivine.

In English language usage, the term dolerite is European in origin and functionally equivalent to the North American usage of the term diabase, which is the IODP standard term. However, in Japanese, the term diabase has a distinctly different meaning, referring to strongly altered (green) basaltic rocks and is expressed differently in Kanji script. This usage of "diabase" is also prevalent in Europe. We therefore agreed to use "dolerite."

Basalt was divided according to phenocryst content, using the following convention:

Aphyric = <1% phenocrysts.
Sparsely phyric = 1%–5% phenocrysts.
Moderately phyric = >5%–10% phenocrysts.
Highly phyric = >10% phenocrysts.

If present, phenocryst phase names were used as modifiers in front of the rock name with a hyphen. If <1% phenocrysts, the rock was given the modifier "aphyric."

Mineralogy

Plutonic rock

In oceanic plutonic rock, the primary rock-forming minerals are olivine, plagioclase, clinopyroxene, orthopyroxene, amphibole, Fe-Ti oxide, sulfides, and rarely quartz. The following data were recorded in the LIMS database for each primary silicate:

- Visually estimated modal percent, which in fresh rock represents the modal mineralogy as observed; in (partially) altered rock, this represents the estimated igneous modes prior to alteration. Where a mineral occurs in trace quantities (i.e., too low to assign a meaningful percentage), 0.1% was recorded. Accessory phases are also noted where observed. Modal estimates were made independently for each phase by a different team member and summed. If the total deviated significantly from 100%, the interval was reexamined by the team and estimates were adjusted. Where totals were close to 100%, the mode of the most abundant mineral (generally plagioclase) was adjusted, retaining the original estimates of phases that occur in minor abundance (generally oxides, olivine, and/or orthopyroxene). The rationale behind this procedure was that the absolute uncertainty in estimating modal proportions is largest for the most abundant minerals;
- Minimum, median, and maximum grain size for each mineral phase;
- Mineral shape: euhedral, euhedral-subhedral, subhedral, subhedral-anhedral, and anhedral; and

- Mineral habit: equant (aspect ratio < 1:2), sub-equant (aspect ratio = 1:2 to 1:3), tabular (aspect ratio > 1:3 to 1:5), and elongate (aspect ratio > 1:5), as well as many additional terms often specific for the different habits of individual minerals (e.g., interstitial, poikilitic, acicular, lath-shaped, fibrous, flaky, skeletal, columnar; for more terms used see Shelley, 1993), were used.

Some troctolite and lesser gabbro contains spectacular clinopyroxene oikocrysts. These oikocrysts are a macroscopic feature with a distinctive texture clearly observable in the core. The oikocrysts have a well-defined spherical or augen-like habit that shows a clear boundary to the troctolitic or, less commonly, gabbroic matrix. Chadacrysts (enclosed grains) within the oikocrysts are clearly visible and typically are plagioclase. Olivine only occurs at the outermost rim. Because of their well-defined habit and clear relationships with other minerals, the oikocrysts are easily identified with the naked eye. Clinopyroxene is defined as poikilitic if characterized by interstitial with the matrix. Poikilitic clinopyroxene grains are often very irregular in shape, forming large irregular clusters, with much less defined contact relations relative to the matrix. In more olivine rich gabbros, these clinopyroxenes also include olivine as chadacryst, irrespective of whether they are located in the central part or in the rim of the clinopyroxene. The macroscopic observations concerning the oikocrysts are consistent with microscopic observations.

Volcanic rock

In volcanic and hypabyssal rock, the groundmass, phenocrysts (if any), and vesicles were described. For the groundmass, grain size was recorded using the following definitions:

Glassy.
Cryptocrystalline = <0.1 mm.
Microcrystalline = 0.1–0.2 mm.
Fine grained = >0.2–1 mm.
Medium grained = >1–5 mm.
Coarse grained = >5–30 mm.

For phenocrysts, the abundance (in percent); maximum, minimum, and median grain size (in millimeters); and shape were recorded for each phase. Phenocrysts and groundmass crystals were described based on the identification of phenocrysts in hand sample following the criteria listed below:

Aphyric = <1% phenocrysts.
Sparsely phyric = 1%–5% phenocrysts.
Moderately phyric = 5%–10% phenocrysts.
Highly phyric = >10% phenocrysts.

Rock names were further classified by types of phenocrysts present (e.g., sparsely plagioclase-olivine phyric, in which the amount of olivine exceeds the amount of plagioclase).

For vesicles, abundance (in percent); vesicularity; size distribution; minimum, maximum, and modal size (in millimeters); roundness (rounded, sub-rounded, or well rounded); sphericity (highly spherical, moderately spherical, or slightly spherical or elongate); filling (in percent); and fill composition were documented. If vesicles are elongate, the direction was noted.

Contacts

For igneous contacts between units, the type, definition, geometry, and interpretation were described. We noted when the contact was not recovered. For more details on contacts see "Structural geology."

Contact types include

- Grain size contact: units on either side have markedly different grain sizes,
- Modal contact: units on either side have markedly different mineral proportions, and
- Color contact: units on either side have markedly different primary (i.e., not alteration related) color.

If contacts were characterized by combinations of the above parameters, the terms were combined (e.g., grain size and modal contact).

Where contacts are obscured by deformation and/or metamorphism, they were called

- Sheared: if an interval with deformation fabric is in contact with an undeformed interval,
- Foliated: if both intervals have deformation fabrics, or
- Tectonic: if the contact appears to be the result of faulting.

Contact definitions describe how well defined a contact is, using the terms sharp, gradational, and sutured. "Sutured" refers to contacts in which individual mineral grains interlock across the contact. Contact geometry can be planar, curved, or irregular.

Following description, contacts were interpreted as being extrusive, intrusive, or igneous. The latter term is used for contacts in plutonic rocks where the lithologies on either side of the contact were interpreted to form part of the same igneous sequence (e.g., a modal contact between cumulate layers or a grain size contact in a graded sequence).

The term "dike" refers to any sharp, well-defined, and relatively thick (>1 cm) crosscutting feature formed by injection of magma. This contrasts with "igneous vein," which describes a thin (<1 cm) cross-

cutting feature formed by injection of magma with generally less well defined contacts. Dikes and veins are generally designated as individual intervals.

Texture

Plutonic rock

Textures were defined on the basis of three categories: grain size, grain size distribution, and the relationships between different grains.

Grain sizes were defined as

Less than fine grained = < 0.2 mm.
Fine grained = >0.2–1 mm.
Medium grained = >1–5 mm.
Coarse grained = >5–30 mm.
Pegmatitic = >30 mm.

For plutonic rock, grain size distributions (Fig. **F10**) were classed as

- Equigranular: all minerals are of similar size,
- Inequigranular: two populations of grain sizes occur, or
- Seriate: a continuous range of crystal sizes.

For defining textures, we used the terms

- Granular: aggregation of grains of approximately equal size;
- Subophitic: partial inclusion of plagioclase in clinopyroxene;
- Ophitic: total inclusion of plagioclase in clinopyroxene;
- Comb structure: comb-like arrangement of crystals growing inward from a contact;
- Dendritic: branching arrangement of elongate crystals;
- Poikilitic: relatively large oikocrysts enclosing smaller crystals, termed chadacrysts, of one or more other minerals; and
- Varitextured: domains with contrasting grain size are present.

Similar to the silicate minerals, the textures of oxide and sulfide minerals are described in terms of grain size and their relationship to adjacent minerals. In plutonic rock, oxides commonly occur as aggregates, and for grain size determination, an aggregate is counted as a single grain.

Layering, where present, is divided into modal layering and grain size layering; when neither term describes the observations well, the term "layering (other)" is used and the nature of layering is described in the comments. If layering is present, the geometry of layering is described in the comments (e.g., sharp, gradational, or irregular). For more details see also **"Structural geology."**

Volcanic rock

Textures were defined on the basis of three categories: grain size, grain size distribution, and the relationships between different grains.

Grain sizes were defined as follows:

Less than fine grained = < 0.2 mm.
Fine grained = >0.2–1 mm.
Medium grained = >1–5 mm.

For volcanic rock, grain size distribution applies to phenocrysts only, using the terms "unimodal" when all phenocrysts are of similar size, "bimodal" when two size populations are defined, or "seriate" when they form a continuous range of sizes.

The following terms were used to describe the textural relationships between different silicate grains (Fig. **F10**):

- Phaneritic: phenocrysts are observable in hand sample and with the naked eye.
- Aphanitic: phenocrysts are not observable in hand sample but are observable under the microscope.
- Porphyritic: discrete isolated crystals (phenocrysts) are present in a groundmass of finer grain size.
- Aphyric: no phenocrysts were observable in hand sample or under the microscope.
- Intergranular: coarser grains (typically plagioclase) form a touching framework of the rock with interstices filled by crystalline material.
- Intersertal: coarser touching grains form a framework of the rock with interstices filled by glass.
- Subophitic: partial inclusion of plagioclase in clinopyroxene.
- Ophitic: total inclusion of plagioclase in clinopyroxene.
- Comb structure: comb-like arrangement of crystals growing inward from a contact.
- Dendritic: branching arrangement of elongate crystals.

Similar to the silicate minerals, the textures of oxide and sulfide minerals were described in terms of grain size and their relationship to adjacent minerals.

Thin section descriptions

Each thin section was photographed in both plane light and under crossed polars (see thin section images in WEBIMAGE in **"Supplementary material"**). Thin section descriptions closely follow the procedure for macroscopic core description. Where a thin section contained areas with different primary (i.e., not alteration related) lithology, mineralogy, and/or texture, these were defined as domains (e.g., Domain 1, Domain 2, etc.). For thin sections with multiple ig-

neous domains, a map of the domains is shown in the full thin section photomicrograph (Fig. F11), with different domains described separately and their relative abundance noted. For each hole, a table is provided listing the corresponding thin sections, the number and nature of the individual domains, the characteristics of the contact between the domains, and a link to the corresponding image of the thin section with the domain boundaries marked.

The following data were recorded and entered into the LIMS database through separate tabs within the thin section workbook in DESClogik.

Lithology and texture

The following definitions were used for plutonic, volcanic, and ultramafic rock:

- Rock name (based on thin section observations), using the same definitions as those for macroscopic descriptions;
- A comment for the whole rock (for all domains);
- Number of igneous domains within the thin section;
- Nature of igneous domains, if any (e.g., contact between two units, mix of two lithologies in one section, or presence of texturally different regions within one thin section);
- Igneous domain relative abundance (in percent);
- Igneous domain number within the thin section (igneous Domain 1, igneous Domain 2, igneous Domain 3, etc.); this parameter identifies each domain described in the Mineralogy tab;
- Igneous domain lithology name; if only one domain is present, this is identical to the rock name;
- Igneous domain grain size modal name (aphanitic, cryptocrystalline, microcrystalline, fine grained, medium grained, coarse grained, and pegmatitic); and
- Igneous domain comment.

Textural definitions were used for the three different rock types (plutonic, volcanic, and ultramafic) individually, as outlined in the following sections.

Plutonic rock

For the domain grain size distribution in plutonic rock, we used the terms equigranular and seriate. For the description of the texture of each domain, the terms granular, subophitic, ophitic, granophyric, and poikilitic were used.

Volcanic rock

For the textures in volcanic rock, we followed the definitions from Expedition 309/312 (Expedition 309/312 Scientists, 2006).

Volcanic rock is described as holohyaline (100% glass) to holocrystalline (100% crystals). The terms "phyric" and "glomeroporphyritic" indicate the presence of phenocrysts and clusters of phenocrysts, respectively. For a continuous range in grain size, the texture is seriate. In cases where there is no significant grain size difference between groundmass crystals and somewhat larger and more euhedral crystals, which do not adhere to the definition of phenocrysts, the term "microphenocryst" is used. In holohyaline to hypohyaline rock, glass was divided into four distinct types:

1. Fresh glass (amber in transmitted polarized light and isotropic under crossed polars, commonly found in the outermost parts of preserved chilled margins,
2. Dark (because of abundant crystallites) interstitial volcanic glass of basaltic composition termed "tachylytic,"
3. Glass that contains abundant fibrous spherulites, and
4. Glass that has been altered to clay minerals.

As grain size distribution, the terms equigranular or seriate were used. For groundmass, the following terms were used to describe textures:

- Intergranular (olivine and pyroxene grains between plagioclase laths),
- Intersertal (glass between plagioclase laths),
- Variolitic (fan-like arrangement of divergent microlites),
- Subophitic (partial inclusion of plagioclase in clinopyroxene), and
- Ophitic (total inclusion of plagioclase in clinopyroxene).

Flow textures were described as

- Trachytic (subparallel arrangement of plagioclase laths in the groundmass),
- Pilotaxitic (aligned plagioclase microlites embedded in a matrix of granular and usually smaller clinopyroxene grains), and
- Hyalopilitic (aligned plagioclase microlites with glassy matrix).

Mineralogy

Igneous domain mineralogy was described using abundance (in percent) of primary minerals preserved; estimated abundance (in percent) of primary minerals prior to alteration; computed value of mineral replacement by alteration; minimum, maxi-

mum, and median size; shape; habit; and special features of primary minerals, using the same conventions as during macroscopic description; individual comments for primary minerals; and absorption colors/pleochroism for clinopyroxene, orthopyroxene, and amphibole.

For plagioclase, a qualifier for zoning was recorded using the following convention:

0 = none.
1 = zoning is rare and weakly developed.
2 = abundant zoning that can range from weak to strong.
3 = nearly ubiquitous, generally strong zoning.

The type of zoning in plagioclase was also documented as

- Continuous: zoning is optically continuous from core to rim;
- Discontinuous: zoning occurs from core to rim, but with distinct break(s);
- Patchy: zoning occurs in patches randomly throughout the grain; and
- Oscillatory.

Alteration and metamorphism

The characteristics of hydrothermal alteration of rock recovered during Expedition 345 were described macroscopically and microscopically. X-ray diffraction (XRD) analyses were used to confirm mineral identification of vein-filling materials and rock coatings. Shipboard observations of altered and metamorphosed rock were recorded using the DESClogik worksheet interface and uploaded to the LIMS database. Alteration and metamorphic features of igneous rock were described in terms of pervasive background alteration, localized alteration patches (zones of more intense alteration), hydrothermal veins and alteration halos, and cataclastic zones. Alteration was generally described on a depth-interval basis. Wherever possible, the depth of any feature was defined by the intersection with the center line of the split face of the archive half. For features that did not intersect the center line, the highest and lowest observed points were recorded. Sections of Leg 147 plutonic cores were redescribed using the techniques and methods outlined below to ensure consistency in descriptions between Expedition 345 and previous ODP legs.

As was done during Legs 176, 206, and 209 and Expeditions 304/305 and 309/312 (Shipboard Scientific Party, 1999a, 2003, 2004; Expedition 304/305 Scientists, 2006; Expedition 309/312 Scientists, 2006), core descriptions were made by the entire metamorphic petrology team working together. Each member

was responsible for one or more aspects of the description (macroscopic description of background alteration and texture, veins and halos, and thin section identification of microscale features) and data entry on the entire core. This approach ensured consistency of recorded observations for all cores. Usually the entire team worked together, particularly when defining metamorphic intervals.

Core characterization was based on individual pieces from a recovered section of core when continuity of core pieces could not be confirmed. In cases where core was continuous, core characterization was tied to igneous units based on magmatic features unless distinct alteration intervals were observed. Macroscopic descriptions were compiled in the DESClogik workbook tabs. A summary comment of the overall nature of the alteration including background and vein halo alteration, as well as the structural characteristics of vein morphology, is captured in the Alteration comment field of the Unit summary tab in DESClogik. This information was then used for the production of VCDs, which summarize the description of each section of core as well as provide a downhole plot of overall alteration intensity expressed as a rank, as described below.

Macroscopic core description

All metamorphic descriptions created during Expedition 345 were made on the archive halves of the cores. Alteration and vein core description logs on a piece-by-piece or interval scale were tabulated to provide consistent characterization of the rock and to quantify the different alteration types. Metamorphic domains are defined as regions with significantly different alteration characteristics. Examples of types of domains include background alteration, vein halos, and cataclastic zones but can also be the same as lithologic intervals, as alteration style and intensity commonly vary with primary igneous mode. Alteration intervals are defined on the basis of major changes in alteration mineralogy and degree of recrystallization or replacement.

Plutonic rock

Alteration of plutonic rock was described systematically in the Plutonic alteration tab in DESClogik. First, we estimated the proportion of different features defined below:

- Background: the dominant alteration style and intensity throughout the rock.
- Pseudomorphic patch: patch of alteration distinct in alteration style from the background alteration in which the original mineralogy can be discerned.

- Recrystallized patch: patch of alteration distinct in alteration style from the background alteration in which the original mineralogy cannot be discerned (e.g., felted actinolite).
- Halo: zone of enhanced alteration adjacent to a vein, vein network, or fracture.

Each of these features (if present) is described separately line by line (e.g., halo is on one line, background is on another) within DESClogik. For each alteration textural type, the volume percentage of each primary mineral replaced and the volume percentage of each secondary mineral replacing each primary mineral were documented.

Rather than assign a percentage to these proportions, an overall rank was assigned based on a range of volume percentages in order to encompass the uncertainty associated with macroscopic mineral identification. The rank scale used for documenting the proportion of each primary mineral (by percentage of volume alteration products) replaced and plotted on the VCD is as follows:

0 = <10%.
1 = 10%–29%.
2 = 30%–59%.
3 = 60%–90%.
4 = >90%.

The overall volume percentage of alteration in the entire alteration interval was estimated, integrated over all features, and reported as alteration intensity using the rank scale outlined above for estimating the volume percentage of each secondary mineral replacing each primary mineral. Alteration intensities are independent of changes in lithologic intervals defined by igneous features. Sulfides and oxides were noted as alteration products where the relationships between a primary phase and sulfide or oxide were obvious. If the relationship was not clear or the oxide or sulfide phase occurred within veins, the abundances were noted in separate columns.

Recrystallized patches are described in terms of their shape and area and the modal abundance of the replacing minerals when we cannot identify the original mineralogy. We conclude with a general comment about the alteration in the metamorphic domain.

Where observed, the following distinctive alteration textures and relationships were also noted in the DESClogik template as

- Corona textures: unless otherwise noted, the term corona texture in the descriptions refers to the reaction between olivine and plagioclase in which tremolite ± talc replaces olivine and chlorite replaces plagioclase;

- Serpentine mesh texture: a texture resembling a network, caused by the alteration of olivine to an interlacing network of microveinlets of fibrous serpentine (0.5–1 mm in width) enclosing cores of more weakly birefringent cryptocrystalline serpentine in which relict polygonal grains of olivine may survive; and
- Breccia/cataclastic textures: fault rocks that consist of angular clasts within a finer grained matrix. Description of the alteration of comminuted rock fragments and clasts within the cataclastite are described separately within DESClogik.

An alteration summary description was entered in DESClogik so that it could be added to the VCDs. The alteration intensity plotted on the VCD corresponds to the background alteration intensity. The VCDs also contain a summary statement of the alteration characteristics for each lithologic interval in a core.

Volcanic and hypabyssal rock

Alteration in volcanic and hypabyssal rock was described systematically in the Volcanic alteration tab in DESClogik following methodology similar to that described above for plutonic and ultramafic rock. For volcanic and hypabyssal rock, we distinguish between groundmass alteration and phenocryst replacement, as well as alteration of glass. If vesicles were present, we made an estimate of the abundance and nature of vesicle filling alteration. Alteration intensity plotted in the VCDs is based on the intensity of phenocrysts.

Veins and alteration halos

Veins were defined as linear cracks partially or completely filled by secondary minerals. Fractures were defined as linear cracks with no mineral fill. The term halo was used to describe alteration spatially related to cracks. Note that both veins and fractures may have halos. Veins and halos were described with the same methods for all rock types.

Data on abundance, width (in millimeters), orientation, texture, connectivity, color, and vein-filling minerals were recorded for each piece containing one or more veins. These observations in cores were recorded in the Veins and halos tab of DESClogik. In pieces with more than one vein, veins were numbered sequentially from the top of the piece; vein numbers are correlated with structural observations of veins (see "Alteration veins"). Data recorded related to vein-related alteration halos included halo type (based on mineralogy), halo width, and abundance of halos as a percentage of the piece containing them. Linear vein density is described in "Struc-

tural geology" of the hole chapters; see also "Structural geology").

Veins were measured on the archive half unless otherwise noted. The classification used for vein geometry, texture, and connectivity is shown in Figure F12. The orientations of veins in oriented core pieces were systematically measured by the structural geology team (see "Structural geology") in close liaison with the metamorphic petrology team to ensure consistency of vein classification. Alteration halos representing zones of increased alteration adjacent to veins were described by width and color in the halo Comments column of the Vein and halo log, and the halo alteration mineralogy was described as a domain in the Background alteration log. Vein networks and breccia/cataclastite were recorded on the Vein and halo log in the Alteration feature column, noting the depth interval, total volume percent of secondary minerals, and percentages of individual secondary phases. A numerical estimate was also made of the percentage of the metamorphic interval that was vein material. Vein types were categorized according to mineralogy, allowing vein types to be illustrated downhole. Plots of vein type with depth are included in "Structural geology" in the hole chapters. Vein-related symbols used in the VCDs are shown in Figure F7.

Thin section description

Thin sections of rock recovered during Expedition 345 were examined to confirm macroscopic identifications of secondary minerals and establish the occurrence, abundance, and distribution of secondary minerals with depth in the core. Each thin section was photographed in both plane-polarized light and under crossed polars (see thin section images in WEBIMAGE in "Supplementary material"). Descriptions of alteration in thin sections for all rock types sampled are described in the Thin section alteration tab within DESClogik. Where a thin section contained areas with different alteration-related lithology, mineralogy, and/or texture, these features were defined as domains (e.g., Domain 1, Domain 2, etc.). For thin sections with multiple alteration domains, a map of the domains is shown on the full thin section photomicrograph (Fig. F13). The different domains were described separately, and the relative abundance of the domains was noted. Thin section descriptions closely follow the procedure for macroscopic core description, except that mineral abundances and alteration are expressed as percentages rather than as ranks. For each thin section, we first determined the relative abundance and number of different alteration domains we could distinguish and described each domain line by line in the Thin

section alteration tab within DESClogik. Observations about the alteration domain, including mineralogy, textural features, veins, and deformation were recorded for both plutonic and volcanic rocks within the Thin section alteration tab within DESClogik. We summed the alteration phases replacing each primary mineral to establish the total alteration of that domain. A weighted average of each domain yielded the total alteration of the rock in thin section. Chronological relationships between different secondary minerals or parageneses were recorded as comments when observed. Comments on any mineral-specific alteration observations (i.e., coronas, mesh texture, and halos) and general comments on the thin sections were included in the thin section reports (see "Core descriptions").

Alteration intensity for thin section descriptions of each primary mineral is defined as

Fresh = <2%.
Slight = 2%–9%.
Moderate = 10%–49%.
High = 50%–95%.
Complete = >90%.

Sediment description

Drill cuttings were inspected in hand samples by the same techniques as used for macroscopic core. In addition, grain mounts were made of each of the drill cuttings intervals, and each slide was point-counted using a mechanical stage.

X-ray diffraction

Phase identification of vein material and, as time permitted, powders for whole rocks and patches were aided by XRD analyses using a Brucker D-4 Endeavor diffractometer with a Vantec-1 detector using nickel-filtered CuKα radiation. XRD was performed on small amounts of powder (usually ~20 mg) that were freeze-dried, crushed, and mounted as smear slides or pressed onto depressions in sample holders. Mineral identification was achieved with the interactive Diffrac.Suite EVA version 1.4 software package (2010) using the powder diffraction file database associated with the program. Identifications were based on multiple peak matches. Instrument conditions were as follows:

Voltage = 40 kV.
Current = 40 mA.
Goniometer scan (bulk samples) 2θ = 2°–70°.
Step size = 0.0087°.
Scan speed = 0.2 s/step.
Divergence slit = 0.3°; 0.6 mm.

Structural geology

Conventions for structural studies established during previous "hard rock" drilling legs (e.g., ODP Legs 118, 131, 140, 147, 153, 176, 179, 206, and 209 and Expeditions 304/305, 309/312, and 335) were generally followed during Expedition 345 (Shipboard Scientific Party, 1989, 1991, 1992, 1993, 1995, 1999a, 1999b, 2003, 2004; Expedition 304/305 Scientists, 2006; Expedition 309/312 Scientists, 2006; Expedition 335 Scientists, 2009). Definitions of structural measurements and descriptive parameters were further refined from Expedition 335 to configure the DESClogik core description software application for hard rock descriptions. DESClogik is used to enter and upload the information into the LIMS database (see **"Introduction"**). Details specific to structural features are illustrated with comments and sketches in STRUCTUR in **"Supplementary Material."** Sections of Leg 147 plutonic cores were redescribed using the techniques and methods outlined below to ensure consistency in descriptions between holes in plutonic crust at Hess Deep.

Structural measurements

Structural features, categorized as magmatic, crystal-plastic, brittle, and veins were logged by interval in centimeters from the top of each section. Descriptions of all features were recorded using curated depths so that structural intervals are correlated with lithologic core descriptions. Depth intervals of structures were recorded as the distance from the top of the section to the top and bottom of the feature, where the feature intersected the center of the core piece. We measured structures on the archive half relative to the standard IODP core reference frame (Fig. **F2**). The plane normal to the axis of the borehole is referred to as the horizontal plane. On this plane, a 360° net is used with pseudosouth (180°) pointing into the archive half and pseudonorth (000°) pointing out of the archive half (Fig. **F14A**). The cut surface of the core, therefore, is a vertical plane (strike 090°–270°).

Apparent dip angles of planar features were measured on the cut face of the archive half. To obtain a true dip value, a second apparent dip was measured, where possible, in a section perpendicular to the core face (second apparent orientation shown in Fig. **F14B**). The two apparent dips and dip directions (or one apparent direction combined with the strike) measured for each planar feature were used to calculate the dip and dip direction in the core reference frame. If the feature intersected the upper or lower surface of the core piece, measurements of the strike were made in the core reference frame, recorded as

the trend (strike) of a line with zero dip angle, and combined with an apparent dip measurement, measured on the cut surface of the core, to calculate the true dip value (Fig. **F14C**). If a feature was exposed on the surface of the core (i.e., a fracture defining the top or bottom of a piece) the true dip and dip azimuth were measured directly on the feature with no need for another measurement or a calculation. True dip and dip direction (azimuth) were calculated using a macro in Microsoft Excel written by Michael Cheadle for Leg 209, or by inputting data into the Stereonet 8 program developed by R. Allmendinger (**www.geo.cornell.edu/geology/faculty/RWA/programs/stereonet-7-for-windows.html**), and imported into DESClogik.

Macroscopic core description and terminology

All descriptions and structural measurements during Expedition 345 were made on the archive halves of the cores unless otherwise noted. Whole cores were oriented by a member of the structural geology group for cutting prior to curation. Cores were marked to maximize dip of planar structures so that the dominant structure dips toward 90° in the CRF (Fig. **F2**). Where no obvious structures were present, cores were marked to maximize contiguity with adjacent core pieces.

During Expedition 345, the structural geologists worked together for the shift to minimize measurement inconsistencies, with each member of the team responsible for making a specific set of observations throughout the entire core (e.g., characterization of crystal-plastic fabric [CPF] intensity). For each section, detailed structural information was described and sketched on handwritten forms and subsequently entered into Excel spreadsheets. This information was then input into the DESClogik framework, which contains four worksheets for the following categories:

1. Magmatic structures: magmatic foliation, compositional or grain size layering, igneous contacts, magmatic veins, and melt percolation features;
2. CPFs: peridotite and gabbro foliation and/or lineation and the preferred orientation of serpentine networks;
3. Brittle structures: breccias, faults, joints, open fractures, drilling induced fractures, and cataclastic fabrics; and
4. Alteration veins.

The DESClogik worksheets contain data on the interval, type of structure, intensity, orientation, any crosscutting relationships, and comments. The work-

sheets record up to six separate types of quantitative measurements using the deformation intensity scales summarized in Figure **F15.** Sketches of structural relations were made to illustrate the most representative structures and crosscutting relationships in a core section. All sketches were scanned and archived in STRUCTUR in **"Supplementary material."**

The most representative and/or prominent structural features in the cores recovered during Expedition 345 are plotted on the VCDs. These include intensity of magmatic and CPF alignment; density of brittle fractures; and precise locations of observed prominent structures, such as igneous contacts, magmatic banding and magmatic veins, alteration veins, vein networks, hydrothermal breccia, cataclastic zones, breccia, shear veins, faults, fractures, and folds, where recognizable.

Short explanations for terms and abbreviations used in the respective categories are based on definitions given in Ramsay and Huber (1987), Twiss and Moores (1992), Passchier and Trouw (1996), and Davis et al. (2011) and are given below.

Magmatic structures

Intrusive contacts, magmatic dikes, and magmatic veins (including plagioclase and pyroxene segregation veins) were measured and described in accordance with the igneous petrology workbook (see **"Igneous petrology"**). Descriptions include

- Contact nature: sharp, gradational, and sutured (contacts where individual mineral grains interlock across the contact);
- Contact geometry: planar, curved, or irregular;
- History and crosscutting relationships of veins and dikes; and
- Orientation (dip azimuth and dip angle of contact dike or vein).

Igneous layering/banding, where present, was measured and described in accordance with the igneous petrology workbook (see **"Igneous petrology"**). Descriptions include

- Nature of layering: modal or grain size layering or both; when neither term describes the observations well, the term "layering (other)" is used, and the nature of layering is described in the comments;
- Layering geometry: sharp or gradational and weak, strong, irregular, planar, curved, or anastomosing;
- The thickness of the layers; and
- Orientation (dip azimuth and dip angle of layering as well as trend and plunge of any lineation in the layering, where measurable.

Magmatic fabrics were defined by the presence and intensity of any shape-preferred orientation (SPO) of magmatic phases. Descriptions of magmatic fabric include

- Geometry of magmatic fabric: linear, planar, planar-linear, or anastomosing/irregular;
- Magmatic fabric intensity accompanied by intensity rank (Fig. **F15**): 0 = isotropic, 1 = weak, 2 = moderate, and 3 = strong;
- Sense of shear: normal (n), reverse (r), dextral (d), sinistral (s), or a combination of these (nd, ns, rd, or rs); and
- Orientation (dip azimuth and dip angle of planar fabric as well as trend and plunge of lineation, where measurable) of magmatic fabric.

Crystal-plastic fabrics

CPFs include planar or linear fabrics defined by grains exhibiting plastic strain. Descriptions for CPF include

- Geometry of CPF: linear (L), planar (S), or planar-linear (L-S);
- Six levels of deformation intensity, ranging from a lack of any CPF (0), through three stages of foliation and porphyroclast development (1–3), to mylonitic and ultramylonitic fabrics (4–5) (Fig. **F15**). Occasionally, it proved difficult to differentiate between crystal-plastic and cataclastic deformation in relatively high strain shear zones based on hand-specimen observations only. In this case, we introduced a new classification: brittle-plastic foliations (Bp);
- CPF boundary geometry (i.e., shear zone boundary): planar or irregular;
- CPF boundary sharpness: sharp or diffuse;
- Sense of shear: normal (n), reverse (r), dextral (d), sinistral (s), or a combination of these (nd, ns, rd, or rs); and
- Orientation (dip azimuth and dip angle of planar fabric as well as trend and plunge of lineation, where measurable) of CPF.

Preferred orientation of serpentine networks

Serpentinization confers a mesh texture in peridotite and/or olivine-rich intrusive rock that defines a macroscopic expression of serpentine growth at the expense of olivine (O'Hanley, 1996). The microscopic serpentine fibers may be randomly oriented and homogeneously distributed in the rock, forming an anastomosing isotropic network, or preferentially oriented and/or unevenly distributed in the rock leading to an anisotropic texture (foliation). Formation of a preferred orientation of serpentine meshes may include protolith anisotropy (either inheritance of a former shape preferred orientation or of an un-

even distribution of the olivine and pyroxene grains/microlayering), serpentine growth in an anisotropic stress field, or transposition of the serpentine during and/or after growth. Descriptions of the preferred orientation of serpentine networks (Fig. F15) include a semiquantitative indication of the degree of preferred orientation from 0 (isotropic) to 3 (strong preferred orientation) and orientation (dip azimuth and dip angle of the planar fabric, where measurable.

Brittle deformation

Brittle fabrics described during Expedition 345 include breccias, faults (defined as fractures with shear displacement), and fractures (including open, drilling induced, and shear). Descriptions of brittle deformation include

- Fault rock type: fault gouge, fault breccia, cataclastite, hydrothermal breccia, magmatic breccia, or pseudotachylite. Fault rock type may be accompanied by identifiers describing any fabric alignment such as foliated and/or lineated;
- Fault rocks, whether cohesive or incohesive;
- Clast/matrix ratio (percent);
- Average size of clast in fault rock (in millimeters);
- Sense of shear: normal (n), reverse (r), dextral (d), sinistral (s), or a combination of these (nd, ns, rd, or rs);
- Fault offset (in millimeters) where measurable;
- Trend and plunge of slickensides/slickenlines/slickenfibers;
- Six levels of deformation intensity for fabrics, based on the percentage of matrix present in each zone of cataclasis (Fig. F15). Thin section descriptions, wherever available, aided this categorization;
- Density of fractures with density scale:
  0 = no open fracture.
  1 = <1 fracture per 10 cm.
  2 = 1–5 fractures per 10 cm.
  3 = >5 per 10 cm.
- Fracture morphology: planar, curved, concave, irregular, stepped, splayed, or anastomosing (Fig. F16);
- Fracture morphology/network: stepped, splayed, or anastomosing (Fig. F16);
- Fracture thickness (in millimeters); and
- Orientation (dip azimuth and dip angle) of fracture and trend and plunge of associated lineation.

Alteration veins

Alteration veins described during Expedition 345 include characterization of the vein margin, structure of the vein fill (undeformed, sheared, or crack-seal),

chronology of vein intrusion, relations with other veins, and crosscutting relations between veins and other structures. The nature of the vein fill material was identified in cooperation with the metamorphic petrology group. For each mineralogical type, individual veins were numbered within each piece sequentially, starting with the first vein encountered (V1) and entered into the spreadsheet successively (V2, V3, etc.). Descriptions include

- Density of fractures (with a density scale across a 10 cm depth interval along the long axis of the core) (Fig. F15):
  0 = no open fracture.
  1 = <1 fracture per 10 cm.
  2 = 1–5 fractures per 10 cm.
  3 = 5–10 fractures per 10 cm.
  4 = 10–20 fractures per 10 cm.
  5 = >20 fractures per 10 cm;
- Vein morphology: planar, curved, concave, irregular, or vein tip (Fig. F17);
- Vein morphology/network: parallel, echelon, overlapping, crosscutting or anastomosing (Fig. F17);
- Mean vein length (in millimeters);
- Mean vein thickness (in millimeters);
- Vein offset (in millimeters), where measurable;
- Sense of offset: normal (n), reverse (r), dextral (d), or sinistral (s); and
- Orientation (dip azimuth and dip angle) of fracture and trend and plunge of associated lineation.

Microstructures

Because of the setting of the sites drilled during Expedition 345 (plate spreading), superposition of microstructures or deformation mechanisms is commonly attributable to different stages of extension and cooling. Thus, the physical state of the material during fabric development may span the transition from hypersolidus to subsolidus. Igneous fabrics defined entirely by minerals with no crystal-plastic deformation microstructures are termed magmatic. To better characterize different types of deformation, we studied the microstructural features of interesting and/or prominent mesoscopic structures. Thin sections of recovered material were examined in order to

- Confirm macroscopic descriptions of structures,
- Characterize the microstructure of the rock,
- Document crystal-plastic and brittle overprints of magmatic fabrics,
- Provide information on the kinematics of brittle and brittle-ductile deformation,

- Identify temporal relationships between magmatic and crystal plastic deformation and alteration processes, and
- Document major structural zones and downhole variations.

For descriptions of microstructures, the terminology of Passchier and Trouw (1996) was used. Shipboard thin sections were oriented, and the orientation is given relative to the CRF and was marked on each thin section. Marking two directions was necessary in rare cases to achieve unambiguous orientation of thin sections cut parallel to the cut surface of the core. Orientation of structures measured during the macroscopic core description was confirmed, and macroscopic observations were refined by the microscopic description. Digital photomicrographs and sketches were taken and annotated to document features described in thin sections, which are all scanned and included in STRUCTUR in "Supplementary material." Microstructural notes were entered into the Structures tab in the thin section workbook of DESClogik.

We followed the terminology used during Legs 153, 176, and 209 and Expedition 304/305 (Shipboard Scientific Party, 1995, 1999a, 2004; Expedition 304/305 Scientists, 2006). In the Structure tab of the thin section description workbook, we described the following microscopic features for each thin section:

- Type of microstructure: magmatic, submagmatic/transitional, crystal-plastic, cataclastic, or metamorphic.
- Morphology of grain boundary: straight, curved, serrate, polygonal, complex, or varied.
- Intensity of magmatic fabric: isotropic, weak, moderate, or strong.
- Intensity of static recrystallization: absent, weak, strong, partial, or complete.
- Presence of submagmatic fracture: absent, rare, or common.
- Intensity of crystal-plastic undulose extinction: absent, weak, moderate, strong, complete, patchy, or subgrains.
- Morphology of crystal-plastic subgrain boundaries: straight, curved, serrate, or polygonal.
- Presence of crystal-plastic deformation twinning: absent, rare, or common.
- Intensity of crystal-plastic dynamic recrystallization: absent, weak, strong, or complete.
- Intensity of overall CPF with intensity rank:
  0 = absent.
  1 = weakly foliated/lineated.
  2 = strongly foliated/lineated.
  3 = porphyroclastic/protomylonitic.
  4 = mylonitic.
  5 = ultramylonitic.

- Sense of shear estimated from CPF: normal (n), reverse (r), dextral (d), or sinistral (s).
- Clast/matrix ratio (percent) of cataclasite/brittle fracture.
- Size (in millimeters) of clasts in cataclasite/brittle fracture.
- Intensity of cataclastic fabric and intensity rank:
  0 = undeformed.
  1 = minor fracturing with no significant grain size reduction.
  2 = moderate fracturing without grain size reduction.
  3 = dense anastomosing fracturing with incipient grain size reduction.
  4 = well-developed grain size reduction with evidence for clast rotation (independent particulate flow).
  5 = cataclastic.

Inorganic geochemistry

During Expedition 345, chemical analyses of rock samples were performed using inductively coupled plasma–atomic emission spectroscopy (ICP-AES) for major and trace element analyses and gas chromatography for sulfur, CO_2, and H_2O. These samples were selected as representative of the rock recovered from Site U1415 by the Shipboard Scientific Party. A thin section was located next to each of the geochemistry samples to precisely determine their modal composition and degree of alteration because of the highly heterogeneous lithologies sampled at Site U1415 (see "Igneous petrology" and "Metamorphic petrology" in each hole chapter for the characterization of the lithologic units). The rock names in the resulting table (see Table T1 in the "Geochemistry summary" chapter [Gillis et al., 2014a]) were determined on the basis of the thin section descriptions (see "Igneous petrology"). A characteristic of Site U1415 gabbroic rock is the abundance of trace orthopyroxene observed in some holes. For simplicity, only samples with >2% orthopyroxene were described as orthopyroxene bearing in figures and in Table T1 in the "Geochemistry summary" chapter (Gillis et al., 2014a).

Sample preparation for geochemistry

Samples were prepared from 15 to 30 cm³ of rock for troctolites, gabbroic rocks, and basalts and 30 cm³ scooped material for drilling-induced disaggregated gabbro samples. The solid rock samples were cut from cores using a diamond saw blade. Whenever possible, a thin section billet was taken from the same rock fragment. Grain mounts were produced

from the batches of drilling-induced disaggregated gabbro samples selected for geochemical analyses. Outer surfaces of rock samples were ground on a diamond-impregnated disk to remove saw marks and altered rinds resulting from drilling. Each cleaned sample was placed in a beaker containing isopropanol and ultrasonicated for 15 min. The isopropanol was decanted, and the samples were then ultrasonicated twice in nanopure deionized water (18 MΩ·cm) for 10 min. The cleaned pieces were then dried for 10–12 h at 110°C. During Expedition 345, this time was shortened to 6 h for the preparation of the igneous rock sampled in Hole U1415P.

The clean, dry whole-rock samples were crushed to <1 cm chips between two disks of Delrin plastic in a hydraulic press. The rock chips were then ground to a fine powder in a tungsten carbide mill in a SPEX 8510 shatterbox. A check on grinding contamination contributed by the tungsten carbide mills was performed during Leg 206 (Shipboard Scientific Party, 2003), and contamination was found to be negligible for major elements and most trace elements measured on board (Sc, V, Cr, Ni, Sr, Y, Zr, Nb, and Ba). A systematic analysis of the shipboard powders from Expeditions 304/305 indicated a possible contamination in Co during grinding (Godard et al., 2009); this element, although analyzed (Table T1), was eliminated from Expedition 345 data.

After grinding, a 5.00 ± 0.05 g aliquot of the sample powder was weighed on a Mettler Toledo balance and ignited at 1025°C for 4 h to determine weight loss on ignition (LOI) with an estimated precision of 0.02 g (0.4%).

The standard shipboard procedure for digestion of rock and subsequent ICP-AES analysis is described in Murray et al. (2000). The following protocol is an abbreviated form of this procedure with minor changes and additions. After determination of LOI, 100.0 ± 0.1 mg aliquots of the ignited whole-rock powder were weighed and mixed with 400.0 ± 0.5 mg of lithium metaborate ($LiBO_2$) flux, which was preweighed on shore. Standard rock powder and full procedural blanks were included with unknowns in each ICP-AES run. All samples and standards were weighed on the Cahn C-29 microbalance (designed to measure on a moving platform), with weighing errors conservatively estimated to be ±0.02 mg.

A 10 μL aliquot of 0.172 mM aqueous LiBr solution was added to the flux and rock powder mixture as a nonwetting agent to prevent the cooled bead from sticking to the crucible. Samples were then individually fused in Pt-Au (95:5) crucibles for ~12 min at a maximum temperature of 1050°C in a Bead Sampler TK-4100 (internally rotating induction furnace). After cooling, beads were transferred to 125 mL high-density polypropylene bottles and dissolved in 50 mL 10% dilution of concentrated trace-metal grade HNO_3 (hereafter referred to as 10% HNO_3), aided by shaking with a Burrell wrist-action bottle shaker for 1 h. After digestion of the glass bead, the solution was passed through a 0.45 μm filter into a clean 60 mL wide-mouth, high-density polypropylene bottle. Next, 1.25 mL of this solution was pipetted into a plastic vial and diluted with 8.75 mL of 10% HNO_3 to bring the total volume to 10 mL. The final solution-to-sample dilution factor for this procedure was ~4000. Dilutions were conducted using a Brinkman Dispensette.

Inductively coupled plasma–atomic emission spectroscopy

Analyses

Major and trace element concentrations of standards and samples were determined using a Teledyne Leeman Labs Prodigy ICP-AES instrument. The analyzed elements and the wavelengths used for sample analysis during Expedition 345 are provided in Table T1. Certified international rock reference materials, calibration and drift solutions, and chemical procedure blanks were included with the unknown samples for each sample run. Detection limits were calculated as three times the standard deviation of the mean for blank solution measurements.

The ICP-AES plasma was ignited at least 30 min before each sample run to allow the instrument to warm up and stabilize. After the warm-up period, a zero-order search was performed to check the mechanical zero of the diffraction grating. After the zero-order search, the mechanical step positions of emission lines were tuned by automatically searching with a 0.002 nm window across each emission peak using two solutions containing 10 ppm concentrations of set elements prepared in 1% HNO_3. During the initial setup, an emission profile was selected for each peak, using the multielement solutions, to determine peak-to-background intensities and set the locations of background levels for each element. The Prodigy data acquisition software uses these background locations to calculate the net intensity for each emission line.

The ICP-AES data presented in the "Inorganic geochemistry" sections for each hole were acquired using the Prodigy software. The intensity curve for each element is defined by 20 measurements within the designated wavelength window. The user selects the two background points that define the baseline. The Prodigy software integrates the area delineated by the baseline and the intensity curve. Each sample was analyzed four times from the same dilute solu-

tion within a given sample run. For several elements, measurements were made at two wavelengths (e.g., Si at 250.690 and 251.611 nm; Table T1). For each run, the wavelength yielding the best calibration line was identified and used for determining concentrations.

A typical ICP-AES run included

- A set of four certified rock standards, analyzed twice per run and chosen for their wide range of compositions in order to calibrate the analyses (basalt BCR-2; granodiorite JG-1A; peridotite JP-1; gabbro MRG-1);
- As many as 15 unknown samples;
- A drift-correcting sample (BHVO-2) analyzed every fourth sample position and at the beginning and end of each run;
- Procedural blank solutions run near the beginning of each run; and
- Two to three "check" standards chosen for their composition similar to that of the analyzed material (dunite DTS-1, gabbro JGb-1, and an ultramafic reference material from Core 147-895D-10W) run as unknowns.

A 10% HNO_3 wash solution was run for 90 s between each sample analysis. Each sample analysis is the average of four measurements. The check standards were used to test analytical accuracy and reproducibility of the obtained data.

Data reduction for inductively coupled plasma–atomic emission spectroscopy

Following each sample run, raw intensities were transferred to a data file, and all analyses were corrected for drift. A drift correction was applied to each element by linear interpolation between drift-monitoring solutions run every fourth analysis. After drift correction and subtraction of procedural blank, a calibration line for each element was calculated using the results for the certified rock standards. Concentrations used for the calibrations were compiled values from the literature recalculated on a volatile-free basis; the compiled values were from Govindaraju (1994) and from the GeoReM website (georem.mpch-mainz.gwdg.de; December 2012; Jochum et al., 2005) (Table T2). Element concentrations in the samples were then calculated from the relevant calibration lines.

Estimates of accuracy and precision of major and trace element analyses were based on replicate analyses of check standards, compared to values published in Govindaraju (1994) and downloaded from the GeoReM database for international rock standard DTS-1 and JGb-1 and to values published in Puchelt et al. (1996) for shipboard laboratory Standard 147-

895D-10W. Results are presented in Table **T3.** During Expedition 345, run-to-run relative standard deviation by ICP-AES was generally ±1% for major elements except for MgO (±5%) and ±10% for trace elements. Accuracy was better than 2% for major elements and better than 5% for most trace elements, with the exception of low-concentration data for Cr, Zr, and Y.

Volatile measurements

Volatile concentrations were measured by gas chromatographic separation on a Thermo Electron Corporation CHNS analyzer (Flash EA 1112 Series). A new calibration strategy for the analysis of H_2O, CO_2, and S in mafic and ultramafic rocks by CHNS elemental analyzer was developed during Expedition 345. This calibration method involves measuring a series of international rock standards that approximate the composition of the unknown samples. All studied samples were powder splits of ICP-AES samples.

Analytical method

Powders were dried for 12 h at 110°C to ensure evaporation of possible adsorbed moisture and kept in a desiccator prior to measurements. Powder samples were typically 40 mg. Samples were weighed on a Cahn Microbalance Model 29, mixed with 10 mg vanadium pentoxide (V_2O_5), an oxidizer used to improve sulfur detection, and packed into CHNS tin containers (Universal Tin Container "light"; Thermo Electron P/N 240-06400). A revolving autosampler dropped sample capsules into a 950°C resistance furnace where they were combusted in a reactor. Tin from the capsule creates a violent flash combustion within an oxygen-enriched atmosphere. The oxidized and liberated volatiles were carried by a constant helium gas flow through a commercial glass column (Costech P/N 061110) packed with an oxidation catalyst of tungsten trioxide (WO_3) and a copper reducer. Sulfide and sulfate minerals liberate SO_2 and SO_3, respectively; however, both were measured as S. When nitrogen oxide is present, the copper reducer in the reactor tube reduces it to N_2. The liberated gases were transported by the helium carrier flow to and separated by a 2 m packed gas chromatography (GC) column (Costech P/N 0581080). During the measuring time of 1000 s, the millivoltage at the detector was continuously recorded. CO_2, H_2O, and S separated by the GC column arrived at the thermal conductivity detector at approximately 94.0 s (CO_2), 250.0 s (H_2O), and 781.0 s (S) for the international gabbro standard JGb-1. During Expedition 345, we were not able to measure nitrogen because of the

particularly low concentrations of this element in the analyzed mafic and ultramafic rock.

Calibration, blanks, and standards

The routine method for quantitative chromatographic geochemical analyses involves the preparation of a series of standard solutions (e.g., 80 mM L-(+)-cysteine hydrochloride). Because of the low volatile concentrations and different mineralogy in mafic to ultramafic plutonic rock, we chose an alternative method using a matrix-match calibration strategy based on international geostandards for CO_2 and H_2O. Because of the lack of silicate standards for the S calibration, S was calibrated using the geostandards and a series of increasing weights (0.1, 0.3, 0.6, and 1 mg) of sulfanilamide (18.62% S). Peak areas of the measured volatiles from the geostandard chromatographs were integrated and plotted weight-corrected as a function of their reference concentration published in Govindaraju (1994) and downloaded from the GeoReM database for the certified dunite DTS-1, syenite SY-2, gabbro JGb-1, and Cody Shale SCo-1 and to values from Puchelt et al. (1996) for the shipboard laboratory ultramafic peridotite Core 147-895D-10W. Procedural blanks were determined by using empty tin capsules (plus V_2O_5) and measured four times during each CHNS run of 8 samples (6 new samples plus 2 duplicates from the prior sample run). A measurement blank was performed after every sample to prevent cross-contamination within the chromatographic column. After weight correction, H_2O, CO_2, and S abundances were calculated by using the function resulting from the linear or polygonal functions of the calibration lines.

Peridotite JP-1 and gabbro MRG-1 were used as quality control by monitoring the analytical accuracy and reproducibility and as sensitivity drift check by replicate measurements. A typical CHNS run included a maximum of 8 unknown samples per run; this approach allowed for the frequent restandardization required for high accuracy. Results of the GC analyses for MRG-1 and JP-1 during Expedition 345 are presented in Table **T4.** Based on 10 runs, the reproducibility was better than 5%–14% for CO_2, better than 12%–13% for H_2O, and better than 13% for S for JP-1 and MRG-1. The average obtained concentrations for peridotite JP-1 and gabbro MRG-1 are in agreement with recommended values (Govindaraju, 1994) and downloaded from the GeoReM database.

In comparing the GC volatile analyses to the LOI results, it is also important to bear in mind that during ignition of the sample in an atmospheric oxygen fugacity, Fe^{2+} will change into Fe^{3+}, which accounts for a weight gain of as much as 11.1% of the proportion of ferrous Fe within the sample. Also, ignition at or above 1000°C may induce a loss of K and Na, as these elements have boiling-point temperatures below 1000°C (759°C for K and 883°C for Na) (Lide, 2000). This can lead to discrepancies between LOI analyses and volatile concentrations determined by GC analysis.

Paleomagnetism

During Expedition 345, routine shipboard paleomagnetism and magnetic anisotropy experiments were carried out. Remanent magnetization was measured on archive section halves and on discrete cube samples taken from the working halves. Continuous archive section halves were demagnetized in an alternating field (AF), whereas discrete samples were subjected to stepwise AF demagnetization, thermal demagnetization, or a combination of low-temperature demagnetization followed by either AF or thermal treatment. Because the azimuthal orientations of core samples recovered by rotary drilling are not constrained, all magnetic data are reported relative to the sample core coordinate system (Fig. **F2**). In this system, $+x$ points into the working section half (i.e., toward the double line), $+z$ is downcore, and $+y$ is orthogonal to x and z in a right-hand sense.

Archive section half remanent magnetization data

Measurement and filtering

The remanent magnetization of archive section halves was measured at 2 cm intervals using the automated pass-through direct-current superconducting quantum interference device (DC-SQUID) cryogenic rock magnetometer (2G Enterprises model 760R). An integrated in-line AF demagnetizer (2G model 600) capable of applying peak fields up to 80 mT was used to progressively demagnetize the core. Demagnetization was conducted in 5 mT steps up to 80 mT, but data from demagnetizations above 30 mT were usually found to be contaminated by instrument-induced anhysteretic magnetization.

With strongly magnetized materials, the maximum intensity that can be reliably measured (i.e., with no residual flux counts) is limited by the slew rate of the sensors. At a track velocity of 2 cm/s, it is possible to measure archive section halves with a magnetization as high as ~10 A/m (Expedition 304/305 Scientists, 2006; Expedition 330 Scientists, 2011). Although the baseline values measured just prior to and just after the archive section half measurements are not saved in the database, the baseline drift, and thus the number of residual flux counts, can be determined indi-

rectly from the archived directional data. We used LabView software developed by Jeff Gee (WebTabularToMag; Expedition 330 Scientists, 2011) to reconstruct the baseline drift, allowing the residual flux counts to be logged while converting the data for further processing.

The compiled version of the WebTabularToMag LabView software (SRM Section) used during Expedition 345 is SRM version 318. This incorporates two modifications to the program and the Galil motor system (Expedition 330 Scientists, 2011). First, the speed at which the archive section was moved when not measuring was increased to 20 cm/s. Second, simultaneous sampling of the magnetometer axes was incorporated into the magnetometer software. During Expedition 330, these changes together resulted in substantial time savings (on the order of 0.5 h per section with 6–8 demagnetization steps) and also allowed multiple measurements at each interval for weakly magnetized cores. Hence, these modifications were retained for Expedition 345.

The response functions of the pick-up coils of the SQUID sensors have a full width of 7–8 cm at half height (Parker and Gee, 2002). Therefore, data collected within ~4 cm of piece boundaries (or voids) are significantly affected by edge effects. Consequently, data points within 4.5 cm of piece boundaries (as documented in the curatorial record) were filtered out prior to further processing. To further reduce artifacts, any pieces smaller than 10 cm were removed from section trays prior to measuring/demagnetizing and replaced afterward.

Remanent magnetization directions were calculated for each 2 cm measurement using principal component analysis (PCA; Kirschvink, 1980). Note that the intensity reported for such PCA directions represents the length of the projection of the lowest and highest treatment vectors used in the PCA calculation onto the best-fit direction. Because the origin is not included in the PCA calculation and the remanence remaining after the highest treatment potentially may be significant, resulting characteristic remanent magnetization (ChRM) intensity values will be systematically lower than those derived from the remanence at the lowest demagnetization step adopted for the PCA calculation.

Discrete sample data

Measurement and instrumentation

All discrete samples taken from working-half cores for shipboard magnetic analysis were 8 cm³ cubes. Although standard 2.5 cm diameter minicores are more commonly used, cubic samples were preferred, as they should have a more precisely determined ver-

tical reference (based on a saw cut perpendicular to the core length) than the minicores, where the arrow on the split-core face must then be transferred to the long axis of the sample.

Remanent magnetization of discrete samples was measured exclusively with the JR-6A spinner magnetometer following tests of the reliability of discrete measurements on the 2G superconducting rock magnetometer conducted during Expedition 335 that showed significant scatter in remanence directions measured in different sample orientations (Expedition 335 Scientists, 2012). For samples measured on the spinner magnetometer, the automated sample holder was used, providing the most accurate discrete sample remanent magnetization directions and intensities. Measurements of the empty automatic sample holder after subtracting the stored holder magnetization yielded intensities of 4.0×10^{-6} A/m, representing the practical noise limit of the system.

Discrete samples were subjected to stepwise AF demagnetization using the DTech AF demagnetizer (model D-2000), which is capable of peak fields up to 200 mT. Fifteen AF demagnetization steps were used, with 5 mT steps up to 50 mT and 10 mT steps up to a maximum peak field of 100 mT. The residual magnetic field at the demagnetizing position in this equipment was ~25 nT.

Discrete samples were thermally demagnetized using an ASC Scientific thermal demagnetizer (model TD-48 SC) capable of demagnetizing samples up to 700°C. The total magnetic field along the length of the TD-48 SC access tube is illustrated in Figure **F18,** demonstrating that the sample chamber from 30 cm onward (measured from the edge of the access opening) has a maximum field of <50 nT. Each sample boat for thermal demagnetization included as many as 22 samples, and sample orientations were varied at alternative steps to allow any interaction between adjacent samples to be identified. Samples were held at the desired temperature for 40 min prior to cooling in the low-field chamber. Magnetic susceptibility was measured (using a Bartington MS2C magnetic susceptibility sensor) after every heating step to monitor thermal alteration of magnetic minerals during heating.

Discrete samples were subjected to low-temperature demagnetization (LTD) (Merrill, 1970; Dunlop, 2003; Yu et al., 2003) prior to subsequent AF or thermal demagnetization in order to remove substantial secondary drilling-related magnetizations. LTD involves cooling samples in a liquid nitrogen bath (T = 77K) and allowing them to warm back up to room temperature in a very low field environment. This cools the samples to below the Verwey transition of magnetite (Dunlop, 2003), resulting in a loss of magnetic

remance by multidomain grains upon subsequent warming to ambient temperature. This technique was employed in shore-based paleomagnetic analysis of discrete samples from gabbroic rock recovered from Atlantis Massif in IODP Hole U1309D (Morris et al., 2009) and successfully removed a large proportion of the drilling-related magnetization that is presumed to be carried by coarse, multidomain magnetite grains. During shipboard experiments, a suitable low-field environment was provided by nesting the two available cylindrical mu-metal shields to produce a six-layer shield with an internal field <10 nT (with shields aligned parallel to the ship orientation of 110°–120°). This was sufficiently low to allow LTD treatment to be performed successfully.

Anisotropy of low-field magnetic susceptibility

In addition to standard paleomagnetic measurements, the anisotropy of low-field magnetic susceptibility was determined for all discrete samples using the KLY 4S Kappabridge with the AMSSpin software (Gee et al., 2008). Each sample was measured three times to assess repeatability. The susceptibility tensor and associated eigenvectors and eigenvalues were calculated off-line following the method of Hext (1963). All bulk susceptibility values reported for discrete samples are based on a sample volume of 8 cm^3.

Inclination-only analysis

For azimuthally unoriented cores, the simple arithmetic mean of inclination data will be biased to shallower values (e.g., Kono, 1980; McFadden and Reid, 1982; Arason and Levi, 2010). To compensate for this bias, we have used the inclination-only statistics of Arason and Levi (2010) to calculate the overall mean inclination for the cored interval and appropriate subintervals.

Although the Arason and Levi technique is more robust than previous inclination-only methods (e.g., Kono, 1980; McFadden and Reid, 1982), this technique nonetheless fails to converge under certain circumstances. For example, if inclinations are steep and the scatter is substantial or if dual polarities (also with steep inclination) are present, no maximum likelihood estimate is possible. Hence, this method is unsuitable for analysis of steep drilling-induced magnetization.

Physical properties

Shipboard measurements of physical properties were undertaken to characterize recovered core material. These data are potentially used to link the geological observations made on the core to the results of downhole logging and regional geophysical survey results.

Prior to physical property measurements, whole-round cores were allowed to thermally equilibrate for ~1 h to ambient room temperature. A 4 h delay time was classically reported in previous hard rock expeditions, based on the protocol used for sediment cores. Because gabbroic rock has thermal conductivities typically 2 or 3 times higher than those of marine sediment, 1 h was considered to be sufficient.

Most core sections were run through the WRMSL to measure GRA density and magnetic susceptibility. The NGRL was used to measure gamma radiation for whole-round sections. We did not use the *P*-wave logger on the WRMSL, as these measurements require full-diameter core and good coupling to the liner; this is generally not the case for hard rock cores.

Following whole-round measurements and core splitting, the archive half of the core was passed through the SHMSL for measurement of magnetic susceptibility with a Bartington MS2E contact sensor probe and measurement of color reflectance with an Ocean Optics photospectrometer.

WRMSL and SHMSL data must be filtered to remove spurious values that correspond to gaps in the core section (empty intervals), cracks in core pieces, and, for bulk volumetric measurements (WRMSL), reduced volume of material (departure from a continuous, cylindrical core) in the vicinity of the sensor. Given the relatively small amount of material recovered during Expedition 345, it was not deemed necessary to develop a filtering algorithm for the various whole-round and half-core measurements. We chose to filter the data by manually editing the data files, following procedures described below for each instrument. Throughout the cruise, raw data were uploaded to the LIMS database. Filtered WRMSL and SHMSL data are available in PHYSPROP in **"Supplementary material."**

Thermal conductivity was measured on pieces from the archive half of the split-core sections, depending on the availability of suitable material. Discrete samples (2 cm × 2 cm × 2 cm cubes) were taken from working section halves for physical property measurements. Most samples were also used for paleomagnetic measurements, as the core material was limited. Shipboard samples were preferentially located close to where shipboard geochemistry and thin section samples were taken. Discrete samples were used for *P*-wave velocity measurements in three orthogonal directions following the standard IODP convention (Fig. **F2**), and moisture and density

(MAD) measurements (IODP shipboard Method C) were used to determine bulk density, grain density, and porosity.

A comprehensive discussion of methodologies and calculations used in the *JOIDES Resolution* Physical Properties Laboratory is presented in Blum (1997).

Whole-Round Multisensor Logger measurements

GRA bulk density and magnetic susceptibility were measured nondestructively with the WRMSL. The sampling interval for WRMSL measurements was first set at 2.5 cm for Hole U1415I and at 1 cm for Hole U1415J and the remainder of the expedition, with an integration time of 5 s for each data point to allow both instruments to acquire values from the same location downcore. Calibration was verified after each core measurement by passing a freshwater-filled calibration core through the WRSML. The nominal accuracy of the calibrated instruments is between 1% and 2%.

Gamma ray attenuation bulk density

The GRA densitometer on the WRMSL operates by passing gamma rays from a ^{137}Cs source through a whole-round core into a 75 mm × 75 mm sodium iodide detector located directly below the core. The input gamma ray peak has a principal energy of 0.662 MeV and is attenuated as it passes through the core. Attenuation of gamma rays, mainly by Compton scattering, is related to electron density, which is related to material bulk density by

$$\rho_b = \rho_e w/2\Sigma N,$$

where

ρ_b = bulk density,
ρ_e = electron density,
w = molecular weight, and
N = atomic number of elements in the material.

For the majority of elements and for rock-forming minerals, $2\Sigma N/w$ is ~1, whereas for hydrogen, $2\Sigma N/w$ is 1.9841. Therefore, for a known thickness of sample the gamma ray count is proportional to density. Calibration of the GRA densitometer was performed using a core liner filled with freshwater and aluminum density standards. A freshwater-filled liner was measured at the end of each core measurement; recalibration was performed if the measured density of the freshwater standard was not 1.00 ± 0.02 g/cm³. The spatial resolution of the GRA densitometer is <1 cm. Raw data were filtered by first removing all values lower than 1 g/cm³ (i.e., water density) and then

removing a series of values acquired close to piece edges that show density gradients too high to correspond to realistic density variations in the recovered rocks (i.e., >0.2 g/cm³/cm). Comparison of the data curves with core scan images confirmed that this procedure efficiently removed spurious data that correspond to empty intervals, small or irregularly shaped pieces, and cracks in large pieces.

Magnetic susceptibility

Magnetic susceptibility, κ, is a dimensionless measure of the degree to which a material can be magnetized by an external magnetic field:

$$\kappa = M/H \text{ (SI)},$$

where M is the magnetization induced in the material by an external field with strength H (very low field; ≤0.5 mT). Magnetic susceptibility varies in response to the type and concentration of magnetic grains, making it useful for the identification of compositional variations.

The WRMSL measures volume magnetic susceptibility using a Bartington Instruments MS2 meter coupled to a MS2C sensor coil with an 88 mm diameter and operates at a frequency of 0.513 kHz. During Expedition 345, the instrument was set to record SI units with an integration period of ~1 s, to give a sensitivity of 1×10^{-5} SI. The core diameter is smaller than the sensor coil aperture. The instrument output (κ_{MEAS}) depends on the diameter of the core (d) passing through the coil diameter (D), so a correction factor (κ_{REL}) is necessary to convert the instrument output to true volume susceptibility (κ in SI), where $\kappa_{REL} = 3.45(d/D)^3$ (Bartington Instruments, Ltd., 2011). κ_{REL} is 1 for d = 58 mm and D = 88 mm; d is typically 57 ± 1 mm for well-cut RCB hard rock cores, and the size of small pieces and rollers varies in an unpredictable manner. Hence, a single correction factor was not justified; therefore, no correction was applied to WRSML magnetic susceptibility measurements; raw data are reported in instrument units (10^{-5} SI).

The along-core response curve of the MS2C coil has a full width of half maximum of ~4 cm (Blum, 1997) and is consistent with the decay in magnetic intensity with distance from a dipole (Fig. F19). Therefore, measurements of susceptibility from core pieces <8 cm long will significantly underestimate magnetic susceptibility by more than 10%. Hence, filtering of the WRMSL magnetic susceptibility data consisted of removing data points that correspond to pieces shorter than 8 cm, as well as 4 cm long edges from pieces longer than 8 cm.

The Bartington sensor has a maximum output threshold of 9,999 instrument units (IU), so any reading ≥10,000 IU loses the most significant digit and is "wrapped" around to lower values. Figure F20 illustrates how data can be corrected for this record offset when measuring high-susceptibility rock. Measurements that were judged to be wrong, based on neighboring high susceptibility values and examination of the core, were corrected by adding $n \times 10,000$ to the raw value. The value of n is arbitrarily chosen to generate the smoothest possible corrected curve (e.g., Fig. F20B).

Natural Gamma Radiation Logger measurements

Gamma radiation is emitted from rock primarily as a result of the radioactive decay of ^{40}K and the decay of isotopes in the ^{238}U and ^{232}Th decay series. Measurement of NGR from the recovered core provides an indication of the concentration of these elements and can also be used to correlate the core with the downhole gamma ray logs (e.g., Révillon et al., 2002).

The NGRL installed on the *JOIDES Resolution* was designed and built by IODP-USIO at Texas A&M University (Vasilyev et al., 2011). The main NGR detector unit consists of 8 sodium iodide (NaI) scintillator detectors (~500 in³ each), 7 plastic scintillation detectors, 22 photomultipliers, and passive lead shielding. The eight NaI detectors are spaced every 20 cm in the detector; the detectors themselves are semicylindrical annuli around the lower half of the core (each crystal is ~13 cm wide along the core). Detectors are shielded by lead to reduce the measurement of external gamma radiation, and the NGRL also employs seven plastic scintillation detectors that detect and actively suppress the effect of high-energy gamma and muon components of cosmic radiation. The NGRL was calibrated using ^{137}Cs and ^{60}Co sources to identify peaks at 662 and 1330 keV, respectively.

Background measurements of an empty core liner counted for 44,000 s (>12 h) were made upon arrival at Site U1415. Over the 100–3000 keV integration range, background counts averaged ~5 cps and contributed at least ~80% of the uncorrected total counts for the low-radioactivity mafic rock measured during Expedition 345.

A single measurement run with the NGRL provides 16 measurements at 10 cm intervals over a 150 cm section of core. To achieve a 10 cm interval using the NGRL's eight sensors spaced every 20 cm, the NGRL records two sets of measurements offset by 10 cm. Total counts are routinely summed over the range of 100–3000 keV. The quality of the energy spectrum measured depends on the concentration of radionuclides in the sample and on the counting time, with longer counting times providing better counting statistics. A live counting time of 1800 s (30 min) was set in each position (total live count time of 1 h per section).

During Expedition 345, Detector 3 was reported to have severe drift behavior. A long-term measurement on the Cs/Co standards revealed a serious distortion of the expected energy bin of the signal peaks. This problem could not be fixed with the available tools on board the ship. Details are given in the technical staff report.

Section Half Multisensor Logger measurements

The SHMSL was used to measure spectral reflectance and magnetic susceptibility on archive section halves. An electronic platform moves along a track above the section half, recording the sample height using a laser sensor. The laser establishes the location of the bottom of the section and the presence of samples to measure by locating gaps and cracks between pieces. The platform then reverses the direction of movement, moving from bottom to top taking measurements of point magnetic susceptibility and spectral reflectance data at 2 cm (Holes U1415E–U1415I) or 1 cm (Hole U1415J and the remainder of the expedition) intervals.

Raw data were manually filtered using the half-core scan images for comparison to remove data points that correspond to cracks, empty intervals, or piece edges (1 cm).

Reflectance spectrophotometry and colorimetry

Reflectance from the archive section half was measured using an Ocean Optics, Inc., system for ultraviolet through visible to near-infrared light (171–1100 nm wavelength at 2 nm intervals). Each measurement takes ~5 s to acquire. Spectral data are routinely reduced to the L*a*b* color space for output and presentation, in which L* is luminescence, a* is the red–green value, and b* is the blue–yellow value. The color reflectance spectrometer calibrates on two spectra, pure white (reference) and pure black (dark). Color calibration was conducted every 24 h.

While conducting test measurements with a smaller measurement interval of 1 mm in order to look for variations of a* and b* with the olivine contents in the layered gabbronorites recovered from Section 345-U1415I-4R-1, we identified a problem with the instrument; it was recording different values of these

parameters over successive series of measurements on the same core pieces (see details in the "Hole U1415I" chapter [Gillis et al., 2014b]). A series of tests with color standards was then conducted. We established that the measured chromaticity values (a* and b*) oscillated over time in an unpredictable manner (Fig. F21A, F21B). This behavior appeared to be related to the sensitivity of the spectrophotometer to temperature changes caused by both room temperature variations (air conditioning cycles) and internal temperature changes when acquiring data. The problem was eventually fixed by the technical staff, who worked over several days on reducing the temperature sensitivity of the spectrometer and implementing changes in the data processing software (see details in Expedition 345 technical staff report). The same series of tests with a purple color standard show that the a* and b* values remained stable over time (Fig. F21C, F21D). For the remainder of the expedition, we continued to run color reflectance measurements with a 1 cm interval. Measurements on cores in Holes U1415E–U1415J were done before the drifting behavior of the spectrometer was diagnosed and fixed; absolute values of a* and b* recorded for these cores were drifting over time and are not reliable.

Point magnetic susceptibility

Point magnetic susceptibility was measured using a Bartington MS2E contact probe with a flat 15 mm diameter sensor operating at a frequency of 0.580 kHz. The sensor takes and averages three measurements at 1 s intervals to an accuracy of 5%. The area of response of the MS2E sensor is 3.8 mm × 10.5 mm, with a depth response of 50% at 1 mm and 10% at 3.5 mm, providing higher resolution measurements than the whole-round magnetic susceptibility instrument (Bartington Instruments, Ltd., 2011). Units are reported in 10^{-5} SI units. The point magnetic susceptibility meter was calibrated by the manufacturer before installation on the ship. The probe was zeroed in air before each measurement point, and a background magnetic field was measured and removed from the data before being output.

As with the Bartington MS2C sensor on the WRMSL, the MS2 recorder attached to the SHMSL has an output threshold of $9,999 \times 10^{-5}$ SI and truncates the most significant digit for measurements over $9,999 \times 10^{-5}$ SI. Unlike WRSML data, SHMSL magnetic susceptibility data are not corrected for values over $9,999 \times 10^{-5}$ SI. Series of point measurements are not expected to produce smooth curves over depth as with the WRSML measurements. It is then impossible to easily locate clipped data and to infer the correction to be applied (10,000, 20,000, or more).

Discrete sample measurements

Cubes (~8 cm³) were cut from working section halves for discrete measurements of P-wave velocity and MAD. Most samples were also used for paleomagnetism measurements, in which case V_P and MAD measurements were conducted following the AF demagnetization and anisotropy of magnetic susceptibility measurements. The samples were subsequently passed on to the paleomagnetists for thermal demagnetization whenever appropriate.

Moisture and density

Mass and volume measurements on discrete samples were made to determine bulk, dry, and grain density and porosity. The shipboard MAD facility for hard rock samples consists of a vacuum water saturator, a dual balance system, and a hexapycnometer.

Vacuum water saturator

We used a vacuum pump system to ensure complete saturation of discrete samples. The system consists of a plastic chamber filled with seawater. A vacuum pump then removes air from the chamber, essentially sucking air from pore spaces. Samples were kept under vacuum for at least 24 h. During this time, pressure in the chamber is monitored periodically by a gauge attached to the vacuum pump to ensure a stable vacuum. After removal from the saturator, cubes were stored in sample containers filled with seawater to maintain saturation.

Dual balance system

A dual balance system was used to measure both wet and dry masses. Two analytical balances (Mettler-Toledo XS204) compensate for ship motion; one acts as a reference and the other measures the unknown (i.e., a sample). A standard mass of similar value to that of the sample was placed on the reference balance to increase accuracy. Using a reference mass within ~10% of the sample mass, an accuracy of 0.005 g is readily attainable. After wet mass determinations and P-wave measurements and prior to the determination of dry masses, samples were placed in an oven at 105° ± 5°C for 24 h and then allowed to cool in a desiccator for a minimum of 1 h.

Hexapycnometer system

The hexapycnometer is an IODP custom-built system using six Micromeritics cell units, custom electronics, and custom control programs. The system measures dry sample volume using pressurized helium-filled chambers with a precision of 0.02 cm³. At the start of the expedition, and whenever the helium gas tank is changed, shipboard technicians perform a

calibration using stainless steel spheres of known volume. For a measurement, we run five cells that contain unknowns and one cell that contains two stainless steel calibration spheres (3 and 7 cm³) with a total volume of ~10 cm³. Calibration spheres were cycled through the cells to identify any systematic error and/or instrument drift. Spheres are assumed to be known to within 1% of their total volume. Individual volume measurements were preceded by three purges of the sample chambers with research-grade (99.995% or better) helium heated to 28°C, followed by three data acquisition cycles.

Moisture and density calculations

For density calculations, both mass and volume are first corrected for the salt content of the pore fluid:

$$M_{salt} = M_{water}\ [s/(1 - s)],$$

where

s = pore water salinity,
M_s = mass of salt,
M_d = dry mass of the sample, and
M_w = wet mass of the sample.

Grain density (ρ_g) is determined from the dry mass (M_d) and dry volume (V_d) measurements:

$$\rho_g = (M_d - M_s)/[V_d - (M_s/\rho_s)],$$

where ρ_s is the density of salt (2.20 g/cm³; Blum, 1997). The salt-corrected mass of pore water (M_{pw}) is calculated as

$$M_{pw} = (M_w - M_d)/(1 - s).$$

Then, the volume of pore water (V_{pw}) is

$$V_{pw} = M_{pw}/\rho_{pw} = (M_w - M_d)/[(1 - s)\rho_{pw}],$$

where we assume the density of the pore fluid (ρ_{pw}) is 1.024 g/cm³ (seawater with salinity of 35 g/L; Blum, 1997).

To calculate sample bulk density (ρ_b), we first computed bulk volume:

$$V_b = V_d + V_{pw}.$$

Then,

$$\rho_b = M_w/V_b.$$

Porosity (ϕ) is calculated from the two volume parameters above:

$$\phi = V_{pw}/V_b.$$

P-wave velocity

P-wave velocity measurements of hard rock samples were performed on the same discrete cube samples that were used for MAD and paleomagnetic determinations. P-wave measurements were performed on seawater-saturated samples immediately after wet mass determinations were made. Measurements were made using the x-axis caliper contact transducers on the P-wave velocity gantry. Samples were oriented following standard IODP conventions, and measurements were made in the x-, y-, and z-directions for each cube (Fig. F2C). The apparent anisotropy was then calculated from these three measurements as

$$V_P \text{ anisotropy} = (V_{Pmax} - V_{Pmin})/V_{Pmean}.$$

The system uses Panametrics-NDT Microscan delay line transducers, which transmit at 0.5 MHz, with stainless steel caps. The stainless steel caps were preferred to the rubber caps used during previous hard rock expeditions (e.g., Expedition 335) because they appeared to improve the quality and reproducibility of measurements. The peak of the first arrival was identified automatically by the installed IODP software. The complete waveform is stored with the data if reanalysis is deemed necessary. Shipboard visual checks of the picks appeared satisfactory. The distance between transducers was measured with a built-in linear voltage displacement transformer.

Measurements on standards were conducted as frequently as necessary. Calibration was made before measuring each sample with a series of acrylic cylinders of different thicknesses and a known P-wave velocity of 2750 ± 20 m/s. We performed 4 series of 11 measurements on a suite of 3 acrylic cylinders of different heights (15, 20, and 30 mm; Fig. F22A). These measurements show that (1) successive measured values tend to become more stable after three or four measurements and (2) the measured values are more consistent and closer to the certified acrylic velocity of 2750 ± 20 m/s when a drop of water is added between the acrylic cylinder surfaces and the transducers.

In addition to the test measurements with acrylic standards, at the beginning of Expedition 345 we also conducted several series of measurements on 10 minicores from Leg 147 Site 894. These samples behaved similarly to the acrylic cylinders; the same trend of increasing values was observed over the first three or four measurements during a series of 10 or more successive measurements (Fig. F23A).

We also tested the small water bath used during Expedition 335 (see Expedition 335 Scientists, 2012, for details on the rationale for using this device), which was designed to maintain saturation during the mea-

surements and deemed to increase the quality of the results. Our tests, conducted with both the Leg 147 samples and acrylic prisms (Figs. **F22B, F23B**), show that the results are more consistent without the water bath, and measured velocities without the water bath are not systematically lower as described during Expedition 335. The small membrane between the lower transducer and the sample lower the measured velocity of acrylic prisms by ~10–15 m/s. We decided not to use this device.

Hence, the measurement protocol established for Expedition 345 was to perform a series of at least 10 successive measurements (or more if the measured velocity took longer to reach a stable value) in each of the three directions for each cube sample and discard the first four (or more, when necessary) measurements before computing the mean velocity. The standard deviation over three test measurements series on Site 894 samples (Fig. **F23B**) ranges from 0.5% to 2% and is 1% on average.

Thermal conductivity

Thermal conductivity (k; in W/[m·K]) is a measure of the rate at which heat is transported through a material. At steady state, thermal conductivity is the coefficient of heat transfer (q) across a steady-state temperature difference over a distance:

$$q = k(dT/dx).$$

Thermal conductivity of rock depends on many factors, including temperature, pressure, porosity, type of saturating fluid, and the composition, distribution, and alignment of mineral phases. Thermal conductivity was measured on split core pieces under ambient conditions using the Teka TK04 system described in Blum (1997). All measurements were made at room temperature and pressure and were not corrected for in situ conditions.

The TK04 system measures thermal conductivity by transient heating of the sample with a known heating power and geometry. Changes in temperature with time during heating are recorded and used to calculate thermal conductivity. Heating power can be adjusted for each sample; as a rule of thumb, heating power (W/m) is set to be ~2 times the expected thermal conductivity (W/[m·K]). The temperature of the superconductive needle probe has a quasilinear relationship with the natural logarithm of the time after the initiation of heating (Blum, 1997). The TK04 device uses a complex special approximation method to calculate conductivity and to assess the fit of the heating curve. This method fits discrete windows of the heating curve to the theoretical temperature (T) with time (t) function:

$$T(t) = A_1 + A_2 \ln(t) + A_3 [\ln(t)/t] + (A_4/t),$$

where A_{1-4} are constants that are calculated by linear regression. A_1 is the initial temperature, whereas A_2, A_3, and A_4 are related to geometry and material properties surrounding the needle probe. Having defined these constants (and how well they fit the data), the apparent conductivity (k_a) for the fitted curve is time dependent and given by

$$k_a(t) = q/4\Pi\{A_2 + A_3[1 - \ln(t)/t] - (A_4/t)\},$$

where q is the input heat flux. The maximum value of k_a and the time, t_{max}, at which it occurs on the fitted curve are used to assess the validity of that time window for calculating the thermal conductivity. The best solutions are those where t_{max} is greatest, and these solutions are selected for output. Fits are considered good if k_a has a maximum value, t_{max} is large, and the standard deviation of the least-squares fit is low. For each heating cycle, several output values can be used to assess the quality of the data, including natural logarithm of extreme time (LET) t_{max}, which should be large; the number of solutions (N), which should also be large; and the contact value, which assesses contact resistance between the probe and the sample and should be small and uniform for repeat measurements.

Half-space determinations of thermal conductivity were made with a needle probe embedded in the bottom of a Plexiglas block with a thermal conductivity of 0.184 W/(m·K). Heat is assumed to be transferred through the sample, and the TK04 documentation indicates that heat flow through the Plexiglas block itself is only significant for sample thermal conductivities <1 W/(m·K). Good thermal contact with the heating needle is required, so the split face of the samples was polished with 240 gauge silicon carbide powder.

During transit to Site U1415, empirical tests were conducted with both a certified MACOR ceramic standard (k = 1.626 W/[m·K] ± 2%) and a gabbroic sample from Leg 147 to evaluate the reproducibility of results (Fig. **F24**). We tested two probes with different needle lengths (7.3 and 4.4 cm). The longer needle (used during previous hard rock IODP expeditions and ODP legs) gives better results with less variability and was preferred for series of measurements with the needle aligned with the axis core pieces (Fig. **F24**). The shorter needle (new during Expedition 345) allows measurements parallel or perpendicular to the trace of the foliation when visible on the cut face and was used for a few apparent anisotropy test measurements. The stability of the measurement series using the short needle (reported in the **"Hole**

U1415I" and "Hole U1415J" chapters [Gillis et al., 2014b, 2014c]) was not good enough to give reliable apparent anisotropy values. The quality of measurements done with the large needle probe was assessed using LET and N (number of solutions); only a few measured values were rejected. Our measurement protocol (with a series of 10 measurements) provided consistent analyses within the analytical error (2%).

Samples were saturated and left to equilibrate to room temperature in a seawater vacuum saturator for ≥24 h, and the sample and sensor needle were equilibrated at room temperature in an isolated Styrofoam-covered seawater bath (k = ~0.6 W/[m·K]) for at least 15 min prior to measurement. Seawater was preferred to improve the needle/sample contact to silicone thermal contact gel in order to avoid contamination of the samples. Isolation of the sample and sensor needle eliminated the effect of small but rapid temperature changes introduced by air currents in the laboratory, as well as the ship's motion. The instrument internally measures temperature drift and does not begin a heating run until sufficient thermal equilibrium is attained.

Core pieces from the archive half were measured at irregular intervals downhole depending on the availability of homogeneous and relatively vein/crack-free pieces long enough to be measured without edge effects (pieces >7 cm long; i.e., longer than the instrument needle). As many as 10 measurements were performed on each sample to verify the consistency of the results and provide an average value. The probe was regularly checked using the MACOR ceramic standard.

Handheld X-ray fluorescence analyses

During Expedition 345, we performed semiquantitative X-ray fluorescence (XRF) chemical analyses of rock surfaces using a ThermoFisher Niton XL3t GOLDD+ handheld XRF analyzer to help identify minerals in selected samples from the working and archive halves. Chemical analysis by handheld XRF is a nondestructive technique that was used on igneous rocks during Expeditions 330 and 335 (Expedition 330 Scientists, 2011; Expedition 335 Scientists, 2012). Analytical procedures were adapted from those developed during Expedition 335 (see the evaluation of this device in XRF in Expedition 335 "Supplementary material").

Analytical methods

The handheld XRF analyzer can measure elemental concentrations of as many as 33 elements simultane-

ously and is equipped with three excitation filters (high range, main range, and light range) for optimizing sensitivity. Calibrations and analytical procedures are preset by the manufacturer and are not adjustable. Analyses were carried out using the Cu/Zn procedure in mining mode. This setting was selected, as it is the recommended method for the elements of interest for petrological characterization. The analyzed elements and their corresponding filter positions are in Table **T5.** Counting time was 150 s for each analysis. An automatically adjusted helium flow was used to avoid interference with the ambient air for the light elements (Mg, Na, and K). For consistency, an 8 mm spot size was used for all measurements on samples and standards except for macroscopically heterogeneous samples, with which a 3 mm spot size was used.

Calibration and standardization

To test the accuracy of the analyses, pressed powders of four certified silicate standards, BHVO-2 (US Geological Survey [USGS] Geochemical Reference Standard-Basalt, Hawaiian Volcano Observatory), JB-2 (basalt, Geological Survey of Japan [GSJ]), JA-2 (andesite, GSJ) and BCR-2 (USGS Geochemical Reference Standard-Basalt, Columbia River), were analyzed (Table **T6**). The measured concentrations differed from published values by 20% or more, except for MnO, CaO, and Cu. The concentration of MgO and trace elements Ba, Cr, Co, and Ni are below detection limits except for BHVO-2.

A tentative effort was made to improve the accuracy of the analyses on major oxides by using a rock standard–based approach similar to that developed during Expedition 335. Calibration curves were defined by plotting the raw concentrations measured on three certified silicate rock standards, BHVO-2, JB-2, and JA-2, with an 8 mm spot size, as a function of their reference concentrations published in Govindaraju (1994) and downloaded from the GeoReM database (Table **T7**); BCR-2 was used as quality control. This approach allowed for improving the accuracy of the measured values for most elements but not enough to allow a quantitative estimate of the major element composition of silicate rocks. The accuracy results obtained for the quality control standard BCR-2 were better than 10% for SiO_2, TiO_2, $FeO^{(T)}$, MnO, CaO, Zr, and Sr (Table **T7**).

Our study indicates that this instrument is not adequate for making quantitative measurements of the oxide contents or the trace element concentrations of igneous rocks. The data produced with this instrument are semiquantitative at best and therefore inappropriate for scientific reports. The handheld XRF analyzer is useful only for rapid qualitative assess-

ment of the compositions of specific geological materials (e.g., identification of Mn crusts or oxides) before more accurate analyses of the samples can be carried out using either shipboard XRD and/or ICP-AES or shore-based analyses. However, the procedure for using and handling the instrument is tedious and time consuming and may not be worth the effort and time of the shipboard scientists.

Collection of core saw cuttings

Following standard IODP procedures, all cores collected during Expedition 345 were cut in half lengthwise to produce an archive half and a working half. The sawing process leaves a ~1.5 mm gap of material ablated by the saw. These saw cuttings should constitute a representative sample of the entire coherent core recovered because the saw does not discriminate between different lithologies. Arguably, this sample may have some advantages for determining bulk core properties over point sampling techniques. This is because the point samples are few in number, preferentially taken on fine-grained, homogeneous and plentiful lithologies in the core, generally avoiding altered, delicate, and "interesting" intervals whose minerals, textures, and structures are of interest for microscopic study, whereas the saw takes everything. Rough calculations show that ~300 g of rock per meter of cut core is produced during the sawing process. The major caveat is that the sawing process itself may introduce some contamination, an effect that should be investigated quantitatively postcruise. The fragments produced by this process are typically <200 μm in diameter, with some fragments reduced to clay size (<4 μm or +8Φ [phi] units). Saw cuttings from each core section cut generated a poorly sorted bulk or "mud" sample (more than ~4 μm), a less than ~4 μm filtrate sample, and a ~30–10 μm filtered sample (Fig. F25).

After the core is removed from its plastic casing, the core pieces are washed and rinsed of all drilling mud and air-dried. The core is then cut using a hand-driven shuttle, forcing the individual pieces through a diamond saw blade lubricated with distilled water. The entire saw and shuttle assembly are enclosed on five sides by a plastic housing. Together with the spray guard at the front of the saw, this ensures that the water and cuttings sprayed from the sample and the drippings from the sample are contained within the housing.

After all pieces in a section (typically 0.5–1.5 m long) are cut, the cuttings are collected. Some of the cuttings lie on the floor of the plastic housing, and as much of this material as possible as is collected using a spatula. The remaining cuttings from the shuttle,

mounts, and farther reaches of the housing are rinsed using a strong spray of deionized water and flushed to the drain of the enclosure. This rinse water flows into a sink in which a temporary sampling drain replaces the original drain so that rinse water and cuttings can be diverted into 10 L plastic containers. A final rinse ensures maximum capture of the total cuttings of all rocks cut in any given section of core and also leaves the saw and housing clean for cutting the next section of core.

Next, the slurry of cuttings and rinse water is decanted from the plastic containers into five 1 US gallon plastic buckets and allowed to settle for at least 12 h to allow most particles to fall to the bottom. In this time, all silt-sized particles (those >4 μm) should settle to the bottom of the 37 cm tall bucket (e.g., Lewis, 1984). The supernatant suspension is then decanted from the bucket, leaving a thick slurry of particles from ~200 to <10 μm in size (Fig. F25A). This slurry, our mud sample, is then air-dried and archived.

The supernatant is free of most silt-sized particles and is passed through a 10 μm Dutron 10 sieve to capture any remaining coarser particles (Fig. F25B). Where a >10 μm fraction is captured, the material is sampled as ">10 μm." In practice, no material was captured in samples where a settling time was 12 h or more, and in no sample did the >10 μm fraction exceed 0.1 g.

A 2 L aliquot of the filtered supernatant with its clay-sized suspended material was centrifuged in 50 mL tubes at 2000 rpm for 10 min, causing the clay-sized particles to settle out. This clay-sized material was then washed in alcohol, dried in air, and weighed. The weight was recorded as grams of suspended material per 2 L of supernatant. The volume of the remaining supernatant was also measured in a burette to ±5 mL. The total amount of clay-sized particles was then calculated as follows:

$$(x \text{ g/L}) \times (\text{total liters}) = \text{total grams of clay-sized particles.}$$

This clay-sized sample (Fig. F25B) typically constitutes ~25% of the total weight of the sample.

To test whether any fractionation occurred between the coarser mud sample and the clay-sized sample, both aliquots were analyzed on board by XRD using a Brucker D-4 Endeavor diffractometer with a Vantec-1 detector and nickel-filtered CuKα radiation. Samples were mounted as smear slides or pressed into depressions in sample holders if the amount of sample was sufficient. Mineral identification was achieved with the interactive Diffrac.Suite Eva, version 1.4, software package (2010 release) using the

powder diffraction file database associated with the program. Identifications were based on multiple peak matches. Instrument conditions were the same as those listed in "X-ray diffraction."

References

Arason, P., and Levi, S., 2010. Maximum likelihood solution for inclination-only data in paleomagnetism. *Geophys. J. Int.,* 182(2):753–771. doi:10.1111/j.1365-246X.2010.04671.x

Bartington Instruments, Ltd., 2011. *Operation Manual for MS2 Magnetic Susceptibility System:* Oxford (Bartington Instruments, Ltd.). http://www.bartington.com/Literaturepdf/Operation%20Manuals/om0408%20MS2.pdf

Blum, P., 1997. Physical properties handbook: a guide to the shipboard measurement of physical properties of deep-sea cores. *ODP Tech. Note,* 26. doi:10.2973/odp.tn.26.1997

Cordier, C., Clément, J.-P., Caroff, M., Hémond, C., Blais, S., Cotten, J., Bollinger, C., Launeau, P., and Guille, G., 2005. Petrogenesis of coarse-grained intrusives from Tahiti Nui and Raiatea (Society Islands, French Polynesia). *J. Petrol.,* 46(11):2281–2312. doi:10.1093/petrology/egi055

Davis, G.H., Reynolds, S.J., and Kluth, C., 2011. *Structural Geology of Rocks and Regions* (3rd ed.): New York (John Wiley & Sons).

Dunlop, D.J., 2003. Stepwise and continuous low-temperature demagnetization. *Geophys. Res. Lett.,* 30(11):1582. doi:10.1029/2003GL017268

Expedition 304/305 Scientists, 2006. Methods. *In* Blackman, D.K., Ildefonse, B., John, B.E., Ohara, Y., Miller, D.J., MacLeod, C.J., and the Expedition 304/305 Scientists, *Proc. IODP,* 304/305: College Station, TX (Integrated Ocean Drilling Program Management International, Inc.). doi:10.2204/iodp.proc.304305.102.2006

Expedition 309/312 Scientists, 2006. Methods. *In* Teagle, D.A.H., Alt, J.C., Umino, S., Miyashita, S., Banerjee, N.R., Wilson, D.S., and the Expedition 309/312 Scientists. *Proc. IODP,* 309/312: Washington, DC (Integrated Ocean Drilling Program Management International, Inc.). doi:10.2204/iodp.proc.309312.102.2006

Expedition 330 Scientists, 2012. Methods. *In* Koppers, A.A.P., Yamazaki, T., Geldmacher, J., and the Expedition 330 Scientists, *Proc. IODP,* 330: Tokyo (Integrated Ocean Drilling Program Management International, Inc.). doi:10.2204/iodp.proc.330.102.2012

Expedition 335 Scientists, 2012. Methods. *In* Teagle, D.A.H., Ildefonse, B., Blum, P., and the Expedition 335 Scientists, *Proc. IODP,* 335: Tokyo (Integrated Ocean Drilling Program Management International, Inc.). doi:10.2204/iodp.proc.335.102.2012

Gee, J.S., Tauxe, L., and Constable, C., 2008. AMSSpin: a LabVIEW program for measuring the anisotropy of magnetic susceptibility with the Kappabridge KLY-4S. *Geochem., Geophys., Geosyst.,* 9(8):Q08Y02. doi:10.1029/2008GC001976

Gillis, K.M., Snow, J.E., Klaus, A., Guerin, G., Abe, N., Akizawa, N., Ceuleneer, G., Cheadle, M.J., Adrião, Á., Faak, K., Falloon, T.J., Friedman, S.A., Godard, M.M., Harigane, Y., Horst, A.J., Hoshide, T., Ildefonse, B., Jean, M.M., John, B.E., Koepke, J.H., Machi, S., Maeda, J., Marks, N.E., McCaig, A.M., Meyer, R., Morris, A., Nozaka, T., Python, M., Saha, A., and Wintsch, R.P., 2014a. Geochemistry summary. *In* Gillis, K.M., Snow, J.E., Klaus, A., and the Expedition 345 Scientists, *Proc. IODP,* 345: College Station, TX (Integrated Ocean Drilling Program). doi:10.2204/iodp.proc.345.114.2014

Gillis, K.M., Snow, J.E., Klaus, A., Guerin, G., Abe, N., Akizawa, N., Ceuleneer, G., Cheadle, M.J., Adrião, Á., Faak, K., Falloon, T.J., Friedman, S.A., Godard, M.M., Harigane, Y., Horst, A.J., Hoshide, T., Ildefonse, B., Jean, M.M., John, B.E., Koepke, J.H., Machi, S., Maeda, J., Marks, N.E., McCaig, A.M., Meyer, R., Morris, A., Nozaka, T., Python, M., Saha, A., and Wintsch, R.P., 2014b. Hole U1415I. *In* Gillis, K.M., Snow, J.E., Klaus, A., and the Expedition 345 Scientists, *Proc. IODP,* 345: College Station, TX (Integrated Ocean Drilling Program). doi:10.2204/iodp.proc.345.109.2014

Gillis, K.M., Snow, J.E., Klaus, A., Guerin, G., Abe, N., Akizawa, N., Ceuleneer, G., Cheadle, M.J., Adrião, Á., Faak, K., Falloon, T.J., Friedman, S.A., Godard, M.M., Harigane, Y., Horst, A.J., Hoshide, T., Ildefonse, B., Jean, M.M., John, B.E., Koepke, J.H., Machi, S., Maeda, J., Marks, N.E., McCaig, A.M., Meyer, R., Morris, A., Nozaka, T., Python, M., Saha, A., and Wintsch, R.P., 2014c. Hole U1415J. *In* Gillis, K.M., Snow, J.E., Klaus, A., and the Expedition 345 Scientists, *Proc. IODP,* 345: College Station, TX (Integrated Ocean Drilling Program). doi:10.2204/iodp.proc.345.110.2014

Godard, M., Awaji, S., Hansen, H., Hellebrand, E., Brunelli, D., Johnson, K., Yamasaki, T., Maeda, J., Abratis, M., Christie, D., Kato, Y., Mariet, C., and Rosner, M., 2009. Geochemistry of a long in-situ section of intrusive slow-spread oceanic lithosphere: results from IODP Site U1309 (Atlantis Massif, 30°N Mid-Atlantic-Ridge). *Earth Planet. Sci. Lett.,* 279(1–2):110–122. doi:10.1016/j.epsl.2008.12.034

Govindaraju, K., 1994. 1994 compilation of working values and sample description for 383 geostandards. *Geostand. Newsl.,* 18(1). doi:10.1111/j.1751-908X.1994.tb00502.x

Hext, G.R., 1963. The estimation of second-order tensors, with related tests and designs. *Biometrika,* 50(3–4):353–373. doi:10.1093/biomet/50.3-4.353

Jochum, K.P., Nohl, U., Herwig, K., Lammel, E., Stoll, B., and Hofmann, A.W., 2005. GeoRem: a new geochemical database for reference materials and isotopic standards. *Geostand. Geoanal. Res.,* 29(3):333–338. doi:10.1111/j.1751-908X.2005.tb00904.x

Kirschvink, J.L., 1980. The least-squares line and plane and the analysis of palaeomagnetic data. *Geophys. J. R. Astron. Soc.,* 62(3):699–718. doi:10.1111/j.1365-246X.1980.tb02601.x

Kono, M., 1980. Statistics of paleomagnetic inclination data. *J. Geophys. Res.: Solid Earth,* 85(B7):3878–3882. doi:10.1029/JB085iB07p03878

Le Maitre, R.W., 1989. *A Classification of Igneous Rocks and Glossary of Terms:* Oxford (IUGS, Blackwell).

Le Maitre, R.W., Steckeisen, A., Zanettin, B., Le Bas, M.J., Bonin, B., and Bateman, P. (Eds.), 2002. *Igneous Rocks: A Classification and Glossary of Terms* (2nd ed.): Cambridge (Cambridge Univ. Press).

Lewis, D.W., 1984. *Practical Sedimentology:* New York (Van Nostrand-Reinhold).

Lide, D.R. (Ed.), 2000. *Handbook of Chemistry and Physics:* Boca Raton, FL (Chemical Rubber Publishing Company).

MacLeod, C.J., Parson, L.M., and Sager, W.W., 1994. Reorientation of cores using the formation microscanner and borehole televiewer: application to structural and paleomagnetic studies with the Ocean Drilling Program. *In* Hawkins, J., Parson, L., Allan, J., et al., *Proc. ODP, Sci. Results,* 135: College Station, TX (Ocean Drilling Program), 301–311. doi:10.2973/odp.proc.sr.135.160.1994

McFadden, P.L., and Reid, A.B., 1982. Analysis of paleomagnetic inclination data. *Geophys. J. R. Astron. Soc.,* 69(2):307–319. doi:10.1111/j.1365-246X.1982.tb04950.x

Merrill, R.T., 1970. Low-temperature treatments of magnetite and magnetite-bearing rocks. *J. Geophys. Res.: Solid Earth,* 75(17):3343–3349. doi:10.1029/JB075i017p03343

Morris, A., Gee, J.S., Pressling, N., John, B.E., MacLeod, C.J., Grimes, C.B., and Searle, R.C., 2009. Footwall rotation in an oceanic core complex quantified using reoriented Integrated Ocean Drilling Program core samples. *Earth Planet. Sci. Lett.,* 287(1–2):217–228. doi:10.1016/j.epsl.2009.08.007

Murray, R.W., Miller, D.J., and Kryc, K.A., 2000. Analysis of major and trace elements in rocks, sediments, and interstitial waters by inductively coupled plasma–atomic emission spectrometry (ICP-AES). *ODP Tech. Note, 29.* doi:10.2973/odp.tn.29.2000

O'Hanley, D.S., 1996. Serpentinites: Records of Tectonic and Petrological History. *Oxford Monogr. Geol. Geophys.,* 34.

Parker, R.L., and Gee, J.S., 2002. Calibration of the pass-through magnetometer—II. Application. *Geophys. J. Int.,* 150:140–152. doi:10.1046/j.1365-246X.2002.01692.x

Passchier, C.W., and Trouw, R.A.J., 1996. *Microtectonics:* Berlin (Springer-Verlag).

Puchelt, H., Malpas, J., Falloon, T., Pedersen, R., Eckhardt, J.-D., and Allan, J.F., 1996. Data report: ultramafic reference material from Core 147-895D-10W. *In* Mével, C., Gillis, K.M., Allan, J.F., and Meyer, P.S. (Eds.), *Proc. ODP, Sci. Results,* 147: College Station, TX (Ocean Drilling Program), 493–496. doi:10.2973/odp.proc.sr.147.033.1996

Ramsay, J.G., and Huber, M.I., 1987. *The Techniques of Modern Structural Geology* (Vol. 2): *Folds and Fractures:* New York (Acad. Press).

Révillon, S., Barr, S.R., Brewer, T.S., Harvey, P.K., and Tarney, J., 2002. An alternative approach using integrated gamma-ray and geochemical data to estimate the inputs to subduction zones from ODP Leg 185, Site 801. *Geochem., Geophys., Geosyst.,* 3(12):8902. doi:10.1029/2002GC000344

Shelley, D., 1983. *Igneous and Metamorphic Rocks Under the Microscope: Classification, Textures, Microstructures and Mineral Preferred Orientations:* London (Chapman and Hall).

Shipboard Scientific Party, 1989. Introduction and explanatory notes. *In* Robinson, P.T., Von Herzen, R., et al., *Proc. ODP, Init. Repts.,* 118: College Station, TX (Ocean Drilling Program), 3–23. doi:10.2973/odp.proc.ir.118.101.1989

Shipboard Scientific Party, 1991. Explanatory notes. *In* Taira, A., Hill, I., Firth, J.V., et al., *Proc. ODP, Init. Repts.,* 131: College Station, TX (Ocean Drilling Program), 25–60. doi:10.2973/odp.proc.ir.131.104.1991

Shipboard Scientific Party, 1992. Explanatory notes. *In* Dick, H.J.B., Erzinger, J., Stokking, L.B., et al., *Proc. ODP, Init. Repts.,* 140: College Station, TX (Ocean Drilling Program), 5–33. doi:10.2973/odp.proc.ir.140.101.1992

Shipboard Scientific Party, 1993. Explanatory notes. *In* Gillis, K., Mével, C, Allan, J., et al., *Proc. ODP, Init. Repts.,* 147: College Station, TX (Ocean Drilling Program), 15–42. doi:10.2973/odp.proc.ir.147.102.1993

Shipboard Scientific Party, 1995. Explanatory notes. *In* Cannat, M., Karson, J.A., Miller, D.J., et al., *Proc. ODP, Init. Repts.,* 153: College Station, TX (Ocean Drilling Program), 15–42. doi:10.2973/odp.proc.ir.153.10X.1995

Shipboard Scientific Party, 1999a. Explanatory notes. *In* Dick, H.J.B., Natland, J.H., Miller, D.J., et al., *Proc. ODP, Init. Repts.,* 176: College Station, TX (Ocean Drilling Program), 1–42. doi:10.2973/odp.proc.ir.176.102.1999

Shipboard Scientific Party, 1999b. Explanatory notes. *In* Pettigrew, T.L., Casey, J.F., Miller, D.J., et al., *Proc. ODP, Init. Repts.,* 179: College Station, TX (Ocean Drilling Program), 1–47. doi:10.2973/odp.proc.ir.179.103.1999

Shipboard Scientific Party, 2003. Explanatory notes. *In* Wilson, D.S., Teagle, D.A.H., Acton, G.D., *Proc. ODP, Init. Repts.,* 206: College Station, TX (Ocean Drilling Program), 1–94. doi:10.2973/odp.proc.ir.206.102.2003

Shipboard Scientific Party, 2004. Explanatory notes. *In* Kelemen, P.B., Kikawa, E., Miller, D.J., et al., *Proc. ODP, Init. Repts.,* 209: College Station, TX (Ocean Drilling Program), 1–75. doi:10.2973/odp.proc.ir.209.102.2004

Streckeisen, A., 1974. Classification and nomenclature of plutonic rocks recommendations of the IUGS subcommission on the systematics of igneous rocks. *Geol. Rundsch.,* 63(2):773–786. doi:10.1007/BF01820841

Twiss, R.J., and Moores, E.M., 1992. *Structural Geology:* New York (Freeman).

Vasiliev, M.A., Blum, P., Chubarian, G., Olsen, R., Bennight, C., Cobine, T., Fackler, D., Hastedt, M., Houpt, D., Mateo, Z., and Vasilieva, Y.B., 2011. A new natural gamma radiation measurement system for marine sediment and rock analysis. *J. Appl. Geophys.,* 75:455–463. doi:10.1016/j.jappgeo.2011.08.008

Yu, Y., Dunlop, D.J., and Özdemir, Ö., 2003. On the resolution of multivectorial remanences. *Earth Planet. Sci. Lett.,* 208(1–2):13–26. doi:10.1016/S0012-821X(02)01149-4

Figure F1. Integrated Ocean Drilling Program labeling scheme used for holes, cores, sections, and samples, Expedition 345.
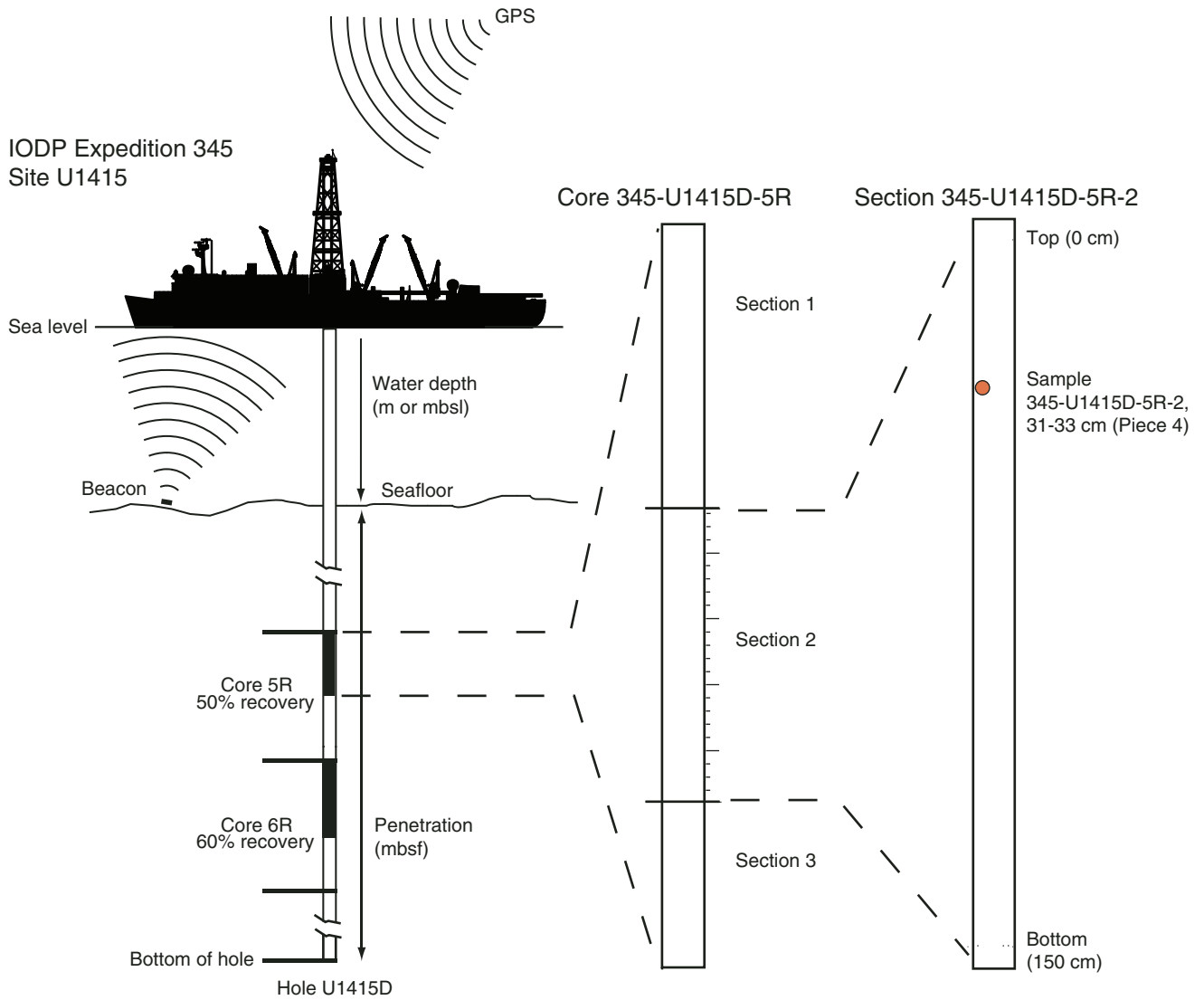
Figure F2. Core reference frame for structural and paleomagnetic orientation measurements, Expedition 345. **A.** The primary orientation of each core piece is up and down along the core axis. **B.** Coordinates in both archive and working section halves. **C.** Conventions for labeling samples and thin sections taken from the working section half.
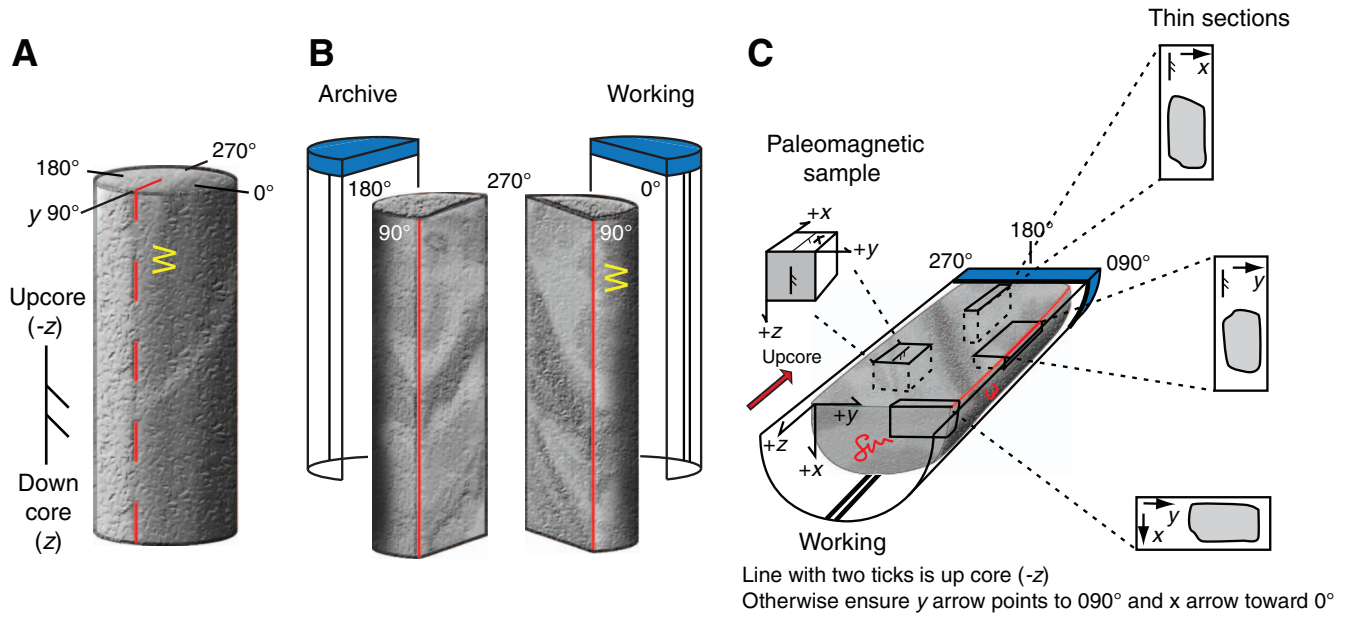
Figure F3. Summary of core handling and workflow from coring to shipboard sampling, Expedition 345. For more information on Step 6, see Figure **F2.** Cur = Curator, ALO = Assistant Laboratory Officer, Struc. = structural geologists, Ig. and Ig. Pet. = igneous petrologists, Phys. props. = physical properties specialist, Met. = metamorphic specialists, TSB = thin section billet, XRD = X-ray diffraction sample, ICP = inductively coupled plasma–atomic emission spectroscopy sample, Mag = paleomagnetism sample, PP = physical properties sample.
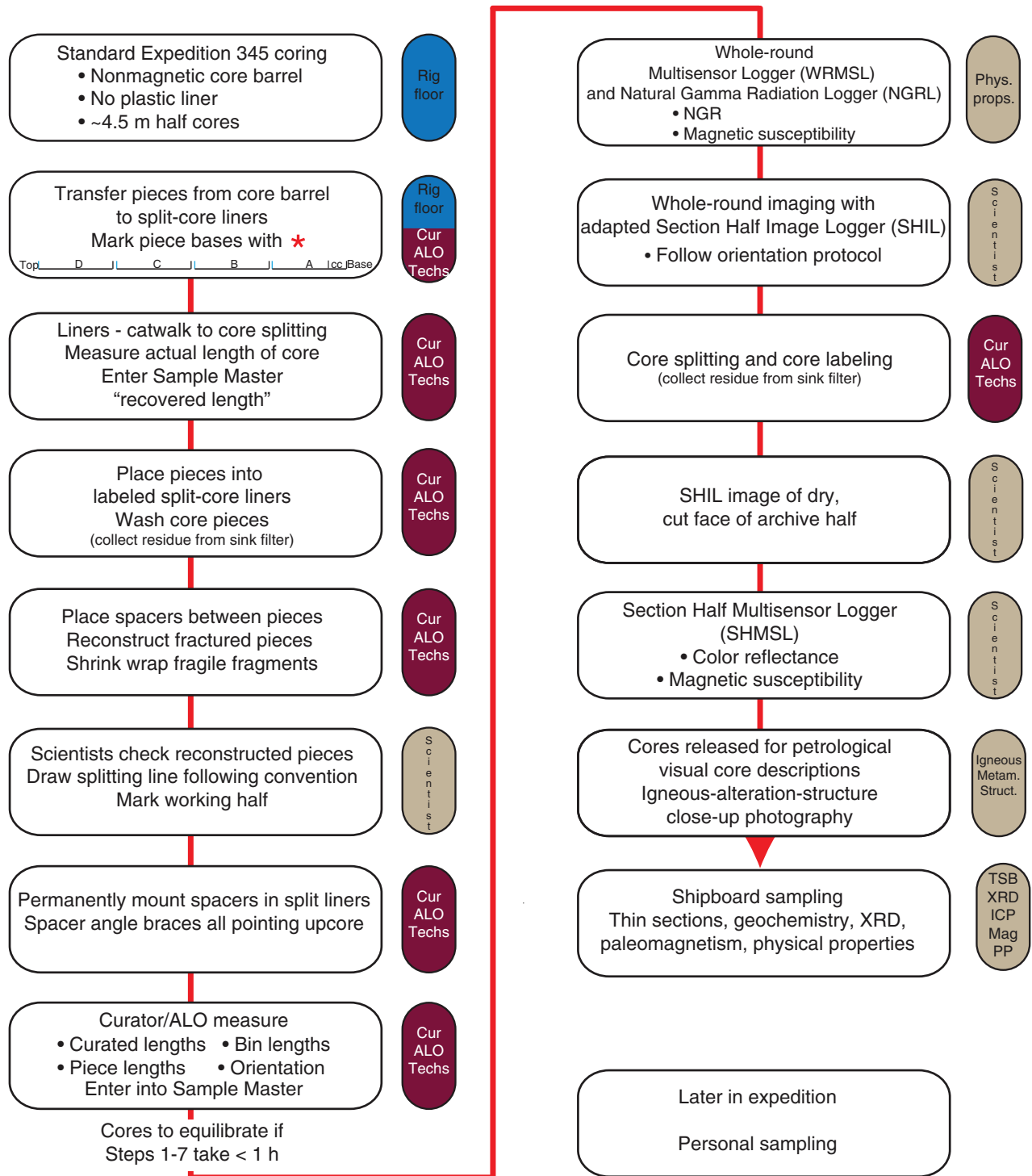
Figure F4. Piece and section lengths defined for curation and scientific purposes, Expedition 345.
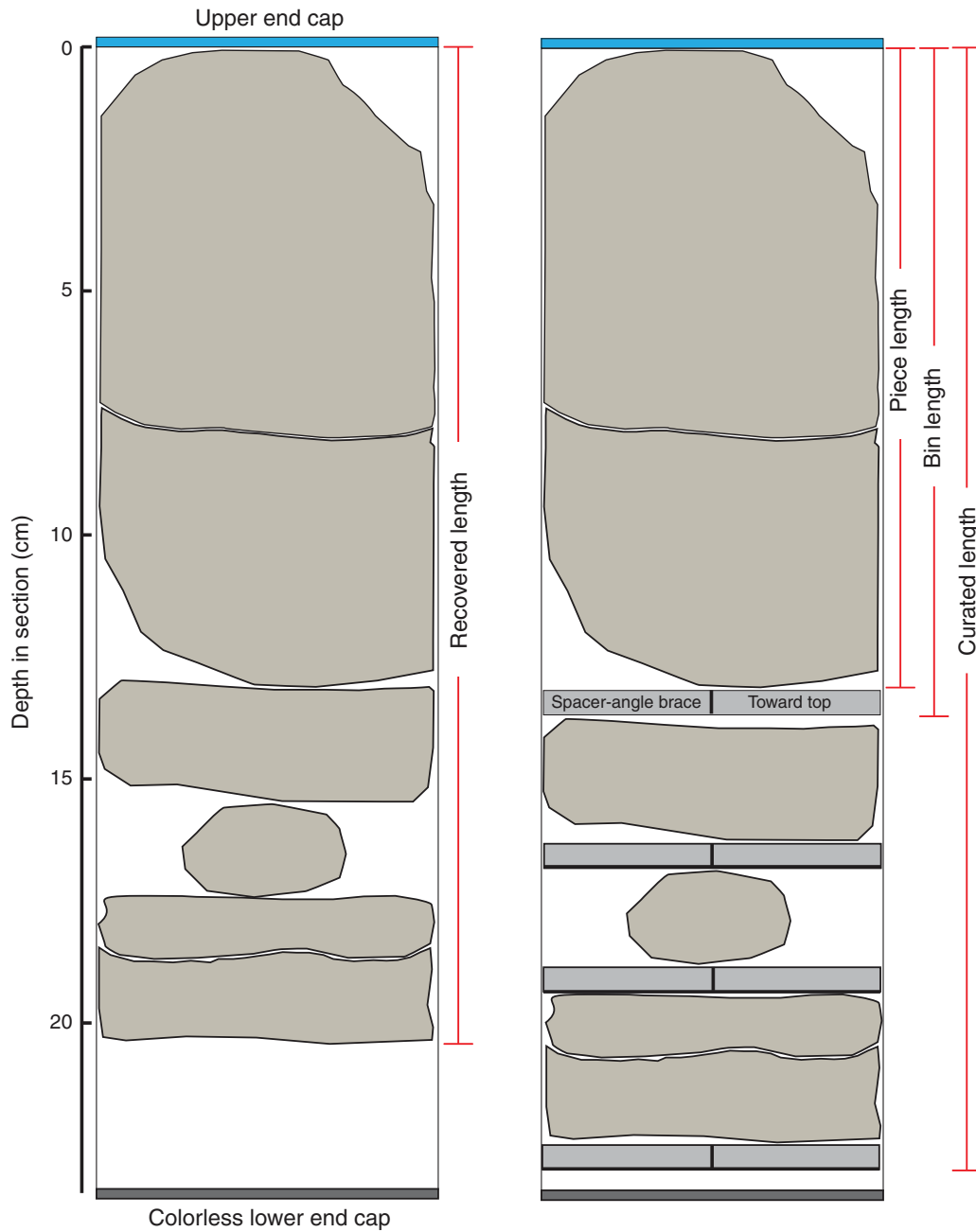
Figure F5. Information capture applications, central Laboratory Information Management System (LIMS) database, data retrieval applications (light green), graphing applications (red), and final documents generated for the Expedition 345 *Proceedings* (yellow). All information is stored in the LIMS database before it is extracted and used for reporting. SHLF = section half, WR = whole round, CSV = comma-separated value, VCD = visual core description.
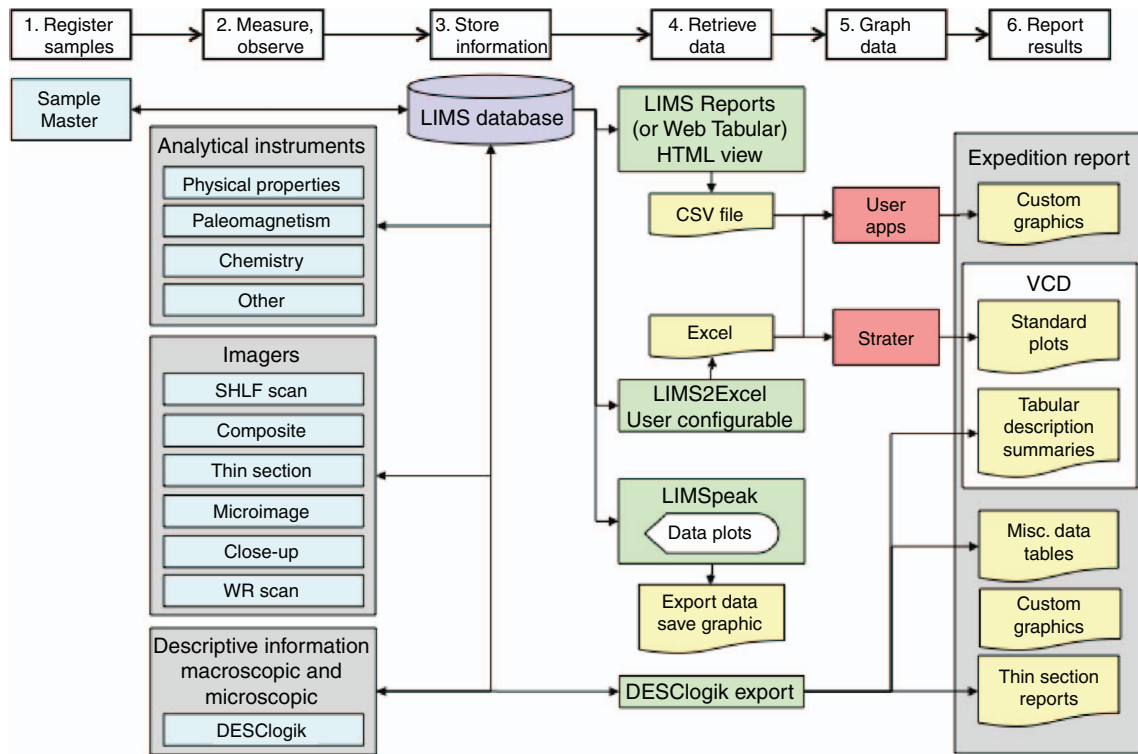
Figure F6. Aluminum frame used for holding whole-round core pieces for imaging, Expedition 345. View of one end of the frame, with one of the four bracing strips removed, as would be the case while imaging the outer core surface.
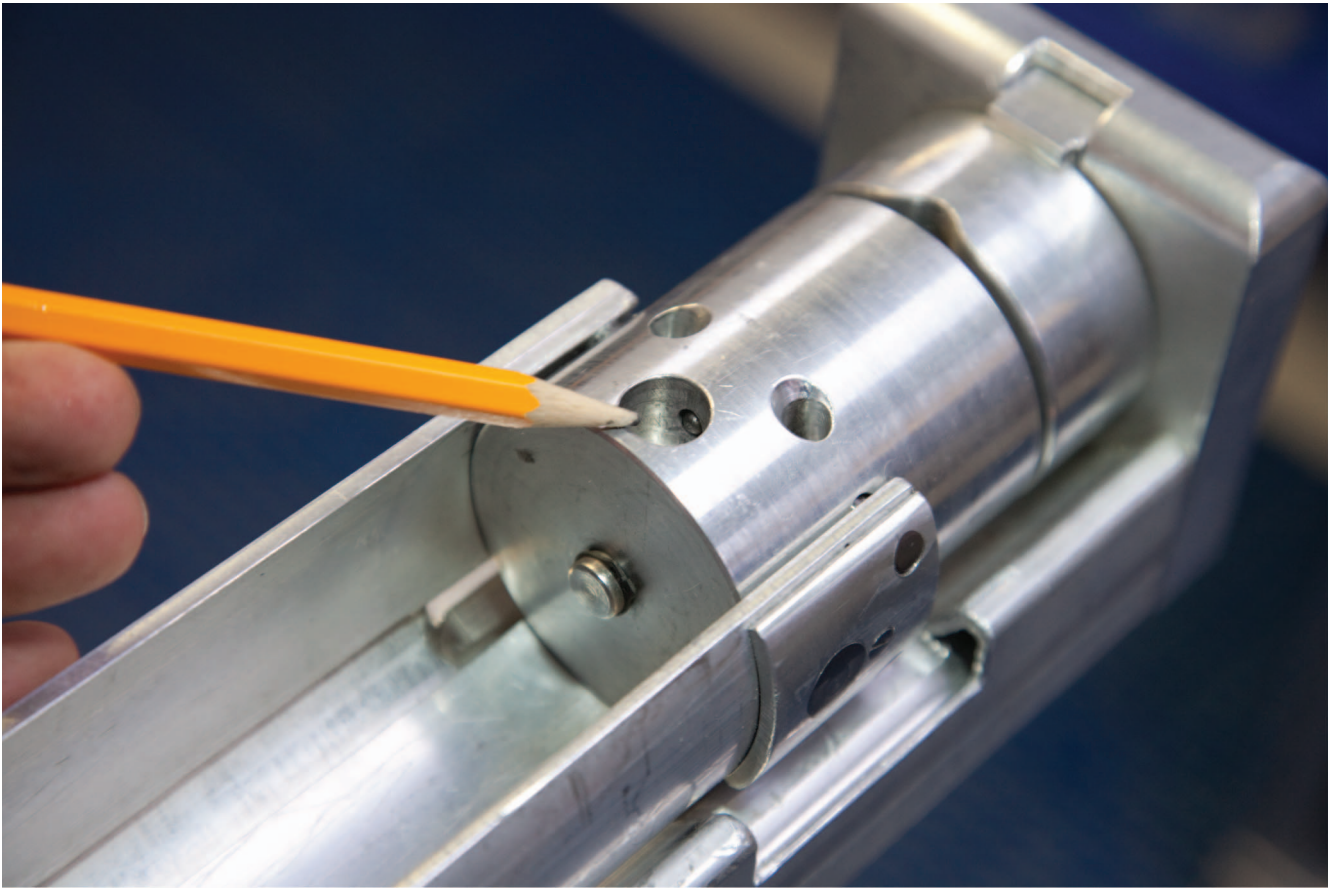
Figure F7. Symbols and abbreviations used in visual core description graphic reports produced during Expedition 345. ICP-AES = inductively coupled plasma–atomic emission spectroscopy.

Lithology

	Basalt
	Dolerite
	Drilling-induced disaggregated gabbro
	Rubble
	Tonalite
	Chromitite
	Completely altered chromitite
	Diorite
	Troctolite
	Drilling-induced disaggregated troctolite
	Quartz-diorite

|	
	Doleritic gabbro
	Olivine gabbro
	Troctolitic olivine gabbro
	Olivine-moderately phyric basalt
	Olivine-sparsely phyric basalt
	Olivine-highly phyric basalt
	Gabbro
	Breccia
	Oxide gabbro
	Oikocryst gabbro

	Oxide gabbronorite
	Gabbronorite
	Olivine gabbronorite
	Silty sand
	Sand
	Pebbly sand
	Felsic material
	Cataclasite
	Alteration vein
	Anorthosite

Shipboard samples

I	M	P	T	X
ICP-AES analysis	Paleomagnetic analysis	Physical property analysis	Petrographic thin section	X-ray diffraction analysis

Structure

	Chilled margin		Crystal-plastic fabric		Cataclastic zone
	Igneous contact		Magmatic fabric		Magmatic and textural banding and patches
	Dike contact		Fault		Modal contact

Veins

	Vein fill		Massive vein		Branched vein		Vein structure
	Vein		Shear vein		Composite Vein		

Alteration intensity

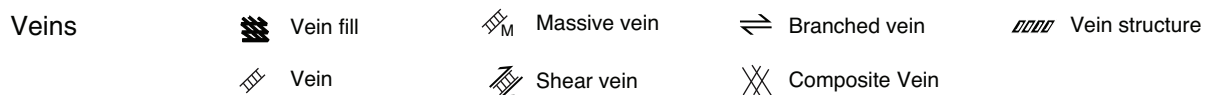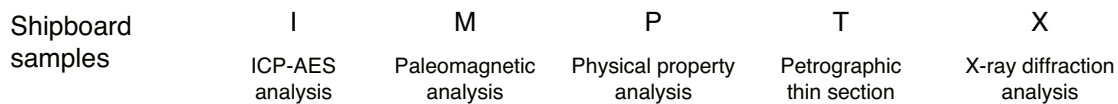| 0	1	2	3	4
<10%	10%-29%	30%-59%	60%-90%	>90%

Figure F8. Modal classification scheme for mafic–ultramafic plutonic igneous rock, Expedition 345 (after Streckeisen, 1974).
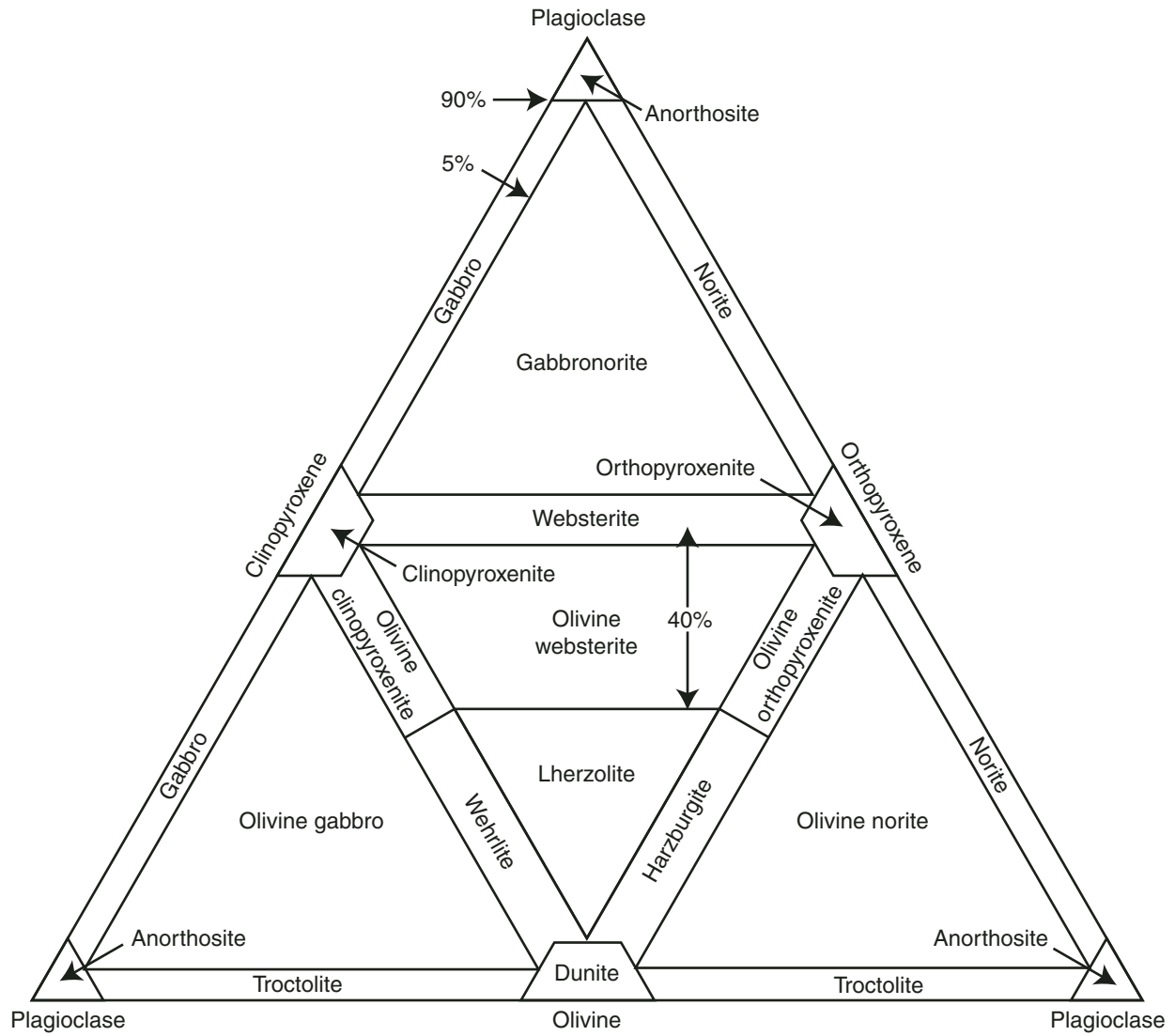
Figure F9. Quartz-alkali feldspar-plagioclase (QAP) modal classification scheme for plutonic igneous rock, Expedition 345 (from Le Maitre et al., 2002).
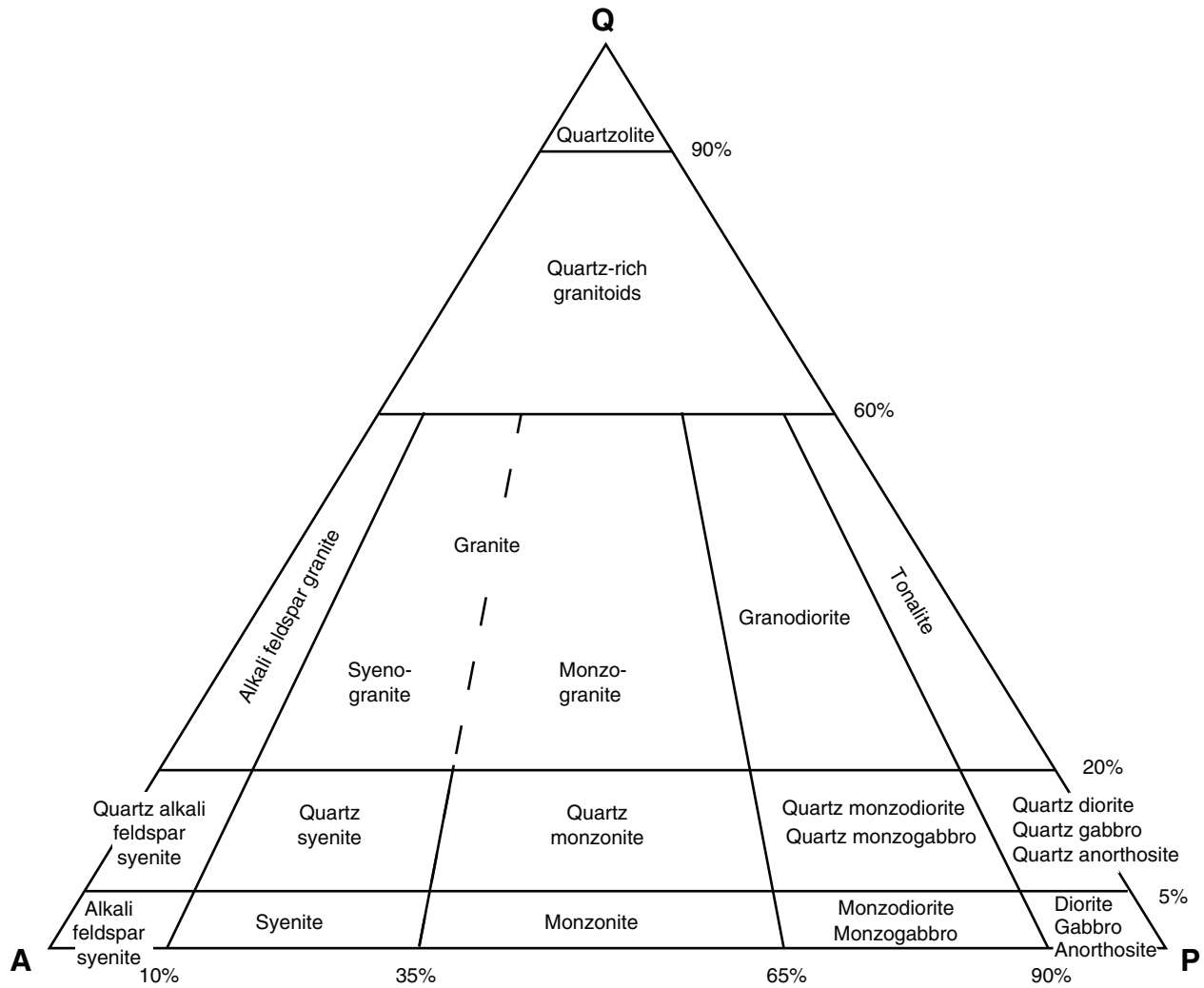
Figure F10. Textural classifications for igneous rock, Expedition 345 (modified from Cordier et al., 2005).

Granular

Intergranular
(intersertal if glass)

Subophitic

Ophitic

Comb

Dendritic

Major phase (feldspar)

Second phase (pyroxene)

Figure F11. Full thin section photomicrographs in which multiple igneous domains were defined, Expedition 345.
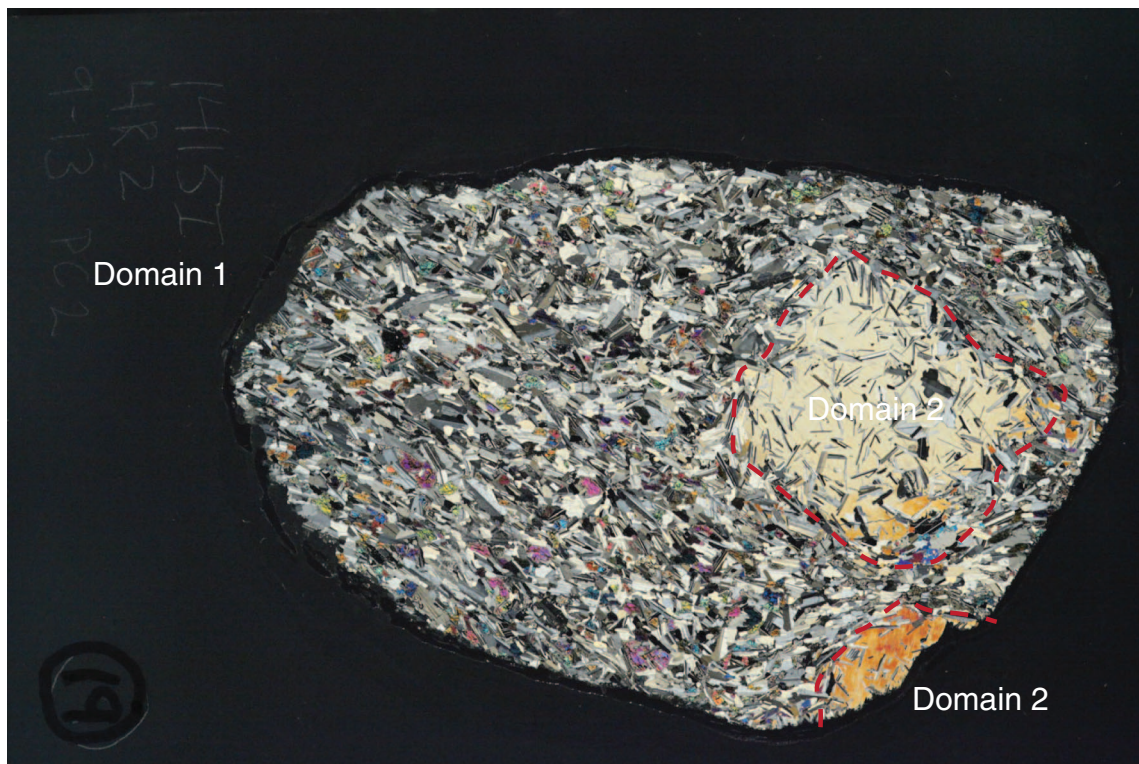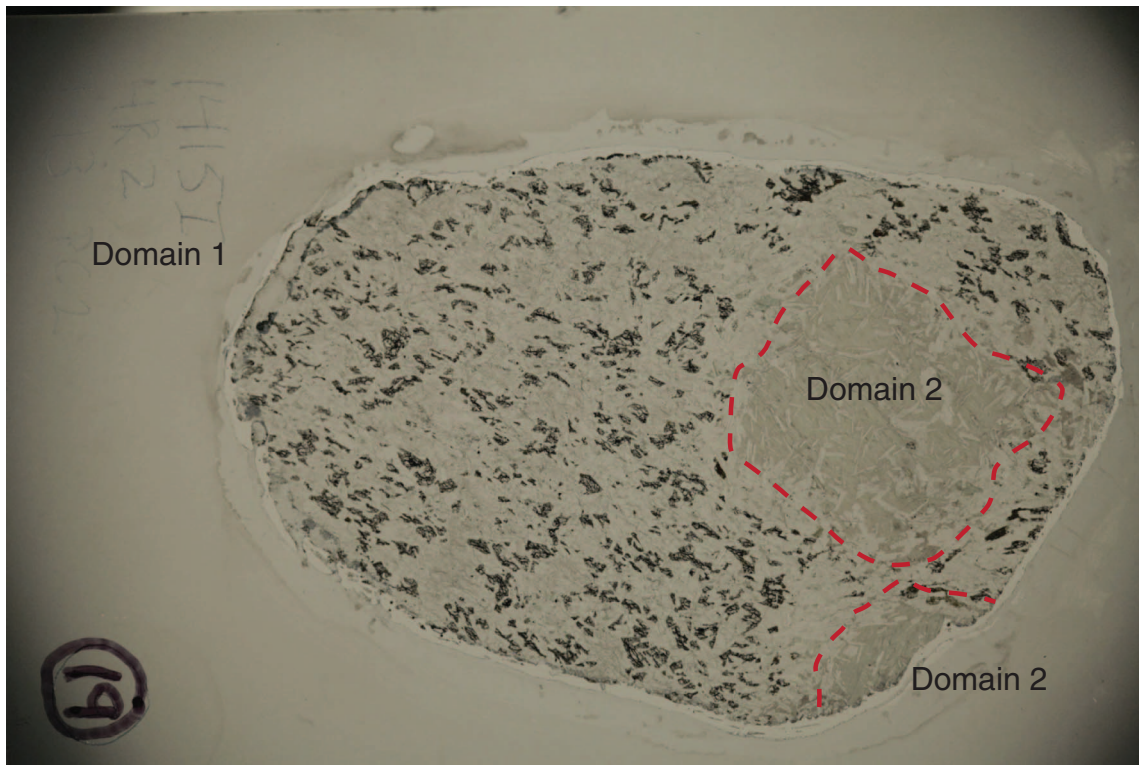
Figure F12. Diagrams and terms used for vein classification and description, Expedition 345.

Vein shape

| Planar | Curved | Irregular | Pull-apart | Fault vein |

Vein connectivity

| Isolated | Single | Branched | Network | En echelon |

| Cross-cutting | Ribbon | Parallel | Anastomosing |

Vein texture

| Massive | Cross fiber | Slip fiber | Vuggy | Polycrystalline |

Vein structure

| Uniform | Banded | Composite | Haloed | Intraveinous |
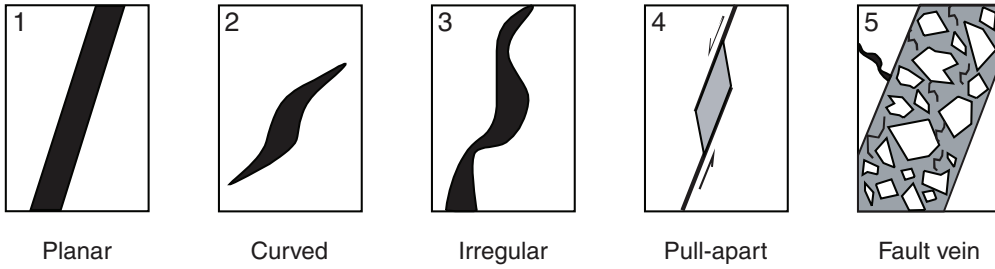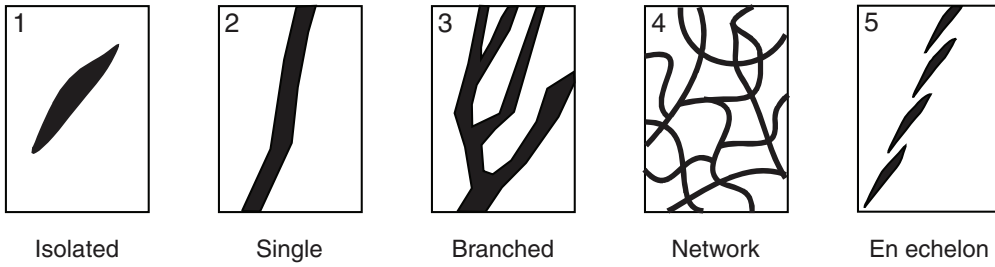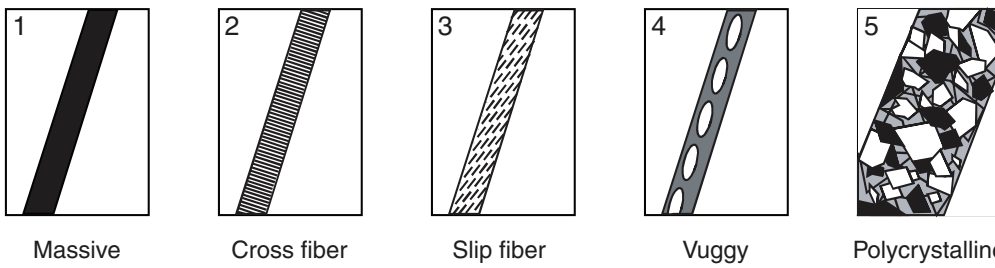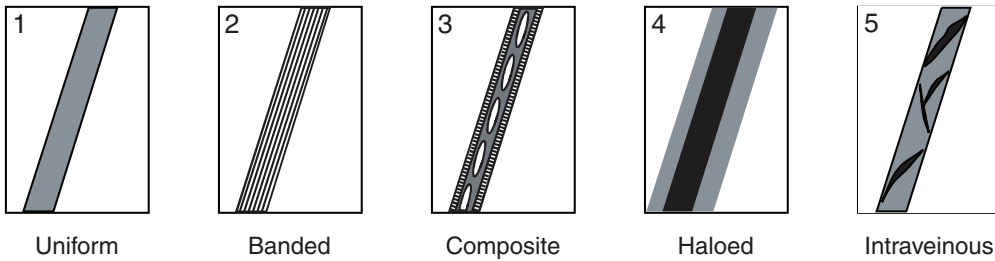
Figure F13. Example of full thin section photomicrographs in which multiple metamorphic domains were defined, Expedition 345 (Sample 345-U1415J-10R-1, 53–55 cm [Piece 6B]). Cpx = clinopyroxene.
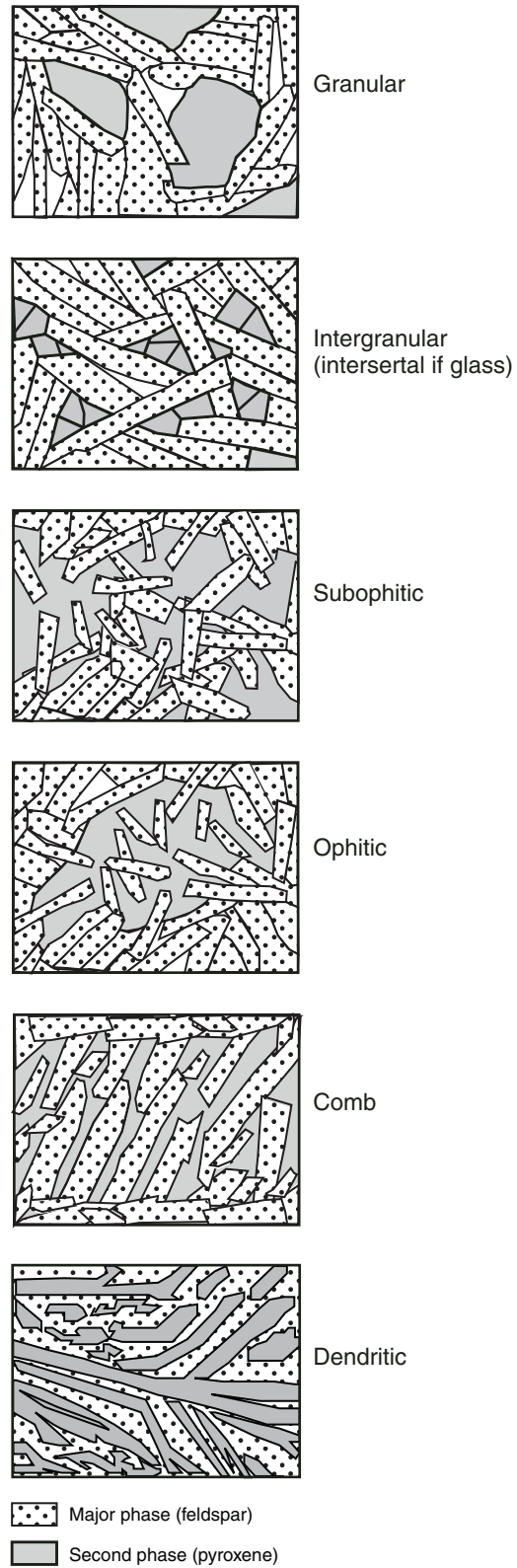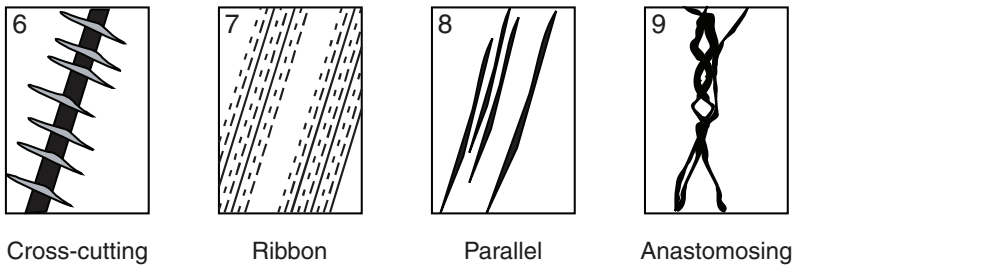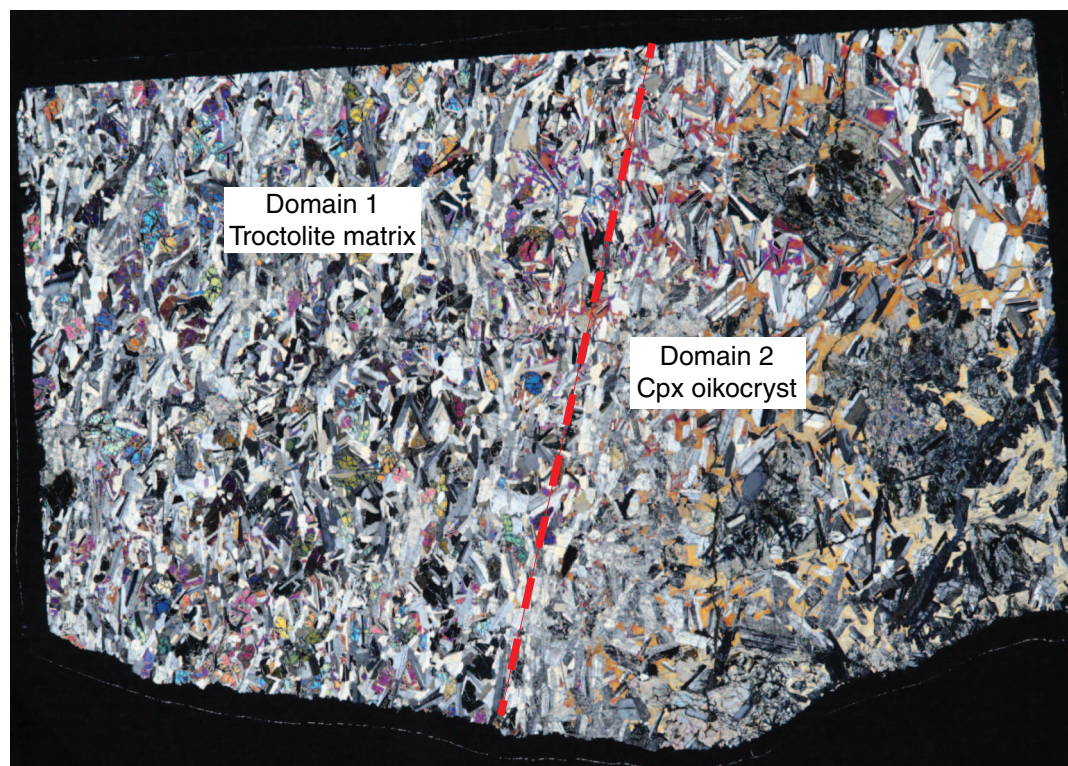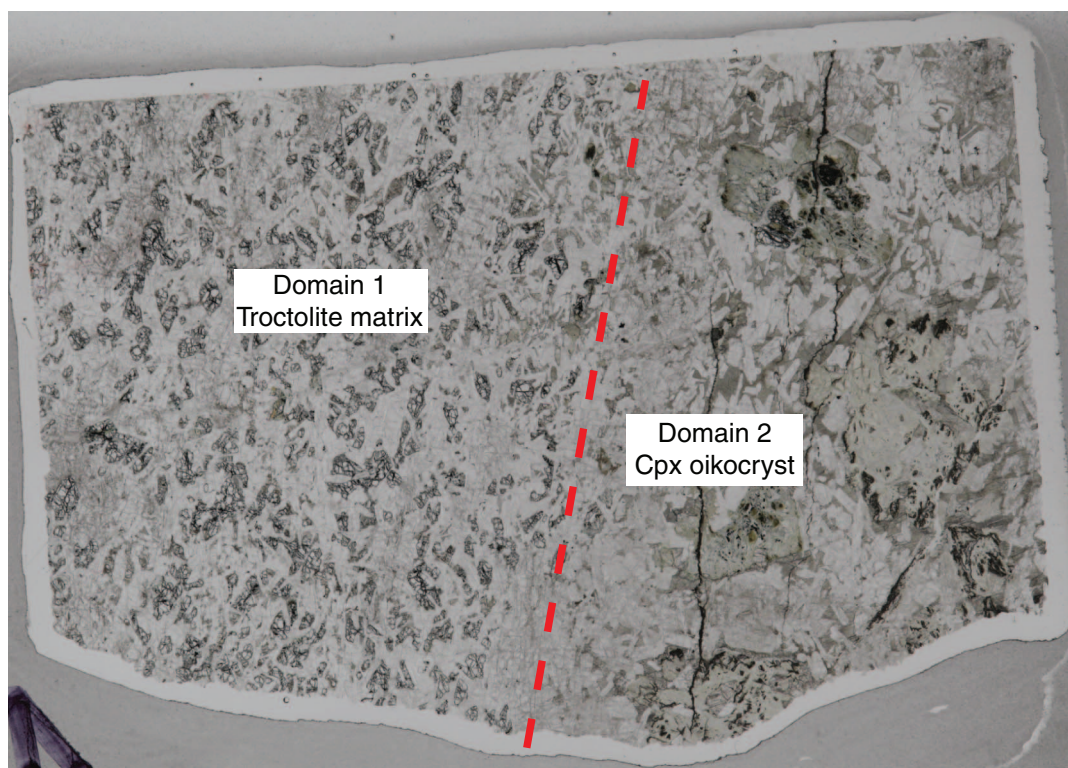
Figure F14. A–C. Reference frame and method of measuring a planar feature to describe the orientation of observed structures, Expedition 345.
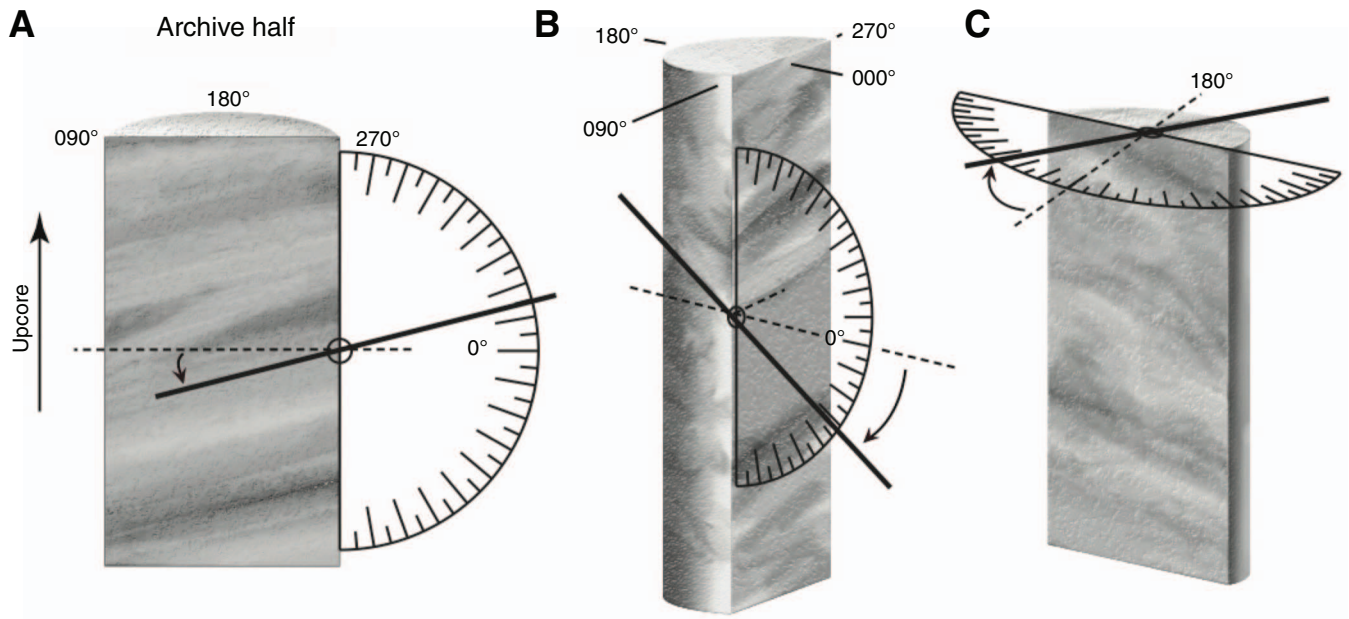
Figure F15. Intensity and intensity rank for magmatic, crystal-plastic, and brittle/cataclastic deformation fabrics and veins, Expedition 345.

Feature	0	1	2	3	4	5
Open fractures	No open fractures	<1 per 10 cm	1-5 per 10 cm	>5 per 10 cm		
Veins	No veins	<1 per 10 cm	1-5 per 10 cm	5-10 per 10 cm	10-20 per 10 cm	>20 per 10 cm
Serpentine network orientation	Random	Weakly oriented	Moderately oriented	Strongly oriented		
Cataclastic deformation	Undeformed	Minor fracturing No significant grain size reduction	Moderate fracturing No significant grain size reduction	Dense anastomosing fracturing and incipient breccia (<20% matrix)	Well-developed fault brecciation; clast rotation (20% - 70% matrix)	Cataclasite (>70% matrix)
Gabbro crystal-plastic deformation	Undeformed	Weakly foliated	Strongly foliated	Porphyroclastic (protomylonite)	Mylonite	Ultramylonite
Magmatic foliation	Isotropic: no shape fabric	Weak shape fabric	Moderate shape fabric	Strong shape fabric		

Figure F16. Morphologies of fracture and fracture networks, Expedition 345.
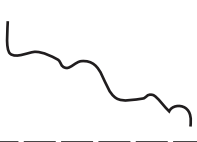
Figure F17. Morphologies of vein and vein networks used by the structural geology group, Expedition 345.

Vein morphology						
	No veins	Planar	Curved	Irregular	Vein tip	Stepped
Vein network morphology						
	Parallel	En echelon	Overlapping	Cross-cutting	Anastomosing	Branching

Figure F18. Total magnetic field profile through the ASC Scientific Model TD-48 SC thermal demagnetizer, measured with an Applied Physics three-axis fluxgate sensor while the R/V *JOIDES Resolution* was at Site U1415 with a ship orientation of 111° (i.e., with the TD-48 SC axis nearly orthogonal to the local geomagnetic field direction). Survey conducted on 14 January 2013.
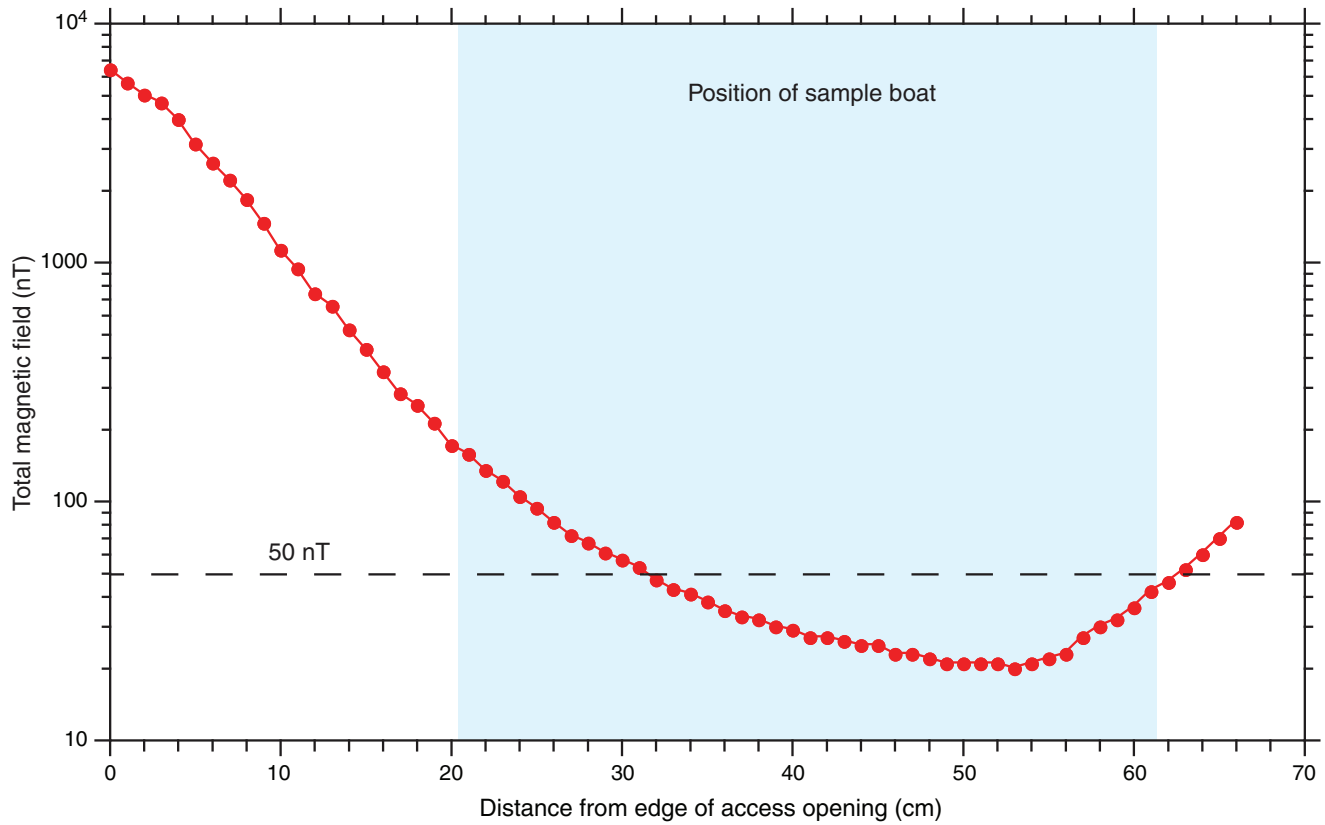
Figure F19. Normalized response curve of the MS2C Bartington magnetic susceptibility meter on the Whole-Round Multisensor Logger (modified after Blum, 1997), Expedition 345. Normalized amplitude (*A*) of magnetic susceptibility of thin discs against distance from the center of the MS2C coil (*x*). Amplitudes are normalized against the peak value at zero distance. Black line shows fitted curve based on the inset equation, where the fitted scaling length (*C*) is about one-fourth of the coil diameter. Gray line shows the cumulative probability function for the fitted curve, indicating that 90% of the measured signal is sourced from within ~4 cm of the coil.

$$A \approx \frac{A_0}{[X/C]^3 + 1},$$

where $C = 2.135$ cm
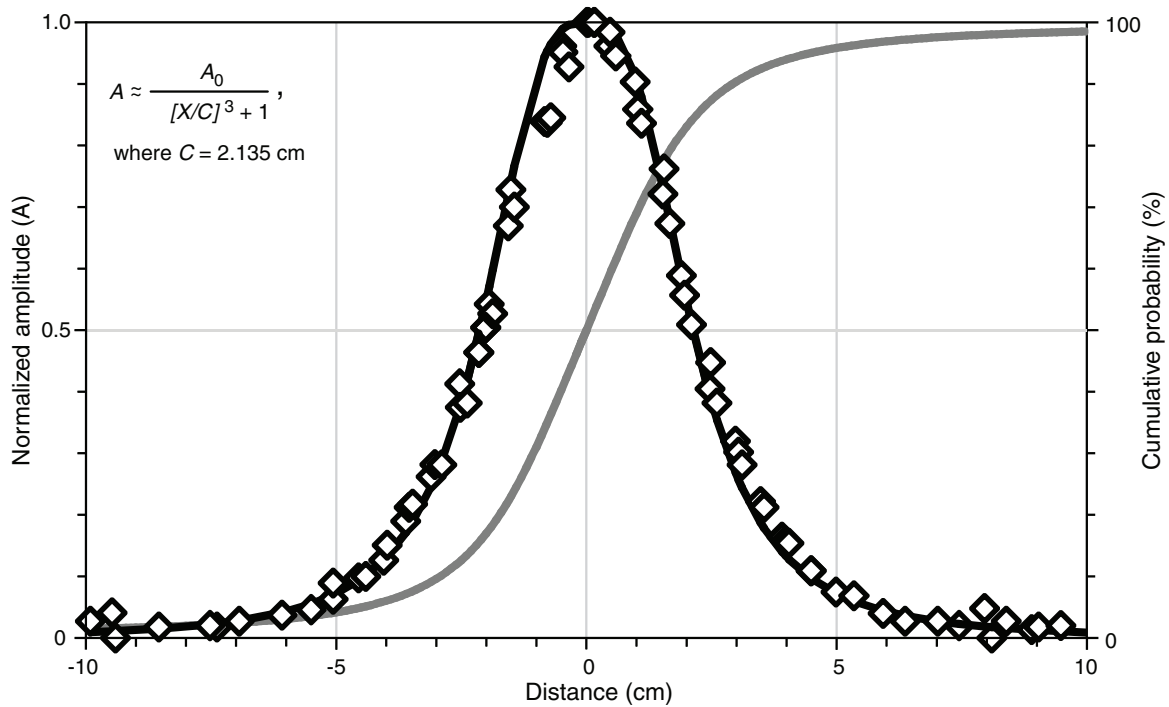
Figure F20. Corrected magnetic susceptibility (MS) data from the Whole-Round Multisensor Logger when the susceptibility is higher than the maximum value recorded by the instrument (9999 × 10^{-5} SI), Expedition 345. The corrected curve (red) is obtained by adding 10,000 (or more; 20,000 for one point in B) to the clipped data points. **A.** Interval 345-U1415J-18R-1, 55–80 cm. **B.** Interval 345-U1415J-21R-1, 0–25 cm.
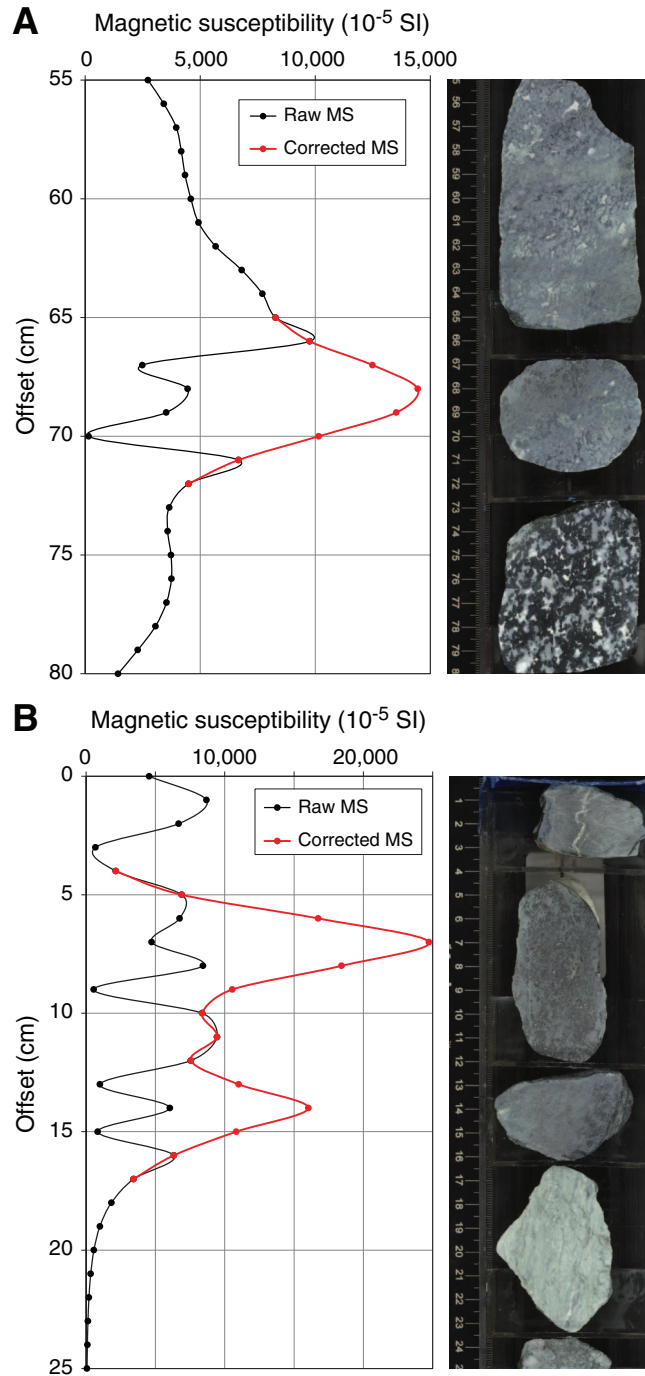
Figure F21. Chromaticity measurement tests on a purple color standard (a* ≈ 12, b* ≈ −4) over a period of ~3–4 h, Expedition 345. See text for further explanations. **A, B.** Tests performed before the data drifting problem was fixed. Note the drift of a* and b* values. **C, D.** Tests performed after the data drifting problem was fixed.
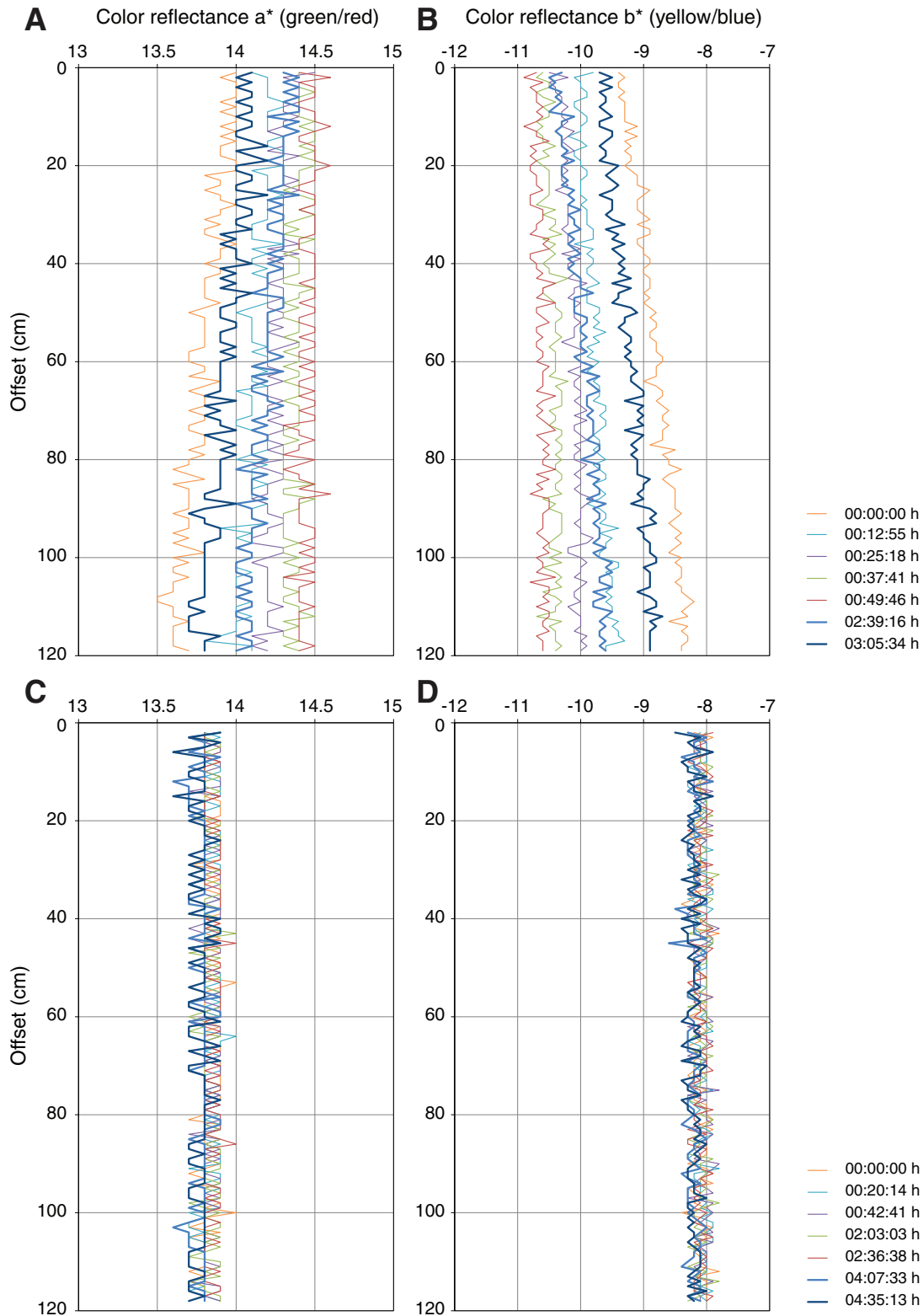
Figure F22. *P*-wave velocity (V_P) measurements using acrylic standards, Expedition 345. **A.** Measurements on cylinders with and without a drop of water to enhance contact between the measured sample and the transducer caps. Acrylic cylinder diameters: circles = 15 mm, squares = 20 mm, triangles = 30 mm. **B.** Measurements on prisms with and without the water bath. Squares = with water bath, circles = without water bath.
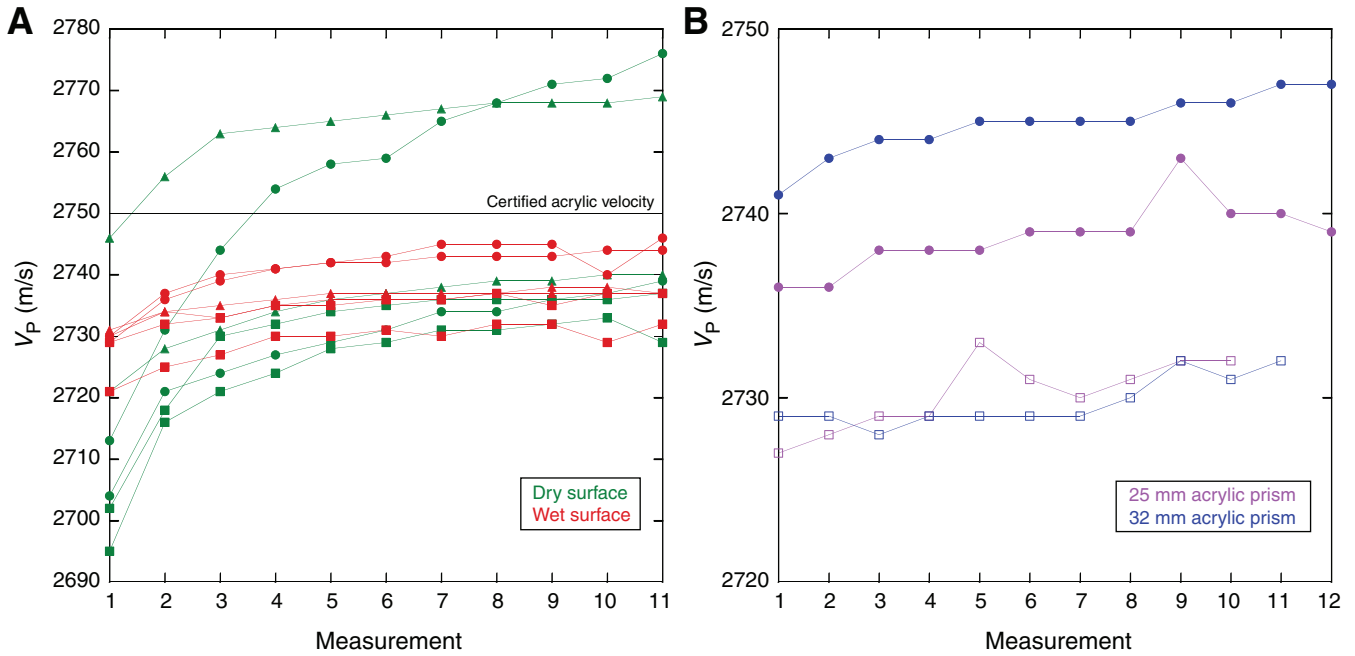
Figure F23. *P*-wave velocity (V_P) measurements made during Expedition 345 using minicores from Ocean Drilling Program Leg 147 Site 894 gabbroic samples. **A.** Measurement series on three samples. **B.** Averages of three measurement series on the 10 Site 894 samples compared with a series of measurements on the same samples using the water bath. White circles and associated bars are the averages and standard deviation (st. dev.), respectively, of the measurements without the water bath. Averages do not take into account the first four measurements of each series.
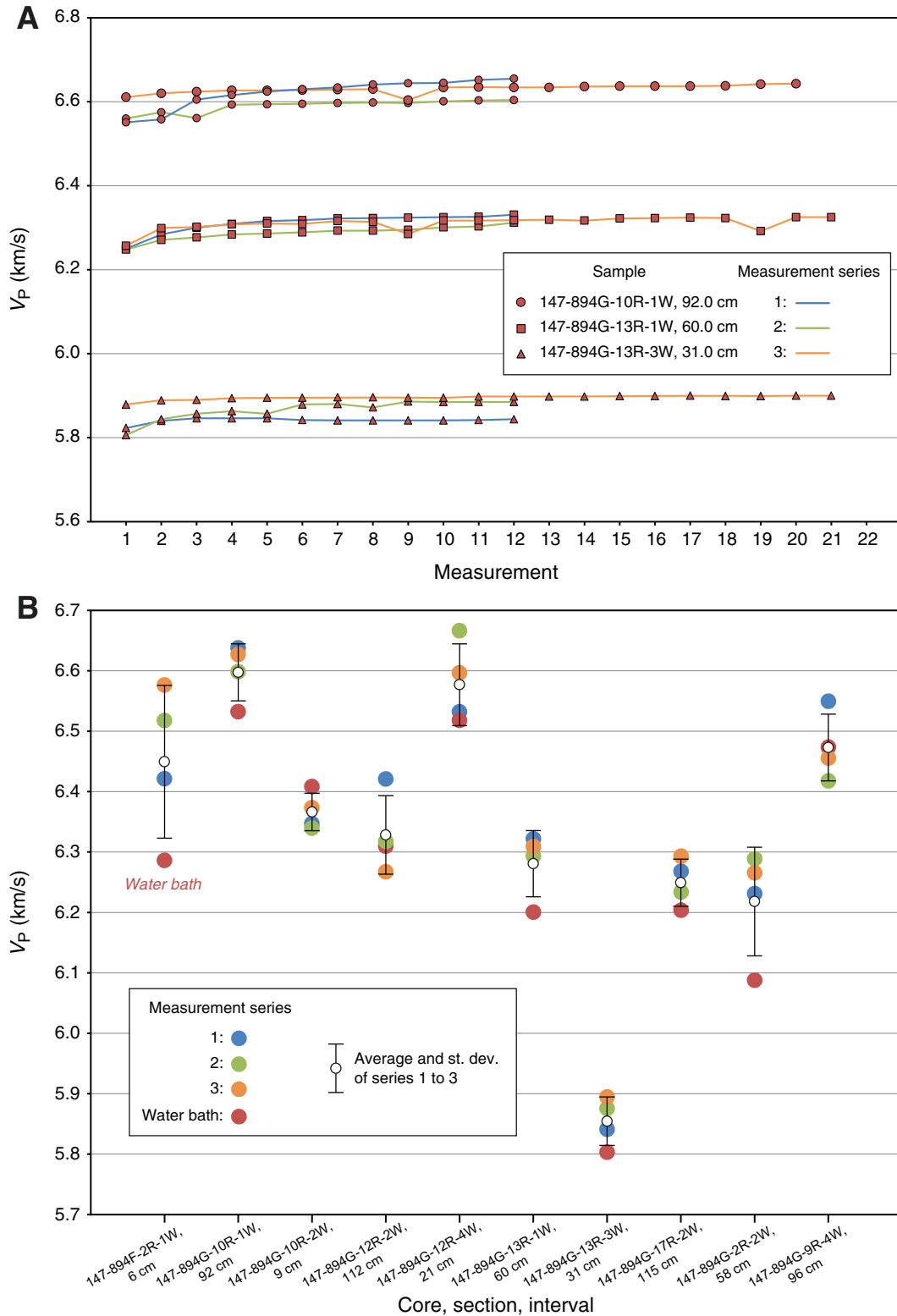
Figure F24. Thermal conductivity measurement tests using (**A**) MACOR standard and (**B**) core piece from Ocean Drilling Program Leg 147 (Sample 147-894C-1M-1A [Piece 1]). Blue = short probe (4.4 cm), green = long probe (7.3 cm).
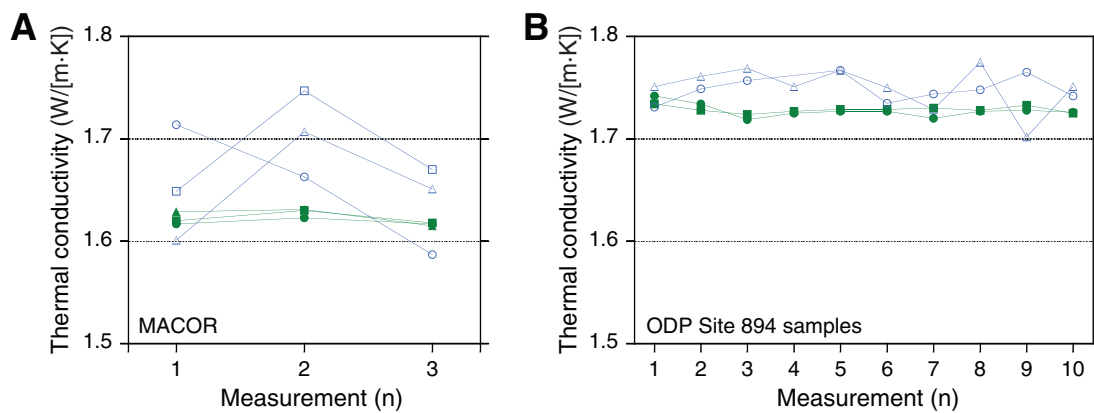
Figure F25. Method of sampling and isolation of three samples of saw cuttings, Expedition 345. For other explanation, see text. **A.** The unsorted "mud sample" is acquired by allowing the cuttings and wash water to stand for 12 h. **B.** The supernatant suspension is filtered to remove lingering silt-sized particles (the >10 µm sample), and the suspended clay-size particles are isolated in a centrifuge.
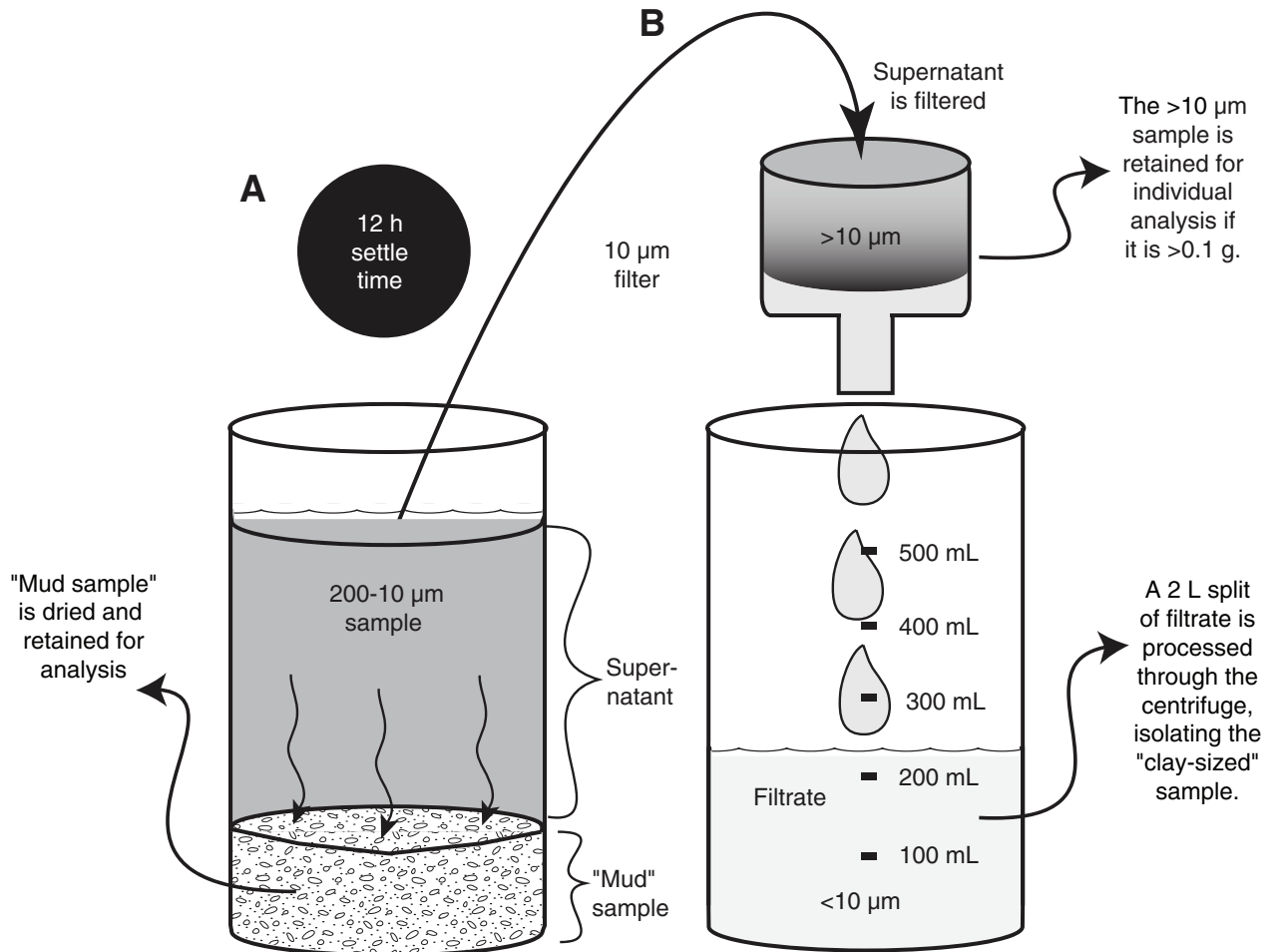
Table T1. Wavelengths used for major and trace element analyses on the Teledyne Leeman Labs Prodigy inductively coupled plasma–atomic emission spectroscopy instrument.

Element	Wavelength (nm)	
Major:		
Si	250.690	251.611
Ti	336.122	337.280
Al	308.215	396.152
Fe	239.563	238.204
Mn	257.610	
Mg	280.271	285.213
Ca	315.887	317.933
Na	588.995	589.592
K	769.897	
P	213.618	214.914
Trace:		
Rb	780.027	
Ba	493.409	
Sr	407.771	421.552
Sc	361.383	
Y	360.073	371.03
Zr	339.198	343.823
Cu	324.754	327.396
Nb	309.418	316.34
V	310.230	292.401
Ni	231.604	
Co	228.615	
W	207.911	
Zn	206.200	202.548
Cr	205.552	267.716

For elements listed with two wavelengths, the wavelength yielding the best calibration line was used.

Table T2. Preferred values for the rock standards used for calibration of major and trace element inductively coupled plasma–atomic emission spectroscopy analyses (volatile-free basis), Expedition 345.

Standard:	JP-1	MRG-1	BCR-2	JG-1a
Concentration (wt%):				
SiO_2	43.28	39.59	54.17	72.36
TiO_2	0.01	3.79	2.26	0.25
Al_2O_3	0.71	8.55	13.52	14.3
$Fe_2O_3^{(T)}$	8.52	18.26	13.82	2.06
MgO	45.6	13.67	3.59	0.69
MnO	0.12	0.17	0.2	0.06
CaO	0.56	14.98	7.13	2.18
Na_2O	0.021	0.74	3.16	3.46
K_2O	0.003	0.18	1.79	4.06
P_2O_5	0.002	0.07	0.35	0.08
Total:	98.83	100	99.99	100
Concentration (ppm):				
Sc	7.4	56.1	33	6.11
V	27.7	532.4	416.5	22.93
Cr	2935	451	18	18.62
Co	113	86	37	5.9
Ni	2424	187	18	6.41
Cu	4.9	135.5	21	1.5
Zn	42.9	192.5	127.2	37.55
Sr	0.65	272.7	340.44	179.23
Y	0.09	13.26	37.048	30.24
Zr	5.53	105.78	184.24	116.75
Ba	9.74	54.76	677.88	464.6
Nb	0.04	21.26	12.62	11.13
Rb	0.36	8	46.96	178.23
W	0.863	—	2.103	13.32

— = not applicable.

Table T3. Analyses of International Rock reference material DTS-1 and JGb-1 and in-house rock standard 147-895D-10W, Expedition 345.

Date (2013)	SiO₂ (wt%)	TiO₂ (wt%)	Al₂O₃ (wt%)	Fe₂O₃(T) (wt%)	MgO (wt%)	MnO (wt%)	CaO (wt%)	Na₂O (wt%)	K₂O (wt%)	P₂O₅ (wt%)	Total	Sc (ppm)	V (ppm)	Cr (ppm)	Co (ppm)	Ni (ppm)	Cu (ppm)	Zn (ppm)	Sr (ppm)	Y (ppm)	Zr (ppm)	Ba (ppm)	Nb (ppm)	Rb (ppm)
DTS-1:																								
9 Jan	39.58	<0.01	0.17	8.68	46.83	0.12	<0.2	<0.02	ND	<0.70	95.40	2.7	<30	3969	106	2316	ND	ND	<0.70	<1.5	ND	ND	ND	ND
9 Jan	39.62	<0.01	0.18	8.68	47.35	0.12	<0.2	<0.02	ND	<0.70	95.98	3.9	<30	3982	101	2381	ND	ND	<0.70	<1.5	ND	ND	ND	ND
13 Jan	40.33	<0.01	0.15	8.69	46.94	0.12	<0.2	<0.02	<0.02	<0.07	96.23	2.9	<30	3999	102	2267	<10	39	<0.70	<1.5	<20	<65	<5	<5
13 Jan	40.17	<0.01	0.15	8.68	47.41	0.12	<0.2	<0.02	<0.02	<0.07	96.52	3.1	<30	3991	106	2256	<10	39	<0.70	<1.5	<20	<65	<5	<5
19 Jan	40.66	<0.01	0.16	8.71	48.35	0.12	<0.2	<0.02	<0.1	<0.07	98.00	3.8	12	4122	114	2530	<10	44	<0.70	<20	<10	ND	<5	<5
19 Jan	40.36	<0.01	0.20	8.67	48.61	0.12	<0.2	<0.02	<0.1	<0.07	97.96	2.5	20	4168	110	2267	<10	43	<0.70	<20	<10	ND	<5	<5
2 Feb	40.00	<0.01	0.15	8.89	48.06	0.12	<0.2	<0.02	<0.04	<0.07	97.24	3.8	15.7	3814	105	2222	<10	32	<0.7	<1.1	9	<11.3	<21	<47
2 Feb	39.69	<0.01	0.16	8.91	48.24	0.12	<0.2	<0.02	<0.04	<0.07	97.15	ND	9.6	3813	101	2346	<10	34	<0.7	<1.1	<5.5	<11.3	<21	<47
6 Feb	39.77	<0.01	0.20	8.71	46.67	0.12	<0.2	<0.02	<0.04	<0.07	95.47	3.0	12.8	3940	104	2282	<6	39	ND	ND	<2	ND	ND	ND
6 Feb	39.98	<0.01	0.20	8.73	46.92	0.12	<0.2	<0.02	<0.04	<0.07	95.96	2.9	ND	3982	107	2172	<6	39	ND	ND	<2	ND	ND	ND
Average:	40.02	—	0.17	8.73	47.54	0.12	—	—	—	—	96.58	3.2	14.2	3978	106	2304	—	39	—	—	—	—	—	—
Preferred values:	40.04	0.01	0.19	8.71	49.30	0.12	0.16	0.02	0.001	0.002	98.54	3.50	10.00	3993	132	2304	6	44.8	0.31	0.04	0.19	0.36	0.02	0.06
Precision (%):	0.9		12.3	1.0	0.6							16.7	28.1	2.8	3.8	4.3	—	10.0						
Accuracy (%):	−0.06		−9.8	0.3	−3.6	2.0						−9.6	41.6	−0.4	−19.9	0.0		−13.6						
147-895D-10W:																								
19 Jan	45.41	0.48	3.82	10.52	38.28	0.14	3.90	0.49	<0.1	<0.07	103.06	16	117	2724	91	1369	29	77	236	<20	51	ND	<5	<5
19 Jan	45.06	0.46	3.80	10.40	38.07	0.14	3.85	0.48	<0.1	<0.07	102.27	15	130	2692	90	1214	24	74	233	<20	63	ND	<5	<5
2 Feb	45.14	0.63	4.21	10.80	34.90	0.14	3.70	0.72	0.05	<0.07	100.28	14	114	2486	76	1817	10	66	242	14	38	<11.3	<21	<47
2 Feb	45.60	0.63	4.24	10.80	35.11	0.14	3.74	0.73	0.05	<0.07	101.04	15	119	2489	74	1818	12	68	245	13	41	<11.3	<21	<47
6 Feb	43.28	0.46	3.67	9.80	35.73	0.13	3.65	0.51	0.07	<0.07	97.31	15	92	2297	79	1946	21	133	248	13	21	ND	ND	ND
6 Feb	43.28	0.46	3.66	9.83	35.61	0.13	3.68	0.51	0.07	<0.07	97.22	16	95	2302	78	1960	21	134	247	13	21	ND	ND	ND
Average:	45.30	0.55	4.02	10.63	36.59	0.14	3.80	0.60	0.05	—	101.68	15	111	2498	81	1687	20	92	242	13	39	—	—	—
Preferred values:	44.37	0.49	4.03	10.57	35.22	0.17	3.70	0.50	0.06	0.06	99.17	17	181.1	2067	97	1851	40.8	87.2	209	11.32	31.7	11	1.04	1.47
Precision (%):	0.6	16.6	5.9	1.9	5.0	1.1	2.4	22.6	2.2			5.1	13.2	7.3	8.9	18.8	37.0	35.2	2.5	3.7	42.0			
Accuracy (%):	2.1	11.7	−0.4	0.6	3.9	−16.7	2.6	20.9	−15.4			−9.9	−38.5	20.9	−16.2	−8.8	−51.7	5.4	15.5	16.7	23.8			
JGb 1:																								
9 Jan	44.00	1.68	17.73	15.23	8.82	0.19	12.02	1.39	ND	<0.70	101.06	35	631	52	54	17	ND	ND	326	10	ND	ND	ND	ND
9 Jan	44.13	1.69	17.76	15.39	8.86	0.19	12.06	1.40	ND	<0.70	101.48	35	632	49	55	24	ND	ND	328	8	ND	ND	ND	ND
13 Jan	43.86	1.68	17.38	15.18	8.85	0.19	11.83	1.33	0.23	<0.07	100.52	35	669	49	59	23	70	104	327	9	34	<65	<5	<5
13 Jan	44.75	1.70	17.48	15.31	8.89	0.19	11.85	1.34	0.23	<0.07	101.74	35	673	49	58	25	71	106	328	8	29	<65	<5	<5
19 Jan	43.90	1.75	17.38	15.43	8.80	0.19	11.99	1.31	0.20	<0.07	100.94	36	652	52	63	<30	76	114	323	<20	31	ND	<5	<5
19 Jan	44.32	1.75	17.74	15.55	8.82	0.19	12.22	1.30	0.20	<0.07	102.09	35	621	48	63	<30	73	115	320	<20	51	ND	<5	<5
2 Feb	43.86	1.71	17.76	15.37	7.80	0.19	11.88	1.31	0.23	<0.07	100.10	36	644	47	59	24	72	98	321	13	39	63	<21	<47
2 Feb	43.93	1.70	17.79	15.19	7.82	0.19	11.94	1.31	0.22	<0.07	100.09	36	654	51	60	18	76	97	320	11	34	45	<21	<47
6 Feb	43.94	1.69	17.56	15.38	8.74	0.19	11.99	1.34	0.27	<0.07	101.09	35	644	50	60	24	85	106	321	7	27	ND	ND	ND
6 Feb	43.85	1.69	17.53	15.33	8.71	0.19	11.97	1.33	0.27	<0.07	100.86	35	642	53	60	30	80	106	319	9	30	ND	ND	ND
Average:	44.05	1.70	17.61	15.33	8.61	0.19	11.97	1.34	0.23	—	101.04	35	646	50	59	23	75	106	323	9	34	54	—	—
Preferred values:	44.00	1.62	17.74	15.09	8.03	0.18	11.87	1.19	0.22	0.06	100.00	35.4	649	61	62	25	75	106	328	9.8	29.0	64.4	2.5	5.59
Precision (%):	0.7	1.5	0.9	0.7	4.9	0.7	0.9	2.6	12.1			1.3	2.6	4.0	4.9	18.6	6.6	6.1	1.2	18.8	22.2	24.1		
Accuracy (%):	0.1	5.2	−0.7	1.6	7.2	5.1	0.9	12.2	5.1			−0.6	−0.4	−18.1	−4.6	−7.8	1.1	0.2	−1.3	−4.0	19.0	−16.1		

These data provide estimates of the run-to-run accuracy and precision for major and trace element inductively coupled plasma–atomic emission spectroscopy analyses. ND = not determined, — = not applicable.

Table T4. Standard reproducibility and accuracy and precision estimates for gas chromatography analyses of CO_2, H_2O and S, Expedition 345.

Standard	Date	CO_2 (wt%)	H_2O (wt%)	S (ppm)
JP-1	24 Dec 2012	0.28	2.50	ND
	26 Dec 2012	0.33	2.48	ND
	3 Jan 2013	0.35	3.02	ND
	8 Jan 2013	ND	2.13	ND
	12 Jan 2013	0.26	2.61	ND
	13 Jan 2013	0.29	2.09	ND
	17 Jan 2013	0.29	2.44	ND
	28 Jan 2013	0.27	2.53	ND
	3 Feb 2013	0.25	2.62	ND
	8 Feb 2013	0.28	2.66	ND
	Average (wt%/ppm):	0.289	2.507	ND
	Preferred value (wt%/ppm):	0.280	2.540	
	Standard deviation (wt%):	0.030	0.26	ND
	Precision (%):	11	11	ND
	Accuracy (%):	3	−1	ND
MRG-1	24 Dec 2012	1.09	0.80	ND
	26 Dec 2012	1.07	0.90	589
	3 Jan 2013	1.19	1.16	ND
	8 Jan 2013	ND	0.96	666
	12 Jan 2013	1.04	0.89	521
	13 Jan 2013	1.17	0.92	ND
	17 Jan 2013	1.18	0.82	ND
	28 Jan 2013	1.15	0.99	504
	3 Feb 2013	1.10	0.96	ND
	8 Feb 2013	1.15	0.94	ND
	Average (wt%/ppm):	1.126	0.93	570
	Preferred value (wt%/ppm):	1.070	1.02	605
	Standard deviation (wt%):	0.053	0.099	74
	Precision (%):	5	11	13
	Accuracy (%):	5	−8	−6

ND = not determined.

Table T5. List of elements of interest and their detection limits as provided by the handheld X-ray fluorescence instrument manufacturer, Expedition 345.

Analyzed element	Filter position	Detection limit (ppm)
Ba	High	45
Sr	Main	3
Zn	Main	8
Cu	Main	15
Ni	Main	25
Co	Main	20
Fe	Main	30
Mn	Main	25
Cr	Main/Light	25
V	Main/Light	15
Ti	Main/Light	30
Ca	Light	40
K	Light	75
Al	Light	310
Si	Light	750
Mg	Light	13,000

Table T6. Handheld X-ray fluorescence measurements for four certified silicate standards, Expedition 345.

	BCR-2				BHVO-2				JB-2				JA-1			
	Compiled values	Measured (N = 5)	Accuracy (%)	Precision (%)	Compiled values	Measured (N = 5)	Accuracy (%)	Precision (%)	Compiled values	Measured (N = 5)	Accuracy (%)	Precision (%)	Compiled values	Measured (N = 5)	Accuracy (%)	Precision (%)
Major element (wt%):																
SiO_2	54.1	44.51	−17.73	5.35	49.9	39.50	−20.85	4.52	53.20	43.27	−18.67	5.37	63.97	44.14	−31.00	6.89
TiO_2	2.26	1.74	−22.82	1.20	2.73	2.08	−23.95	0.97	1.19	0.90	−24.33	0.98	0.85	0.49	−41.90	1.85
Al_2O_3	13.5	8.16	−39.54	8.72	13.5	8.53	−36.83	8.07	14.67	9.25	−36.92	10.97	15.22	7.52	−50.59	12.85
FeO^T	12.28	10.20	−16.95	0.18	10.95	8.30	−24.18	0.35	12.76	9.70	−24.00	0.54	6.29	5.41	−14.01	0.42
MnO	0.2	0.22	8.30	4.52	0.17	0.19	10.89	5.33	0.20	0.21	5.00	1.80	0.157	0.17	8.28	4.86
MgO	3.59	BDL	—	—	7.23	4.30	−40.53	22.32	4.66	BDL	—	—	1.57	BDL	—	—
CaO	7.12	6.89	−3.28	0.63	11.4	10.70	−6.14	0.68	9.89	9.81	−0.81	0.82	5.7	5.61	−1.58	1.55
Na_2O	3.16	—	—	—	2.22	—	—	—	2.03	0.35	−82.72	—	3.84	—	—	—
K_2O	1.79	1.46	−18.44	1.23	0.52	0.44	−15.96	3.30	0.42	0.35	−16.46	2.50	0.763	0.35	−54.13	0.95
P_2O_5	0.35	BDL	—	—	0.27	0.17	−37.04	43.41	0.10	BDL	—	—	0.165	—	—	—
Total:	98.35	73.18			98.89	74.20			99.12				98.53	63.70		
Trace element (ppm):																
Ba	677	BDL	—	—	131	BDL	—	—	208	BDL	—	—	303	BDL	—	—
Sr	340	240	−29.41	—	396	275	−31	2.10	178	125	−30	4.62	264	160	−39	12.60
Zr	184.00	153	−17.12	3.28	172.00	140	−19	5.83	51	40	−22	10.70	84	72	−14	6.20
V	416	135	−67.55	6.01	317	214	−32	7.39	578	788	36	6.70	108	270	150	3.02
Cr	18.0	BDL	—	—	280.0	232	−17	3.28	27	BDL	—	—	6.4	BDL	—	—
Co	37	BDL		—	45	BDL	—	—	39.8	BDL	—	—	11	BDL	—	—
Ni	18	BDL	—	—	119	92	−23	19.47	14.2	BDL	—	—	1.7	BDL	—	—
Cu	21.0	BDL	—	—	127.0	118	−7	8.15	227	223	−2	2.25	41	BDL	—	—
Zn	127.0	113	−11.42	8.51	103.0	90	−13	8.16	110	103	−7	9.34	91	55	−40	10.50

N = number of measurements on the same spot for each analysis. FeO^T = all Fe measured as FeO, BDL = below detection limit, — = not applicable. Compilation data from Govindaraju (1994) and GeoReM (**georem.mpch-mainz.gwdg.de;** 31 December 2012).

Table T7. Handheld X-ray fluorescence measurements of BCR-2 standard by using rock standard calibration, Expedition 345.

		Expedition 335		Expedition 345		
	Preferred value*	Calibration	Accuracy (%)	Calibration ($N = 5$)	Precision (%)	Accuracy (%)
Major element (wt%):						
SiO_2	54.1	48.14	–11.02	52.61	1.52	–2.75
TiO_2	2.26	1.77	–21.62	2.27	0.92	0.38
Al_2O_3	13.5	8.9	–34.07	9.4	6.2	–30.37
FeO^T	12.28	12.41	1.07	12.10	0.18	–1.48
MnO	0.2	0.22	8.86	0.19	1.21	–5.88
MgO	3.59	BDL	—	BDL	—	—
CaO	7.12	7.03	–1.33	6.77	0.87	–4.92
Na_2O	3.16	—	—	—	—	—
K_2O	1.79	1.12	–37.43	0.97	3.08	–45.81
P_2O_5	0.35	BDL	—	BDL	—	—
Total:	98.35					
Trace element (ppm):						
Ba	677	BDL	—	BDL	—	—
Sr	340	240	–29.41	353	2.98	3.82
Zr	184	151	–17.80	178	3.44	–3.26
V	416	150	–63.94	535	7.49	28.61
Cr	18	BDL	—	BDL	—	—
Co	37	BDL	—	BDL	—	—
Ni	18	BDL	—	BDL	—	—
Cu	21	BDL	—	BDL	—	—
Zn	127	105	–17.32	109	4.43	–14.17

* = compilation data from Govindaraju (1994) and GeoReM (**georem.mpch-mainz.gwdg.de;** 31 December 2012). A spreadsheet from Expedition 335 was also used as another quality control to check measurements. N = number of analyses. FeO^T = all Fe as FeO. BDL = below detection limit, — = not applicable.